



Norwegian University of  
Science and Technology

# On Modern IGBT Modules: Characterization, Reliability and Failure Mechanisms

Di Xiao

Master of Science in Electric Power Engineering

Submission date: June 2010

Supervisor: Tore Marvin Undeland, ELKRAFT

Co-supervisor: Astrid Petterteig, SINTEF Energiforskning A/S



# Problem Description

Description: Power systems containing a high percentage of power electronics loads are known to be complex systems with a lot of uncertainties concerning worst case electrical and thermal stress applied to the individual components, and the component ability to survive specific stress conditions. For remote and inaccessible power electronic conversion systems, like offshore wind applications and subsea oil and gas applications, the reliability issues are of still more concern than for traditional industrial applications. That is why power electronics reliability issues have high priority in two R&D projects at SINTEF Energy Research.

The ability of verifying new design ideas and reducing the demand of laboratory testing, which might be time-consuming and cumbersome, is one salient feature of power electronic converters prototyping using device model. Moreover, better understanding of devices behaviour and related physical phenomena can be gained while developing such a model. Devices based on new emerging materials like SiC and GaN are expected to have better performance. However, being a new technology devices characteristics and behaviour need more investigation. Knowledge about the reliability of these devices is still immature which increase the need to have a model where devices behaviour and stresses can be studied in depth.

In the proposed topic the candidate will be guided by the project team at SINTEF. The candidate will get both theoretical (e.g. literature study) and practical (laboratory work) tasks within one or more of the following subjects:

- General fault mechanisms for power semiconductors
- Fault mechanisms related to type of device, but with special focus on IGBTs
- Fault mechanisms related encapsulation (e.g. press-pack devices, modules etc)
- Fault mechanisms related to materials, and especially new materials like SiC
- Application specific reliability, and especially related to driver characteristics
- Influence from pressure and temperature
- Physics-based modelling for SiC devices
- Combined electro-thermal modelling for reliability studies

The candidate may be offered a summer job at SINTEF Energy Research related to ongoing research projects within this field.

A cluster has applied for an EU project in applications of SiC devices in MW converters for wind energy integration. Parts of this project may be included.

Assignment given: 01. February 2010

Supervisor: Tore Marvin Undeland, ELKRAFT





**Faculty of Information Technology, Mathematics and  
Electrical Engineering**

**[Department of Electric Power Engineering](#)**

**On Modern IGBT Modules: Characterization,  
Reliability and Failure Mechanisms**

**Student:** Di Xiao

**Supervisor:** Tore M. Undeland

**Co-Supervisor:** Astrid Petterteig

Ibrahim Abuishmais



---

# On Modern IGBT Modules: Characterization, Reliability and Failure Mechanisms

Master Thesis

By

**Di Xiao**

Faculty of Information Technology, Mathematics and Electrical Engineering

Department of Electric Power Engineering

NORWEGIAN UNIVERSITY OF SCIENCE AND TECHNOLOGY (NTNU)

Trondheim, Norway 2010

---

*This page intentionally left blank*



---

## Content

|   |        |
|---|--------|
| Foreword.....   | i      |
| Abstract.....   | iii    |
| 1. Introduction.....  | - 1 -  |
| 2. IGBT Overview.....                                       | - 3 -  |
| 2.1 Operation Principle.....                                | - 3 -  |
| 2.2 IGBT Turn-on and Turn-off.....                          | - 6 -  |
| 2.3 FWD Performance.....                                    | - 9 -  |
| 3. State-of-the-art Technology of IGBT Module .....         | - 11 - |
| 3.1 Planar- vs. Trench- IGBT .....                          | - 11 - |
| 3.2 PT-, NPT-, FS-, vs. SPT- IGBT .....                     | - 12 - |
| 3.3 SPT <sup>+</sup> IGBT .....                             | - 13 - |
| 3.4 Press-Pack IGBT Module vs. Standard IGBT Module .....   | - 14 - |
| 3.5 SiC Overview .....                                      | - 15 - |
| 4. Failure Mechanisms Summary .....                         | - 19 - |
| 4.1 Package-related Failure Mechanisms .....                | - 19 - |
| 4.2 Failure Mechanisms during Application .....             | - 22 - |
| 5. Experimental Standards and Principles.....               | - 23 - |
| 5.1 Parameters Definitions .....                            | - 23 - |
| 5.2 Testing Standard .....                                  | - 25 - |
| 5.3 Double Pulse Switch Testing.....                        | - 26 - |
| 5.4 Repetitive Switch Testing.....                          | - 27 - |
| 5.5 Power Cycling Testing.....                              | - 28 - |
| 6. Setup and Measurement Description .....                  | - 31 - |
| 6.1 Testing Object Description .....                        | - 31 - |
| 6.2 Measurements and Instruments .....                      | - 32 - |
| 6.3 Double Pulse Switch Testing Setup.....                  | - 35 - |
| 6.4 Repetitive Switch Testing Setup.....                    | - 38 - |
| 6.5 Power Cycling Testing Setup .....                       | - 39 - |
| 7. Results and Analysis .....                               | - 43 - |
| 7.1 Conduction Voltage .....                                | - 43 - |
| 7.2 Gate Resistance Influence .....                         | - 44 - |
| 7.3 Influence of Temperature.....                           | - 45 - |
| 7.4 Influence of Power .....                                | - 49 - |
| 7.5 FWD Performance.....                                    | - 51 - |
| 7.6 Long-term Stability .....                               | - 52 - |
| 7.7 Tyco-IGBT Performance .....                             | - 54 - |
| 7.8 Tyco vs. IXYS IGBT Module.....                          | - 55 - |
| 7.9 Verification of Test Results and Error Evaluation ..... | - 56 - |
| 8. Conclusion and Outlook .....                             | - 57 - |
| Reference .....   | - 59 - |
| Appendix.....   | - 63 - |

---

*This page intentionally left blank*



---

## Foreword

This is a report for the master project in the 2<sup>nd</sup> year of International Master Degree Program of the department of Electric Power Engineering at NTNU. The project has a weight of 30 ECTS credits.

‘Reliable Power Electronics Converters for Offshore Wind Turbines and Subsea Oil Development’ is the subject of this project which is a part of an ongoing research launched by SINTEF Energy Research.

As the continue work of summer job and semester project, this thesis investigates switching characteristics and losses of commercially available IGBT modules to be used for this application. It focuses on switching time and switching energy losses depending on gate resistances, current and voltage levels, operation temperatures, and show differences between several devices of the same type. Some tests also show how device dynamic characteristics and energy losses change when the device has been exposed to stress over some time as well as the long-term stability.

I would like to take this opportunity to thank every people who have helped me during this work. Without your help, I could not have accomplished this much. I would like to thank my supervisor Prof. Tore Undeland, co-supervisors Dr. Astrid Petterteig and Ibrahim Abuishmais, and Riccardo Pittini who tireless support throughout the project and thesis. I would like to thank Mr. Heng Xiao and Ms. Meng Wang for their constructive comments which were useful in refining the thesis finally produced. I also want to thank Kjell Ljøkelsøy and Magnar Hernes at SINTEF Energy Research, Trondheim.

I am solely responsible for any errors or shortcomings.

Trondheim, 28.06.2010

-----  
Di Xiao



---

*This page intentionally left blank*



---

## **Abstract**

The increased demand of offshore power conversion systems is driven by newly initiated offshore projects for wind farms and oil production. Because of long distances to shore and inaccessibility of the equipment long repair times must be expected. At the same time the offshore environment is extremely harsh. Thus, high reliability is required for the converters and it is important to have good knowledge of the switching devices. This thesis investigates switching characteristics and losses of commercially available IGBT modules to be used for this application. It focuses on switching time and switching energy losses depending on gate resistance, current and voltage levels, operation temperatures, and show differences between several devices of the same type. Some test show how device characteristics and losses when the device has been exposed to stress over a certain period.



*This page intentionally left blank*



---

## 1. Introduction

Power systems containing a high percentage of power electronics loads are known to be complex systems with a lot of uncertainties concerning worst case electrical and thermal stress applied to the individual components, and the component ability to survive specific stress conditions. For remote and inaccessible power electronic conversion systems, like offshore wind applications and subsea oil and gas applications, the reliability issues are of still more concern than for traditional industrial applications.

Insulated Gate Bipolar Transistor (IGBT) is becoming more and more important power electronic device in different industrial field because of the advantage of shorter switching time and lower power loss [1-3]. Understanding device fault mechanisms and assessing its lifetime along with other reliability issues of IGBT modules are very important to understand device limits, and thus optimizing converter design later. This thesis first briefly described the structure and operation principle of traditional IGBT, compared the difference between BJT and MOSFET, elaborate the turn-on and turn-off process of IGBT, as well as the freewheeling diode performance in IGBT module at chapter 2. Employing new semiconductor structure to increase the safe operating area (SOA) and improve the stability has attracted much attention. The chapter 3, thus, investigated the state-of-the-art of modern IGBT and the new emerging material SiC which is expected to have better performance.

New developed press-pack IGBT can effectively reduce common faults on traditional IGBT module, but the failure mechanisms of press-pack IGBT did not receive much attention. As the traditional bond-wire IGBT module is still the most popular product for industrial application, investigating the failure mechanisms is still very meaningful. Therefore, common failure mechanisms and the countermeasures were summarized at chapter 4, which paved way for the further experimental research. International standard parameter definitions based on IEC 60747-9 international standard, and the standard testing methods were introduced at chapter 5. Those



---

standards are very important for verification and duplication of the experiments.

Three important experiments were designed and built up to investigate the dynamic characteristics and long-term stability of commercial IGBT modules. Thus chapter 5 also introduced the principles and aims of the experiments theoretically based on the international and industrial standard, and chapter 6 described the build-up processes and operation method of the measurement setups as well as some important tips for mounting the modules, and improving the accuracy of measurements. Finally, chapter 7 analyzed the experimental results, and chapter 8 summarized the thesis and drew some ideas for further research.





## 2. IGBT Overview

The IGBT represents the most commercially advanced device of a new family of power semiconductor devices combining high-input impedance MOS-gate control with low forward-voltage drop bipolar current conduction [1]. At this chapter, the author briefly introduced the basic structure, operation principles and switching behaviors of IGBT as well as the performance of freewheeling diode (FWD).

### 2.1 Operation Principle

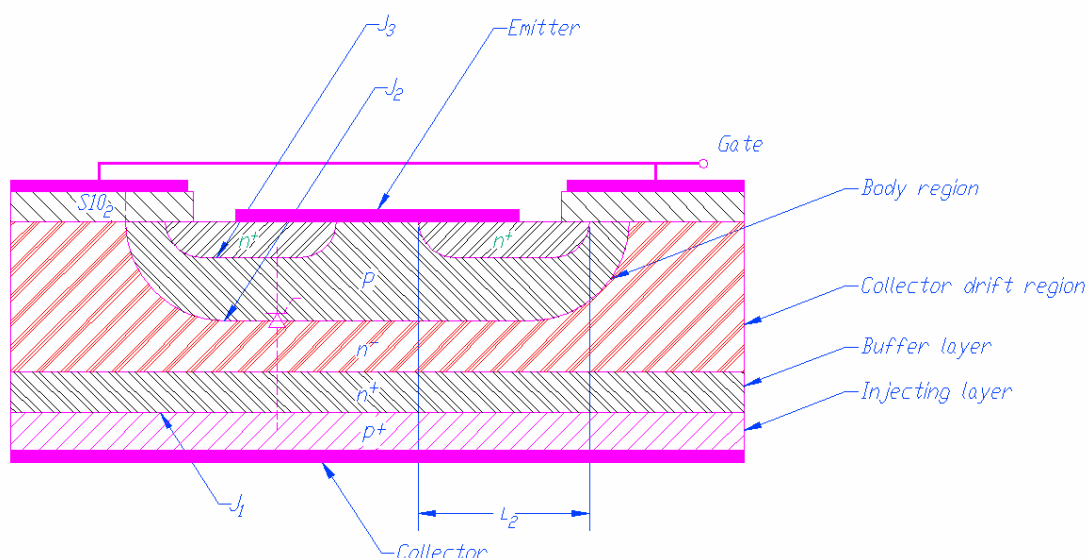


Fig. 1 Sketch of IGBT cross section [4]

IGBT is a byproduct of MOSFET technology which can be self-prove by their structures [1-3]. The only difference is the n-type doped area of drain at MOSFET was replaced by p-layer at IGBT. The structure of (PT-) IGBT as shown in Fig. 1, and the n+ buffer layer is not necessary for NPT- IGBT [5]. The equivalent circuit of the IGBT structure is shown in Fig. 2 which shows the main structure cell: a MOSFET, a BJT and a parasitic thyristor. The interaction of MOSFET and BJT made the IGBT has a better performance than MOSFET and BJT device, and the advantages are summed up in Table 1 [1-3, 6]. However the parasitic thyristor is undesired because it



will destroy IGBT if conducted and this phenomenon is called latch-up.

The equivalent circuit of parasitic capacitance which is important to explain the turn-on and turn-off transition and IGBT symbol as shown in Fig. 3. Based on Fig. 2, the operation principle of IGBT can be explained like that: when Gate-Emitter voltage ( $V_{GE}$ ) excess the gate threshold voltage ( $V_{th}$ ) of MOSFET which leading electrons flow from emitter to drift region. This electrons current is the base-current of PNP-transistor ( $T_1$ ). The emitter of  $T_1$  will inject holes into drift region and most of them will recombination with electrons (injected form MOS channel) because of the larger width of drift region. The remaining holes will diffuse to J2 junction (Collector of PNP transistor) because of the slight reverse-bias of J2, and holes captured by electric field and moved into collector region. So far one should also notice that the IGBT terminal labels are confusing because the IGBT can be used as NPN-BJT but the internal structure is PNP-BJT on the contrary. In addition, the JFET effect often mentioned in many technical papers, but in fact, it does not occur at IGBT [2]. The output current-voltage characteristics of IGBT as shown in Fig. 4

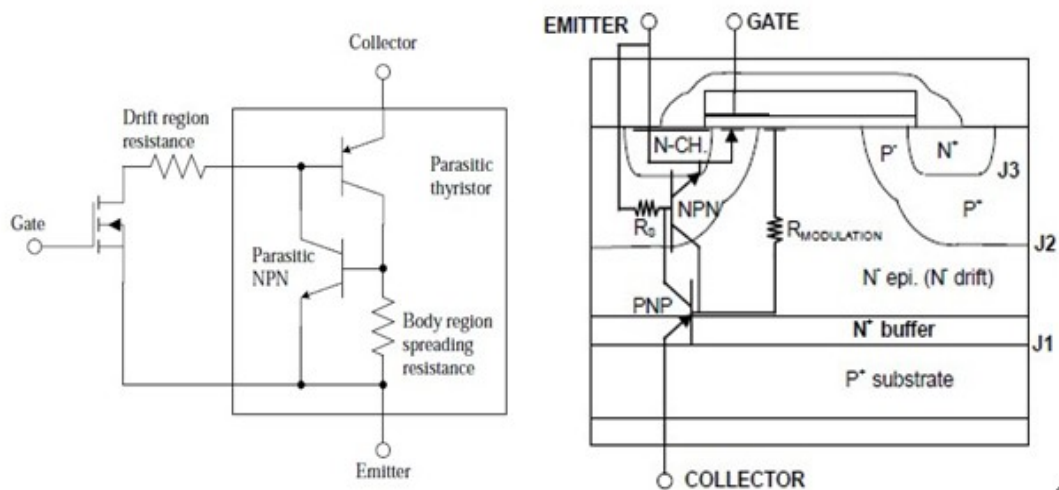


Fig. 2 Equivalent circuit for the IGBT and a cross-section of the IGBT structure (PT & N-Channel)

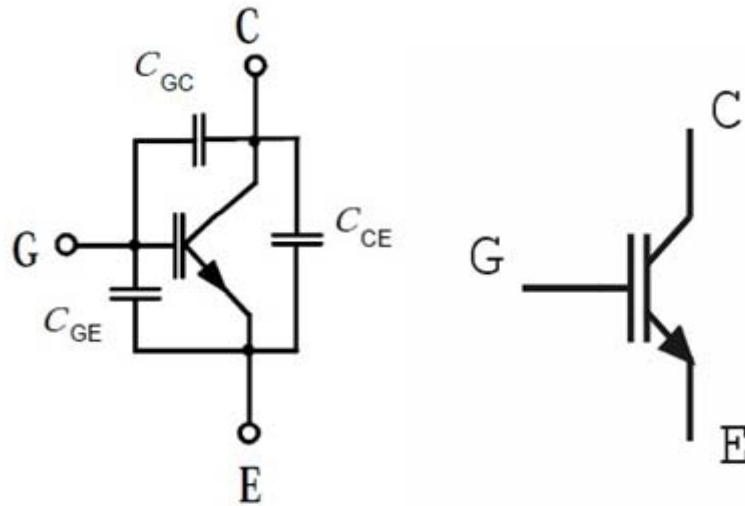


Fig. 3 IGBT Equivalent circuit showing parasitic capacitance (a) and symbol (b) [7]

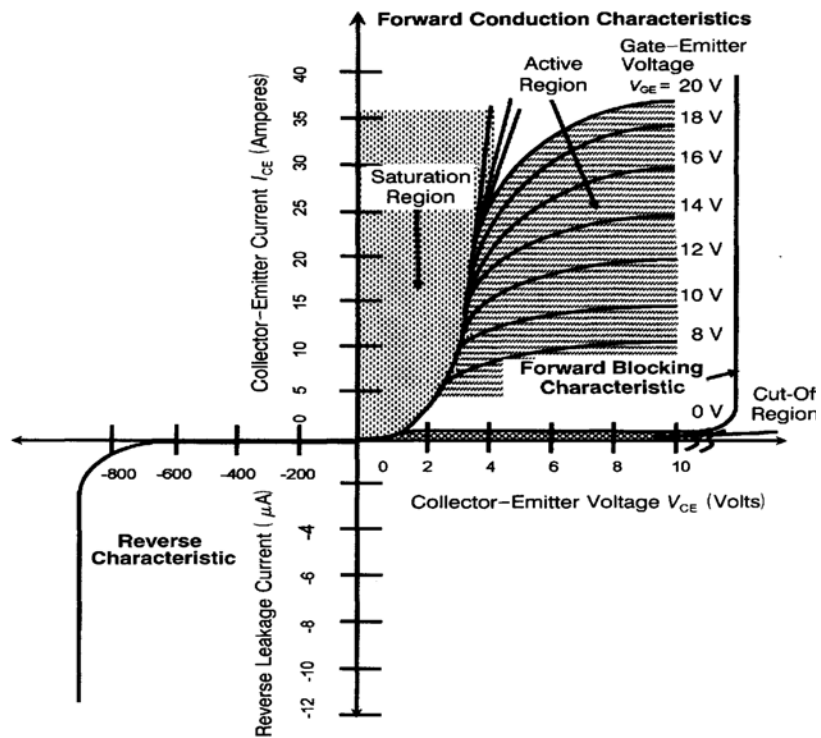


Fig. 4 Output current-voltage characteristic of IGBT [1]



Table 1 The IGBT characteristics vs. BJT & MOSFET

| Features            | BJT             | MOSFET          | IGBT     |
|---------------------|-----------------|-----------------|----------|
| Drive Method        | Current         | Voltage         | Voltage  |
| Drive Circuit       | Complex         | Simple          | Simple   |
| Input impedance     | Low             | High            | High     |
| Drive Power         | High            | Low             | Low      |
| Switching Speed     | Slow ( $\mu$ s) | Fast (ns)       | Moderate |
| Operating frequency | Low (<100 kHz)  | Wide (>200 kHz) | Moderate |
| S.O.A               | Narrow          | Wide            | Wide     |
| Saturation Voltage  | Low             | High            | Low      |

## 2.2 IGBT Turn-on and Turn-off

The IGBT turn-on is controlled by voltage rather than current, but the speed of turn-on increase with the magnitude of gate current. To turn on the IGBT, The input capacitance between gate and emitter is charged to a voltage ( $V_{GE}$ ) greater than the threshold voltage ( $V_{th}$ ). During turn-off the IGBT, the gate-emitter resistance ( $R_{GE}$ ) provides a path for the input gate-to-emitter capacitance to discharge. The  $R_{GE}$  can alter the IGBT turn-off time and so it is under the control of circuit designer. IGBT usually works as a switcher with a resistive load or an inductive load. In the forward testing the IGBT was working with an inductive load, consequently, the theoretical switching behavior of IGBT will based on the case of inductive load which is shown in Fig. 5.

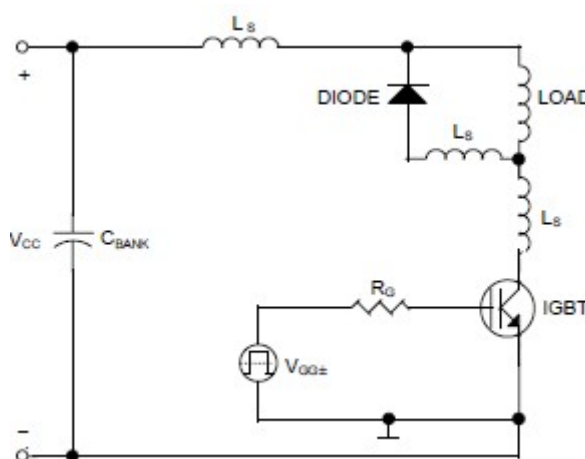


Fig. 5 Diode-clamped inductive load circuit [4]

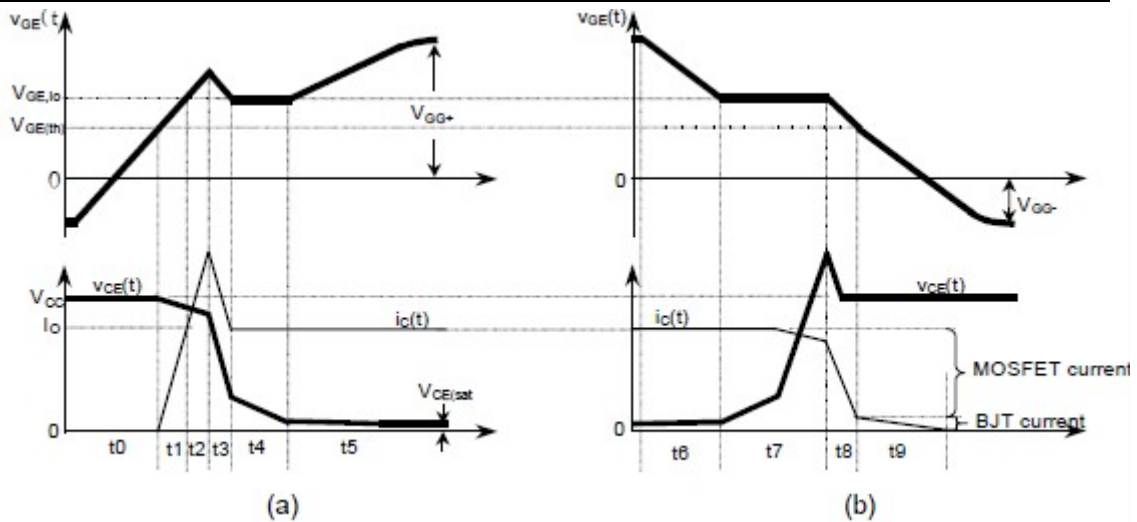


Fig. 6 The waveforms of IGBT turn-on (a) and turn-off (b) process [8]

The waveforms of gate voltage ( $V_G$ ), Collector-Emitter ( $V_{CE}$ ) voltage and collector current ( $I_C$ ) at the IGBT turn-on process as shown in Fig. 6 (a) and at the IGBT turn-off process as shown in Fig. 6 (b). This process can be sum up as following steps [2-3, 9]:

(1)  $t_0$  section:  $V_G$  rises to  $V_{G(th)}$  while  $I_G$  charges the parasitic input capacitance  $C_{GE}$  and  $C_{GC}$ . The  $V_{CE}$  increase pattern is shown to be linear, but it is actually an exponential curve with time  $R_G(C_{GE} + C_{GE, miller})$ . The  $V_{CE}$  is maintained at the  $V_{CC}$  value, and  $I_G$  remains at zero and most of the turn-on delay falls under this section.

(2)  $t_1$  section:  $C_{GE}$  continues to increase exponentially passes  $V_{G(th)}$ . As  $V_G$  increases,  $I_C$  begins to increase to reach the full load current ( $I_0$ ). In the  $t_1$  and  $t_2$  section,  $V_{CE}$  appears to be shaved off than  $V_{CC}$ . This is due to the inductive voltage ( $V_{L_\sigma} = L_\sigma \cdot di_c / dt$ ) which produced by stray inductor ( $L_\sigma$ ).

(3)  $t_2, t_3$  sections: The reverse recovery current of the freewheeling diode is added to  $i_c$  caused the overshoot. Meanwhile, the FWD reverses recovery voltage increases, and  $V_{CE}$  decreases. It is worth to mention that the decrease speed of  $V_{CE}$  depend on  $C_{GC}$  and  $C_{GC}$  also is the function of  $V_{CE}$ . That is why  $dV_{CE} / dt$  is large at  $t_2$  section.



Reverse recovery process of the diode stops at the end of  $t_3$  section.

(4)  $t_4$  section:  $C_{GC}$  charging,  $V_{GE}$  maintains  $V_{GE,I_0}$ , and  $i_c$  maintains  $I_o$ . The  $V_{CE}$  falls at a rate of  $(V_{CG} - V_{GE,I_0}) / (R_G C_{GC})$ . Low  $V_{GE}$  value caused a large  $C_{GC}$  value and this slow discharging produce the voltage tail.

(5)  $t_5$  section:  $V_{GE}$  increases exponentially to  $V_{GG+}$  with a time constant  $R_G(C_{GE} + C_{GC,miller})$  where  $C_{GC,miller}$  is  $C_{GC}$  that rose form low  $V_{CE}$  value due to the Miller Effect.  $V_{CE}$  decreases to on-state voltage and becomes fully saturated. This is because the IGBT (PNP) transistor portion is slower than the MOSFET portion in crossing the active region to reach on-state as well as the effect from  $C_{GC,miller}$

(6)  $t_6$  section: This is turn-off delay time section.  $V_{GE}$  falls from  $V_{GG+}$  to  $V_{GE,I_0}$  with the same time constant as the (5).

(7)  $t_7$  section:  $V_{CE}$  increases at the rate of  $\frac{dV_{CE}}{dt} = \frac{V_{GE,I_0}}{C_{res} \cdot R_G}$  which can be controlled with  $R_G$ .

(8)  $t_8$  section:  $V_{CE}$  maintains the value of  $V_{CC}$ , and  $i_c$  decreases at the rate of  $\frac{di_c}{dt} = g_{fs} \cdot \frac{V_{GE,I_0}}{C_{IES} \cdot R_G}$  which also be controlled with  $R_G$ . There is an over-voltage

$V_{L_\sigma} = L_\sigma \cdot di_c / dt$  due to stray inductance, added to  $V_{CE}$  in  $t_7$  and  $t_8$  sections The MOSFET current disappears at  $t_8$ , which is the first of the two sections where  $i_c$  decreases.

(9)  $t_9$  section: Turn off the PNP transistor (BJT), as shown in Fig. 1, and tail current  $i_c$  disappears. It takes place due to the recombination of the minority carrier (hole), which has been injected into the N- drift region during the on-state. Due to the existence of this region, the switching characteristics of IGBT are inferior to that of power MOSFET.



## 2.3 FWD Performance

The FWD is primarily used to conduct the load current during IGBT turn-off. It must be noticed that in hard switching, turn-on losses increase as the recovery current rises and recovery time is prolonged. To minimize the turn-on losses and withstand surge voltage, a diode having fast, soft recovery characteristic is desirable. The diode with a snappy reverse characteristic and hence high recovery  $di/dt$  is problematic with transient voltage. Therefore, the turn-off current should be diverted through the FWD. When the IGBT is off, the current is carried by the FWD, and due to the conduction of FWD, the voltage across the load terminal is zero. The performance of snappy diode and fast diode is shown in Fig. 7. To improve the FWD performance, three important design techniques are often used: (1) emitter efficiency control, (2) axial lifetime killing, and (3) deep diffusion control. More information related to those techniques can refer to [1, 10-14], and some failure mechanisms related to the FWD will be introduced at chapter 4, more details have been given at the summer job report [15].

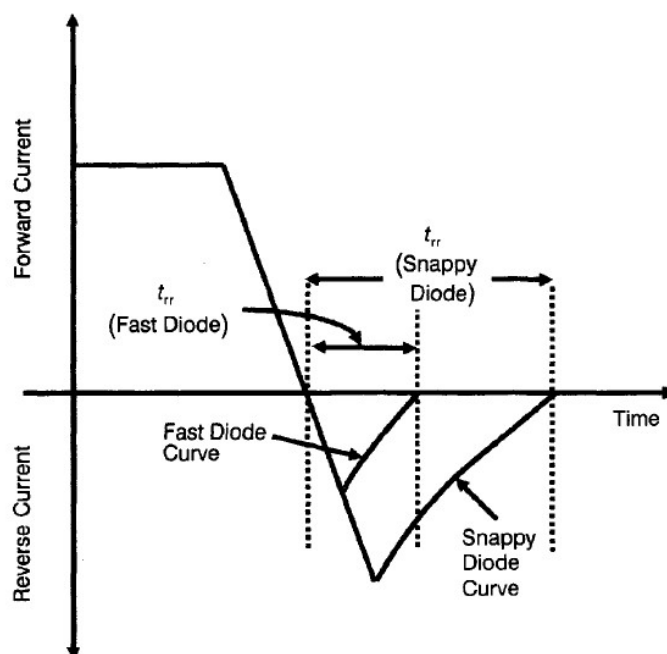


Fig. 7 Reverse recovery waveforms of snappy and fast diodes[1]



---

*This page intentionally left blank*





### **3. State-of-the-art Technology of IGBT Module**

With the development of new technique, more and more new IGBT concepts appeared. The performance also greatly improved. Present IGBT modules are divided into two categories: (a) the conventional module package derived from low-power technology and (b) the new press-pack IGBT based on the classical high-power diode or thyristor technology [1]. This chapter would briefly compare some of the new IGBT concepts like SPT-, FS- and SPT+- IGBT which developed by ABB<sup>TM</sup> with the traditional IGBT concepts like PT-, NPT- IGBT. The difference between Planar- and Trench- IGBT technology [16-18], the advantages of press-pack IGBT module [19-23], and the application of promising semiconductor material SiC [24-29] also covered at this chapter.

#### **3.1 Planar- vs. Trench- IGBT**

The IGBT's gate structure has an important influence on its performance. Iwamoto H., et al. in [30] have evaluated and compared the performance of Planar- and Trench- IGBT under hard- and soft- switching found that trench- IGBT maintains clear advantages: (1) Enhanced electron injection effect, (2) Reduced channel resistance i.e. improved conduction [31], (3) One dimension current flow, (4) No parasitic JFET which can avoid the current crowding occurs, (5) Reduced latch-up effect because the n+ source regions can be make smaller as they are self aligned to the trench, and (6) Better gate contact because the poly-silicon thickness is greater than in the planar case and the reduced gate resistance means the turn-on can be faster. However, a new developed planar- IGBT by ABB<sup>TM</sup> seems challenged this fact [32] . The planar- and trench- IGBT structure are shown in Fig. 8. More details can be found at the semester project report [33].

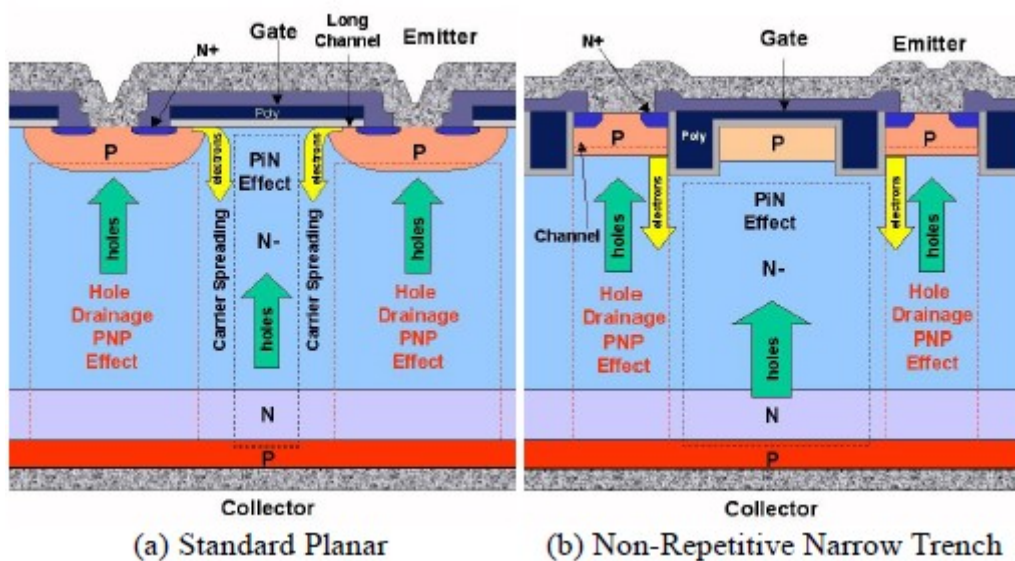


Fig. 8 Planar- (a) and Trench- (b) structures of IGBT [32]

### 3.2 PT-, NPT-, FS-, vs. SPT- IGBT

The traditional PT- as shown in Fig. 9.a , and NPT- IGBT as shown in Fig. 9.b concept has introduced at [3, 33], thus will not pleonastic cover at here. Several manufactures like ABB<sup>TM</sup>, Semikron<sup>TM</sup>, and Westcode<sup>TM</sup> have developed technologies which located between PT and NPT like FS-, and SPT- IGBT. The FS-technology is based on NPT technology. The field stop zone is injected on the shallow p-emitter as shown in Fig. 9.c, and the SPT-technology basically consists of a low-doped n-base and SPT [16-17, 19, 32, 34-36] n-buffer as shown in Fig. 9.d, and makes the switching behavior of normal PT devices softer. In other words,  $di/dt$  during switching (especially turnoff) becomes lower than that of a PT device. Anyway, FS- and SPT- IGBT more or less have the same structure and performance; Udrea F. [37] has investigated the new technology elaborately.

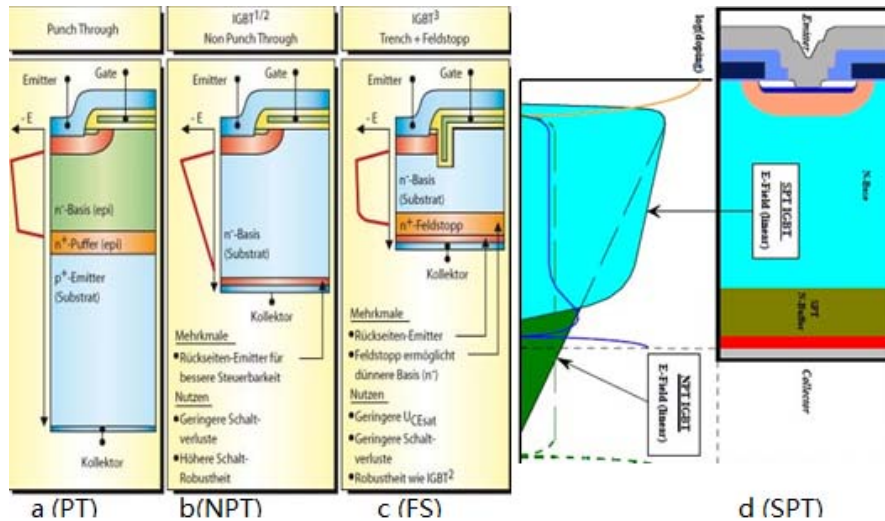


Fig. 9 Chip structure of different IGBT technologies and field distribution [34, 36]

### 3.3 SPT<sup>+</sup> IGBT

The newly developed SPT<sup>+</sup> IGBT from ABB<sup>TM</sup> [16-17, 32, 34] offers significantly lower on-state losses while still maintaining low turn-off losses, and achieve extreme ruggedness during switching and under short circuit conditions and offers the same low EMI levels as for the current SPT platform. Fig. 10 shows a cross-section of the SPT<sup>+</sup> diode. The new technology utilizes a double local lifetime-control technique to optimize the shape of the stored electron-hole plasma. Due to the improved plasma distribution, the overall energy losses could be reduced, while maintaining the soft recovery characteristics of the standard SPT diode technology.

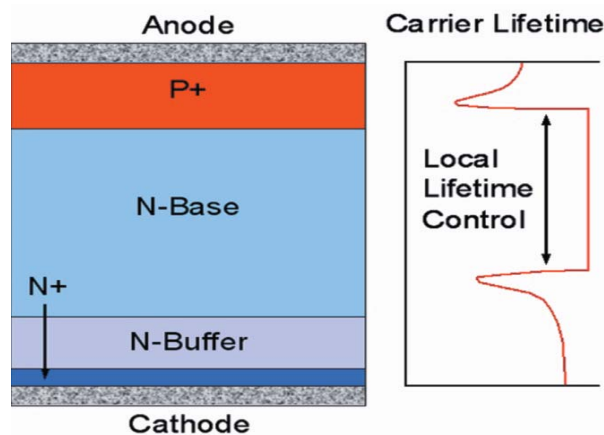


Fig. 10 SPT<sup>+</sup> diode technology [16]



---

### 3.4 Press-Pack IGBT Module vs. Standard IGBT Module

Press-pack encapsulation IGBT offers several advantages over the traditional wire bond package, as point out in Table 2. For press-pack IGBT, the electrical contact is established by pressing the IGBT chips between two high-planarity conducting disks as shown in Fig. 11. An adequate stress relief layer is included to forebear the compression. The chips are housed in a compact both-side cooled hermetic, square flat-packaged ceramic structure is pressure contacts. Low inductance is achieved inside the package because of the absence of Al wire bonding. For compactness, the unused area in the assembly is minimized [1].

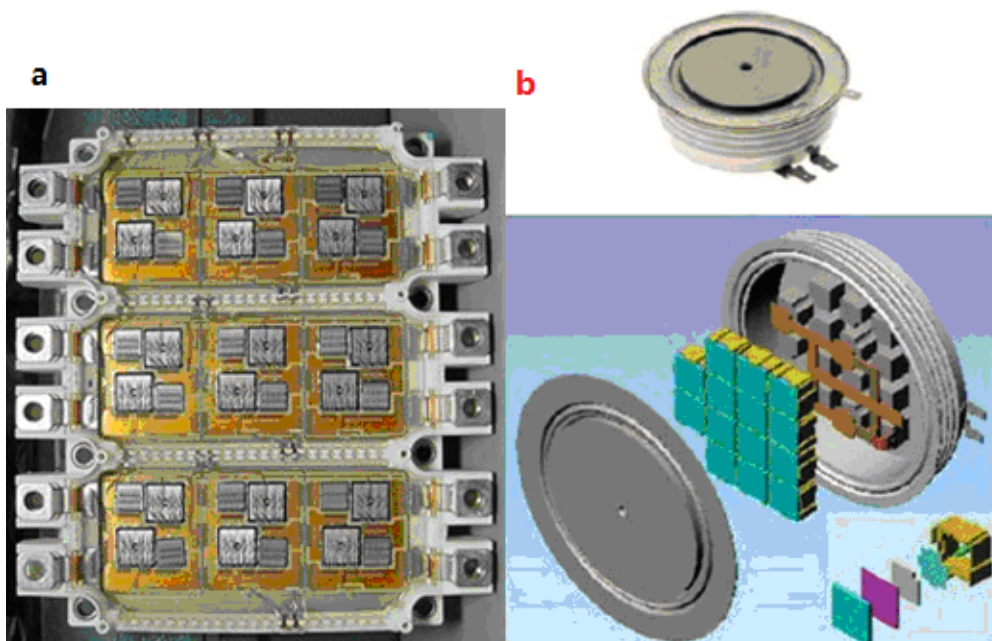


Fig. 11 Bond Package IGBT (a) and Press-pack IGBT (b) (Internet)

Table 2 Comparison of bond pack with press-pack IGBT module [1]

| Bond Package  | Press-pack Package  |
|---|---|
| High inductance   | Low inductance  |
| For good bonded joints, the wire should be small in diameter. The thin wire is also unable to conduct the heat away. So, the wire introduces significant electrical and thermal resistance. | Absence of wires overcomes this limitation                            |
| Nonhermetic and one-side cooling structure  | Hermetic and both-side cooling structure                              |
| The base plate is completely isolated making the cooling simple and lowering the cost   | Insulation of the IGBT and cooling are necessary, increasing the cost |
| Poor power cycling capability   | Superior power cycling ability  |
| Possibility of explosion during failure   | Explosions are avoided  |
| Less reliable   | More reliable   |

### 3.5 SiC Overview

Silicon Carbide (SiC) has many favorable properties making it interesting for high temperature, high frequency and high-power applications. More specifically,



these properties are: wide band gap, high thermal conductivity (better than for example, copper at room temperature), high breakdown electric field strength (approximately 10 times that of Si), one magnitude order higher saturation drift velocity than Si and high thermal stability and chemical inertness [38]. While the smaller on-resistance and faster switching of SiC helps minimize energy loss and heat generation. The higher thermal conductivity of SiC enables more efficient removal of waste heat energy from the active device. Because heat energy radiation efficiency increases greatly with increasing temperature difference between the device and the cooling ambient, operating SiC at high junction temperatures permits much more efficient cooling to take place, so that heat sinks and other device-cooling hardware (i.e., fan cooling, liquid cooling, air conditioning, etc.) typically needed to keep high power devices from overheating can be made much smaller or even eliminated [39-40].

#### A. SiC Diodes

Power diodes made with SiC are expected to show great performance advantage as compared to those made with other semiconductors. A high breakdown electric field allows the design of SiC power diodes with thinner and higher voltage blocking layers. The 4H polytypic of SiC diode is particularly suited for vertical power devices because of higher radiation hardness. The thermal conductivity of SiC is about three times higher than Si. The PiN diodes made using conventional semiconductor materials are restricted to less than 50 kHz and 125 °C. The main features of 4H-SiC PiN diodes are: (1) a voltage drop in the on state comparable to stacked Si diodes at sufficiently high current densities; (2) switching speeds that are at least 30 times faster than any of their Si counterparts because of the use of thinner epitaxial layer; and (3) good high-temperature operating characteristics [27]. SiC Schottky diode, the commercial available power device, has achieved great progress those years and the advantages compare to Si PiN diode is shown in Table 3



Table 3 expect performance for high voltage SiC Schottky diode and Si PiN diode[41]

| Static Characteristics      | SiC Schottky Diode          | Si PiN diode                |
|-----------------------------|-----------------------------|-----------------------------|
| On state Voltage @ 25 °C    | 1 V @ 250 A/cm <sup>2</sup> | 2 V @ 100 A/cm <sup>2</sup> |
| Temperature coefficient     | +Ve                         | +Ve or -Ve                  |
| Leakage current @ 125 °C    | 10 mA/cm <sup>2</sup>       | 0.5 mA/cm <sup>2</sup>      |
| Max Junction Temp.          | 250 °C                      | 150 °C                      |
| Dynamic Characteristics     | SiC Schottky Diode          | Si PIN diode                |
| Reverse Recovery loss       | Small capacitive effect     | High                        |
| IGBT switching losses       | Low                         | High                        |
| EMI                         | Low                         | High@ high di/dt            |
| Stray inductance dependence | Low                         | High                        |
| Forward current dependence  | Low                         | High                        |
| Temperature Dependence      | None                        | High                        |
| Dynamic avalanching         | None                        | Yes at high di/dt           |
| Snappy recovery             | None                        | Yes at high di/dt           |

## B. SiC- IGBT

The availability of SiC IGBT will be delayed because of technical problems, i.e. function density limited and high cost, as previously described by Brown [42]. However some testing has shown that replace the FWD by SiC Schottky diode can greatly improve the IGBT module performance. In addition to providing low switching losses, low voltage and current stress; SiC devices can operate at much higher temperatures. The low switching losses and reverse recovery current will allow power converters to operate with high efficiency and low EMI [43]. Simulation experiment results by J. Wang and BW. Williams [29] also shows that 4H-SiC IGBT exhibit lower on-state voltages at typical operating current and slightly higher on-state voltage at higher current level [29, 41]. This reduces the on-state power losses at typical operating current and ensures current sharing between parallel connected IGBTs [1, 28-29].



---

### C. Si-SiC inverter and Full-SiC inverter

Although there is no SiC inverter commercially available now, there are some experiments have proved the advantages of SiC inverters. Schafmeister F. [44] has evaluated the performance of SiC-JFET three-phase inverter shows that SiC JFET inverters have relatively high efficiency at all powers, switching frequency, and temperature ranges. Compared to Si inverters, the advantage is more obvious at high frequency and high temperature. Motion control, solar energy, wind generation, and vehicle systems might benefit from these SiC inverters in the near future [45]. Replacing Si PiN diodes with their SiC Schottky diode counterparts will decrease the losses of an inverter considerably because the high reverse-recovery losses of Si PiN diodes are negligible at SiC Schottky diodes [45-46]. Thus full-SiC inverter will be an attractive field to explore for researchers and industry applications.





---

## **4. Failure Mechanisms Summary**

Failure mechanisms are physical, chemical, or other processes resulting into a failure. For practical purposes they can be divided in two categories. The first includes mechanisms which result from poorly controlled or poorly designed manufacturing processes. The second category includes those failures, which occur during the normal operation of the device [47-48]. As there is no any literature study involved in the press-pack IGBT (already commercially available), this chapter will just summarize the main failure mechanisms of wire bond IGBT but not cover too much details because those faults and related countermeasures have been discussed in the summer job report [15] and semester project report [33].

### **4.1 Package-related Failure Mechanisms**

Multichip modules for high-power IGBT devices are complex multilayered structures consisting of different materials, which have to provide a good mechanical stability, good electrical insulation properties, and good thermal conduction capabilities. The IGBT and diode chips are soldered on AlN or Al<sub>2</sub>O<sub>3</sub> ceramic substrates (Direct Copper Bonding or Active Metal Braze technologies), which provide high voltage insulation. The substrates are then soldered to a copper or AlSiC base plate, acting as a mechanical support and providing a thermal interface to the cooler. The modules are encapsulated in plastic housings and filled with Silicone gel. The crosses section as shown in Fig. 12 and Fig. 13 [47, 49-51].

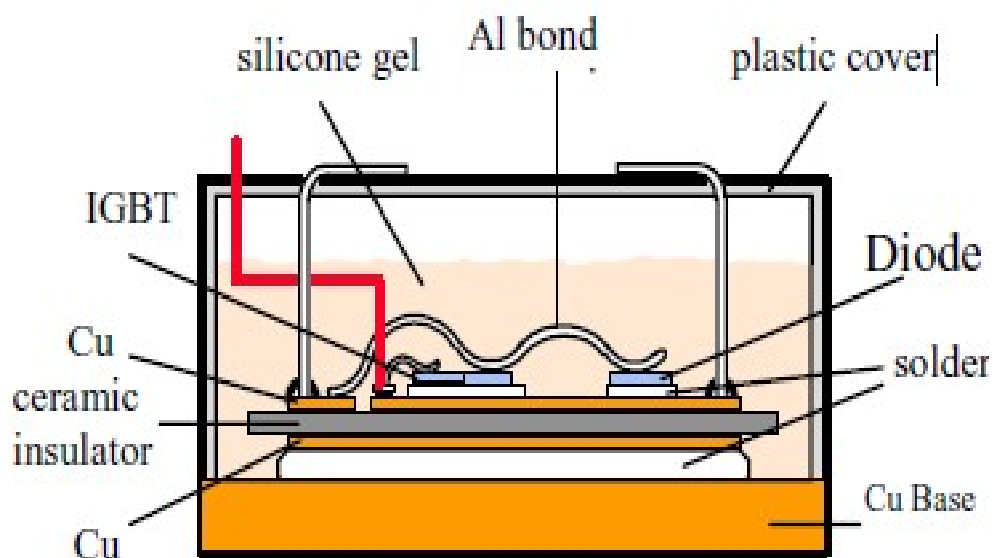


Fig. 12 Cross sectional of a classical IGBT module [48]



Fig. 13 IXYS IGBT inside (without gel)

Due to the different thermal expansion coefficient (CTE) between different materials, wire bonds lift off as shown in Fig. 14 is the most common fault, the mismatch CTE between ceramic and the base-plate also cause the solder interface fatigue as shown in Fig. 15. The faults like fatigue and creep interaction of power terminals as shown in Fig. 16 a, gel related faults [52-53], partial discharge as shown in Fig. 16 b and interconnection corrosion as shown in Fig. 17 are also very common at stressful environment or testing conditions like thermal cycling.

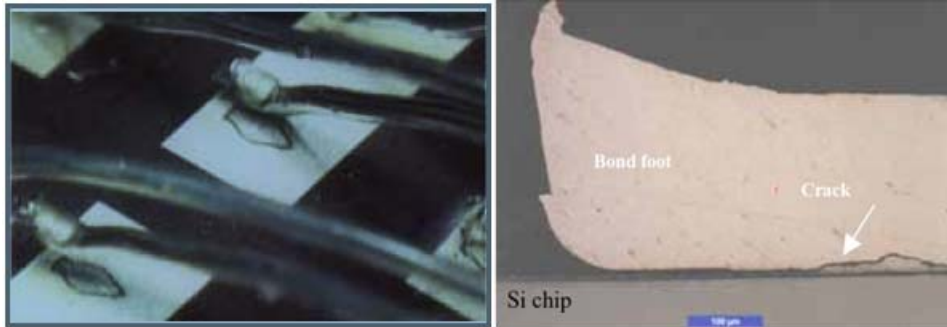


Fig. 14 Wire bonds lift-off (a) and wire bond after a crack has propagated under the bond foot (b) [47]

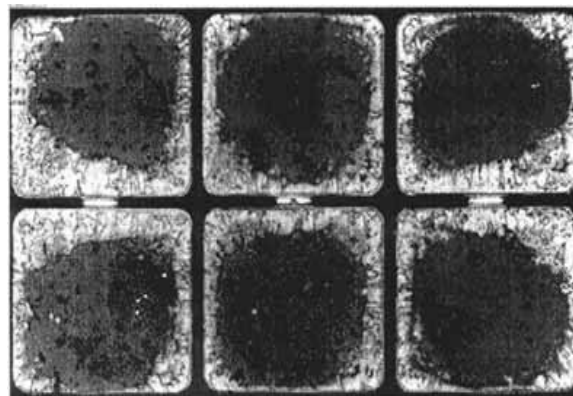


Fig. 15 Delimitation of the solder (white areas) due to thermal fatigue [47]

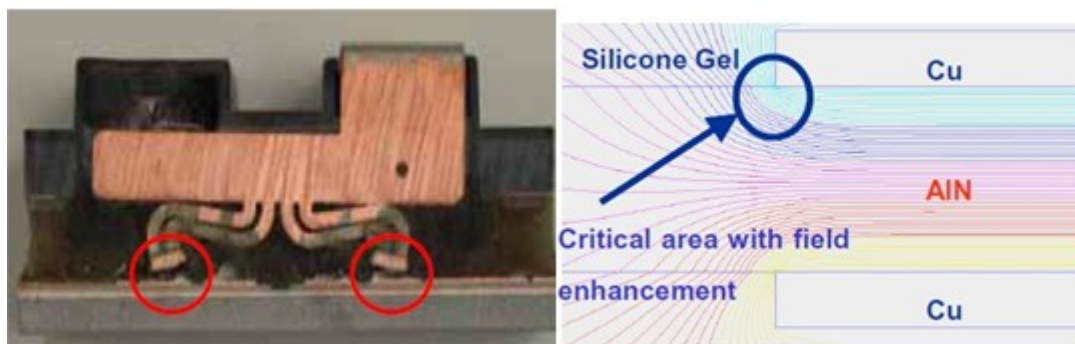


Fig. 16 a. Pull-out of the terminal feet on the ceramic substrate b. E-field simulation of AlN substrate [47]

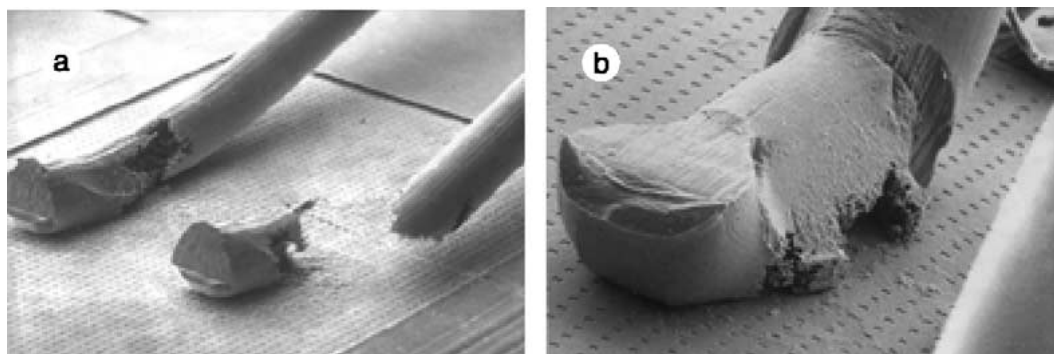


Fig. 17 Rupture of emitter bond wire due to stress corrosion (a), Enlarged picture (b) [52]



## 4.2 Failure Mechanisms during Application

Fault operation or under stressful operation condition can result in faults. Faults caused by short circuit or switching under clamped inductive is very common in real application, the semester project report [33] and summer job report [15] have discussed them deeply. Dynamic avalanche occurs on IGBT [54] and/or FWD [55-56] also can destroy IGBT module if it out of control. In addition, faults caused by cosmic ray and irradiation are not just very important especially in the outer space applications, but also in deep ocean, high temperature, and high power applications. The factor is shown in following formula. However, it did not received enough attention [57].

$$\lambda(V_{DC}, T_{vj}, h) = C_3 \cdot \exp\left(\frac{C_2}{C_1 - V_{DC}}\right) \cdot \exp\left(\frac{25 - T_{vj}}{47.6}\right) \cdot \left(\frac{1 - \left(1 - \frac{h}{44300}\right)^{5.26}}{0.143}\right)$$



## 5. Experimental Standards and Principles

This chapter will focus on the important parameter definitions according to the IEC 60747-9 International Standard [7], and the industrial standard measurement methods which were used in this project. Three different testing principles, that is double pulse switch testing, repetitive switch testing, and power cycling testing, were introduced in this chapter.

### 5.1 Parameter Definitions

The parameters used at the report and measurement were refer to the IEC 60747-9 standard. The definition of turn-on time is the time between gate voltage reaches 10 % of its nominal value and the collector current rise up to 90 % of its desired value. That includes the delay time and rise time. While turn-off time is the time interval between gate voltage decrease to 90 % and the collector current fall down to 10 %. This is also includes turn-off delay time and fall time. Both of the definitions are base on the IEC 60747-9 standard [7]. Some important parameters for this project such as switching time, switching power loss as shown in Table 4, and Fig. 18 and Fig. 19 make it straight. and the full list can refer to [7]. As the power and energy can not be obtained directly form the scope, but the power can be calculated by

$$P = V(t) \times I(t) \quad (1)$$

And the turn-on (turn-off) energy is the energy dissipated inside the IGBT during the turn-on (turn-off) of a single collector current pulse which can be calculated by

$$E_{on} = \int_{t_{on}} V(t) \times I(t) dt \quad (2.1)$$

and

$$E_{off} = \int_{t_{off}} V(t) \times I(t) dt + \int_{t_z} P_{tail} dt \quad (2.2)$$

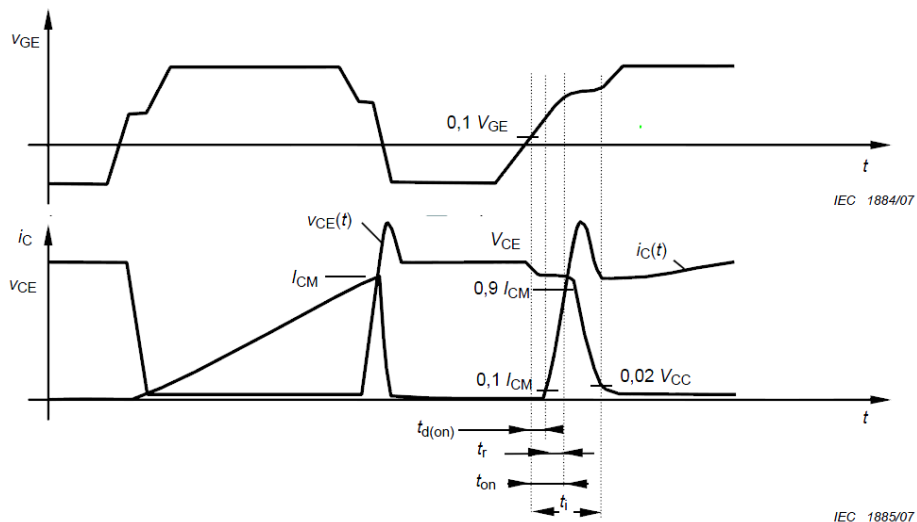


Fig. 18 Waveforms during turn-on times [7]

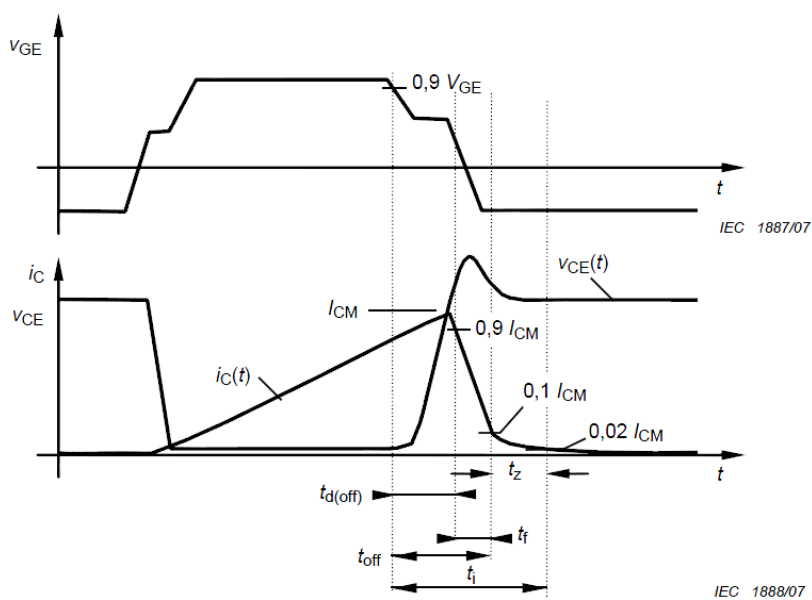


Fig. 19 Waveforms during turn-off times [7]



Table 4: Important Parameters Definition

| Term                | Abbr.     | Definition  |
|---------------------|-----------|---|
| Turn-on delay time  | $t_d$     | time interval between the beginning of a voltage pulse across the input terminals which switches the IGBT from the off-state to the on-state and the beginning of the rise of the collector current                                       |
| Rise time           | $t_r$     | time interval between the instants at which the rise of the collector current reaches specified lower and upper limits, respectively, when the IGBT is being switched from the off-state to the on-state                                  |
| Turn-on time        | $t_{on}$  | sum of the turn-on delay time and the rise time   |
| Turn-off delay time | $t_s$     | time interval between the end of the voltage pulse across the input terminals which has held the IGBT in its on-state and the beginning of the fall of the collector current when the IGBT is switched from the on-state to the off-state |
| Fall time           | $t_f$     | time interval between the instants at which the fall of the collector current reaches specified upper and lower limits, respectively, when the IGBT is switched from the on-state to the off-state  |
| Turn-off time       | $t_{off}$ | sum of the turn-off delay time and the fall time  |
| Tail time           | $t_z$     | time interval from the end of the turn-off time to the instant at which the collector current has fallen to 2 % or lower specified value  |
| Turn-on energy      | $E_{on}$  | energy dissipated inside the IGBT during the turn-on of a single collector current pulse  |
| Turn-off energy     | $E_{off}$ | energy dissipated inside the IGBT during the turn-off time plus the tail time of a single collector current pulse   |

## 5.2 Testing Standard

Investigating the reliability and failure mechanisms of power electronic component (IGBT), experiment should be conducted under much stressful situation such as high temperature, short circuit and vibration. Power cycling and thermal cycling as the strongest challenge in respect to high junction temperatures often employed to evaluate the stability and investigate the failure mechanisms [58-60] is shown Table 5.



Table 5 Stressful testing standard [61]

| Name                       | Condition   | Standard                        |
|----------------------------|---|---------------------------------|
| Thermal Cycling (Infineon) | External heating and cooling<br>$2\text{min} < t_{\text{cycl}} < 6\text{min}$ ; $\Delta T_c = 80\text{K}$ ,<br>$T_{\text{min}} = 25^\circ\text{C}$<br>High power standard: 2000 cycles<br>Medium power: 5000 cycles | IEC<br>60747-2/6<br>IEC 60747-9 |
| Thermal Cycling (Semikron) | external heating and cooling<br>$t_{\text{stgmin}} - t_{\text{stgmax}} = 100\text{cycles}$<br>conventional device (IGBT, diode)<br>modules: 25 cycles   | IEC<br>60068-2-14               |
| Power Cycling (Infineon)   | internal heating and external cooling<br>$0.5 < t_{\text{cyc}} < 10\text{sec}$<br>$\Delta T_j = 60\text{K}$ , $T_{j\text{max}} = 125^\circ\text{C}$ 130,000 cycles  | IEC 60747-9                     |
| Power Cycling (Semikron)   | internal heating and extremal cooling<br>$\Delta T_j = 100\text{K}$ , 20000 cycles  | IEC 60747-9                     |

### 5.3 Double Pulse Switch Testing

Double pulse switch testing [62] (DPS) as shown in Fig. 20 is a standard and efficient method to investigate the switching energies, turn-on and turn-off power loss, turn-on and turn-off time, and conduction loss of power electronic devices (transistor and FWD) at different voltage and current levels. The gate drive circuit is attached to transistors gate, and a double-pulse is applied. The two pulses are composed by one long pulse and followed by a shorter pulse. This allows for turning on and turning off at full current i.e. 400 A in this case. The typical current and voltage waveforms can be seen in Fig. 21.a - Fig. 21.e, the power dissipation and energy loss of transistor can be calculated by formula (1). Energy loss is the integral of power dissipation. The power and energy losses waveforms are shown in Fig. 21.f - Fig. 21.g . Because of the diode reverse recovery, practically observed transistor and diode current waveforms are shown in Fig. 21.h and Fig. 21.i. The more specific details can be found at semester project report [33].



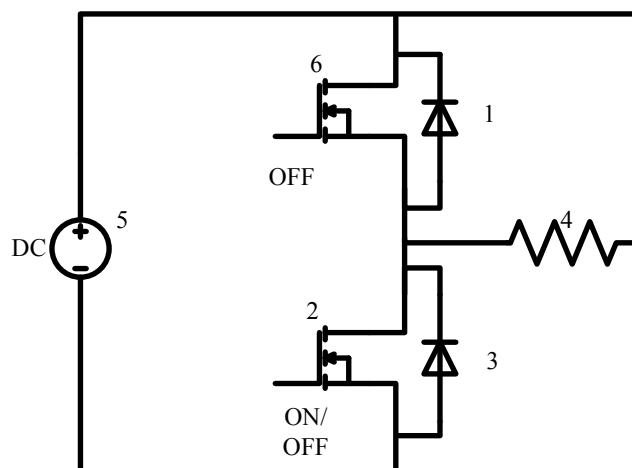


Fig. 20 Schematic of DPS testing circuit

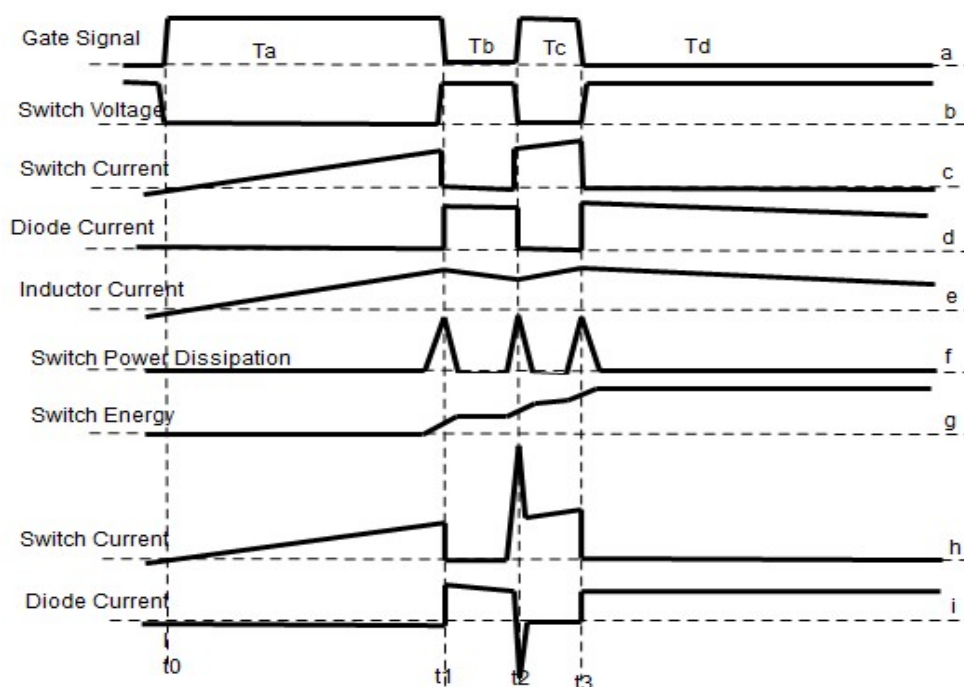


Fig. 21 Principle waveforms at DPS (a~i)

#### 5.4 Repetitive Switch Testing

The long term stability of IGBT modules can be experimentally under multiple switching tests. Two IGBT modules were used to build a full bridge inverter as shown in Fig. 22. The inverter was controlled by PWM switching scheme as shown in Fig. 23 with carrier signal switching at 10 kHz. The system was controlled to keep a constant junction temperature of IGBT chips i.e. 80 °C, for a certain power level (600 V and 105 A in this case). Ambient temperature was 20 °C and test lasted for 90 days.



Then the same double pulse switch testing method was employed to measure the IGBT switching performance, and compared the result with that previously taken. It is worth to mention that this test is not a life time test, but rather an evaluation of module performance in order to gain an optimized inverter design.

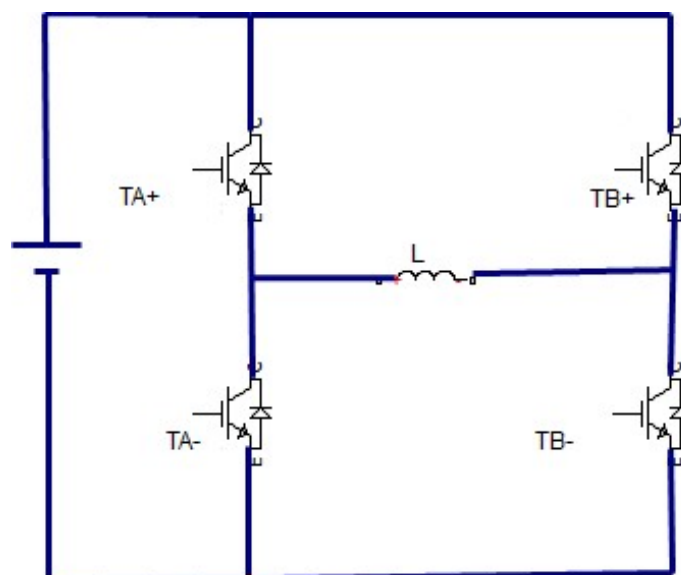


Fig. 22 Principle of repetitive switching test

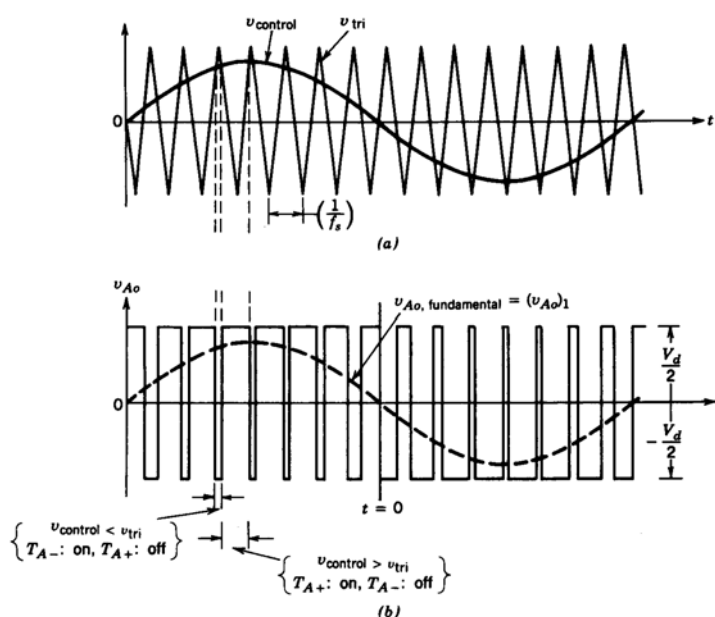


Fig. 23 Scheme of IGBT control signal [3]

## 5.5 Power Cycling Testing

To assess their reliability in these applications and lifetime, power cycling is the most suitable stress test, because the devices are operated in conditions similar to



those encountered in the field. In effect, the main cause of failure is the repetitive thermal cycling, which occurs when power cycling is applied. In spite of the fact that reliability is a key factor for the development of the IGBT technology, only few data are available and no standard test methods have been defined to evaluate the power cycling reliability and the effective impact of the various stress parameters is not yet established [60, 63-64]. The power dissipation losses of the IGBT chip are calculated by  $I_C$  and  $V_{CE}$ . Basically,  $I_C$  is fixed to the rated current value of the chip, and  $V_{CE}$  is adjusted to produce a specified temperature difference between  $T_{jmax}$  and  $T_{jmin}$  ( $\Delta T_j$ ) as shown in Fig. 24.b, and the scheme of setup is shown in Fig. 24.a.

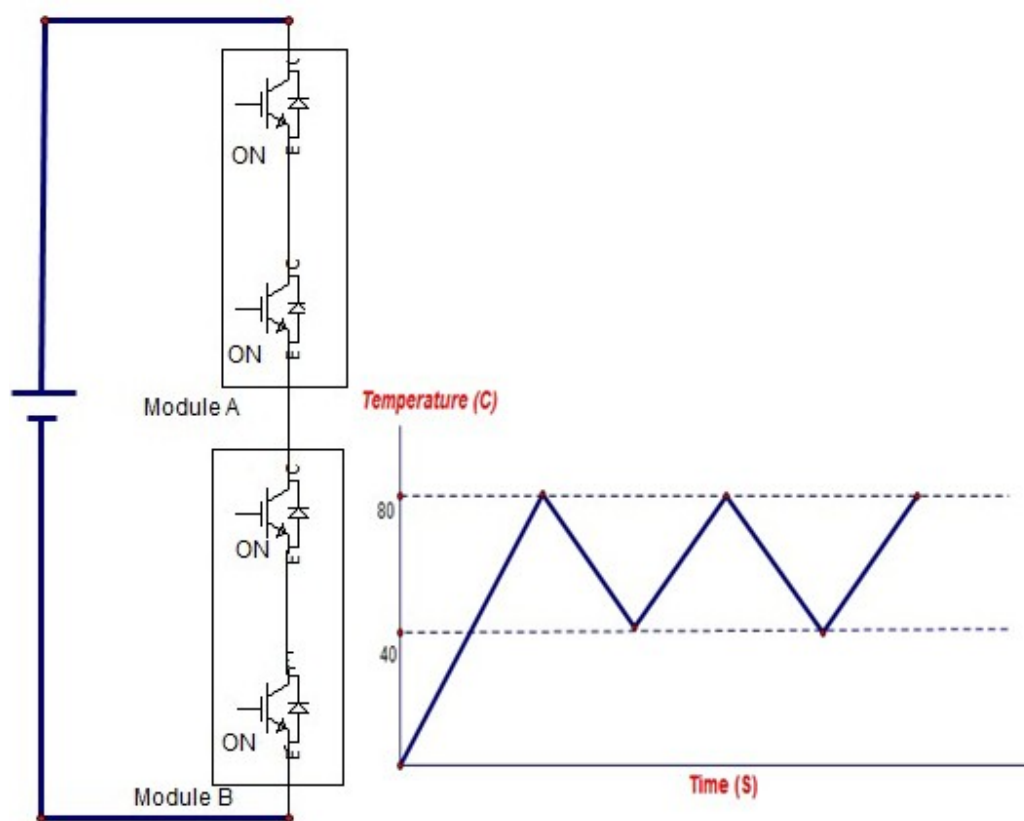


Fig. 24 Scheme of power cycling set and working temperature waveform



*This page intentionally left blank*



## 6. Setup and Measurement Description

This chapter first described two type commercial standard IGBT modules which have been tested at this project, then introduced some of the experimental instruments and mounting tips, finally present the structure and operation method of different setups.

### 6.1 Testing Object Description

Five standard IGBT modules were tested in this project and four of them were manufactured by IXYS, and one of them was produced by Tyco. The tested IXYS IGBT module in this experiment is IXYS<sup>TM</sup> MII 400-12E4 as shown in Fig. 25 which is half bridge structure. Each phase leg contains three NPT IGBT chips and three HiperFRED<sup>TM</sup> diode chips anti-parallel connected. The maximum collector-emitter voltage ( $V_{CE}$ ) and current rating is 1200 V and 420 A, respectively, where the maximum junction temperature defined by the datasheet is 125 °C for this standard module. The Tyco IGBT is V23990-P660-F02-PM as shown in Fig. 26 which is also half bridge structure. The maximum  $V_{CE}$  and  $I_C$  rating is 1200 V and 450 A, and the maximum junction temperature is 150 °C.

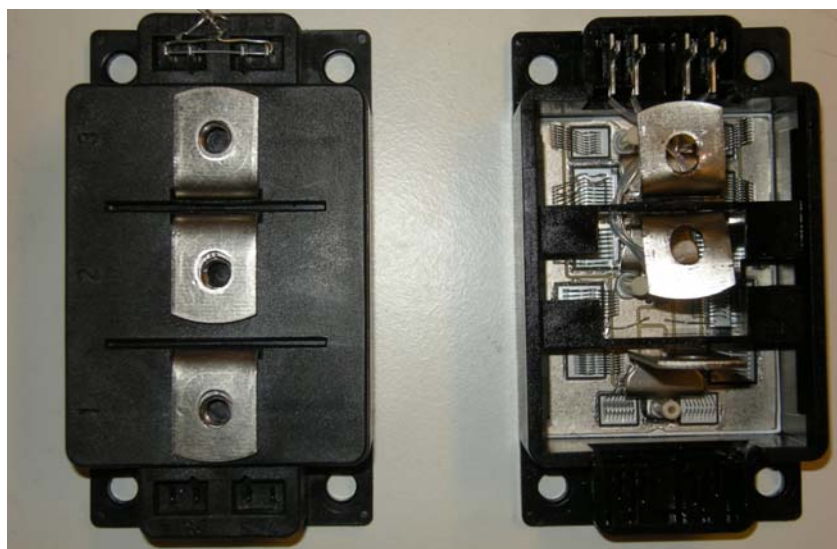


Fig. 25 IXYS MII400-12E4 IGBT

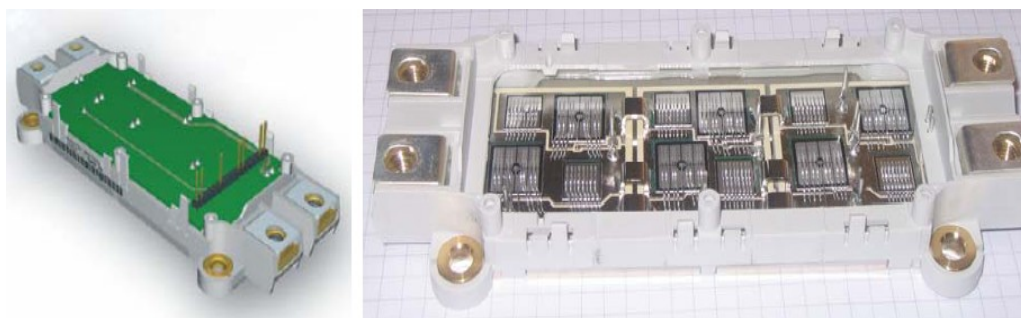


Fig. 26 Tyco IGBT module V23990-P669-F02 [65]

## 6.2 Measurements and Instruments

The main principle of testing is shown in Fig. 27, although different experiments have some different parts which will discuss later. For all of the experiments, the converter, transformer, voltage regulator are the same. In the experiments, the Agilent 74970A was used to acquiring the data of the temperature, voltage and current. Tektronix DPO4050 Digital Phopher Oscilloscope was used to collecting the testing waveforms and the data of waveform. For the sake of convenient comparison, keep the probe at the same channel and testing the same parameter as shown in Table 6.

Table 6 Probe position vs. channel

| Probe name    | Chanel | Parameter  | Comment                                   |
|---------------|--------|------------|---|
| DPO106-0481   | CH1    | $V_{FWD}$  | 50X                                       |
| DPO106-0485   | CH2    | $V_{IGBT}$ | 50X, current probe when measure $I_{FWD}$ |
| DPO106-0484   | CH3    | $V_G$      | 50X                                       |
| Current Probe | CH4    | $I_C$      | 20mA/div                                  |

Keep the switching waveform at same reference time for each test at the oscilloscope (ie. 200 ns/div and reference time is 600 ns for turn on waveform, and 400 ns/div and reference time fixed to 1.2  $\mu s$  for turn-off wave form). All of the data were recorded in excel which is easy to analysis and compare with different experiments.

At the starting of the experiments of repetitive switch and power cycling test,



some faults observed because of the bad thermal grease contacting as shown in Fig. 29 (a) result in the generated heat can not dissipate quickly. As high temperature is the most important reason to cause the IGBT faults, the thermal grease should cover the IGBT module base plant carefully. By trial and error, the method as shown in Fig. 29 (b), with strong vertical force and bit more thermal grease proves to be the best method. In addition, gate driver signal noise also may fail the measurement. Twist is around a coil as show in Fig. 30 is a good method to reduce it. This method applied to both repetitive switch and double pulse switch testing. In addition, stray inductance as shown in Fig. 28 is another important factor to influence the accuracy of the measurement. Moving the DC-capacitor close to the IGBT module and keeping cables as short as possible are effective methods to reduce the inductance [33].

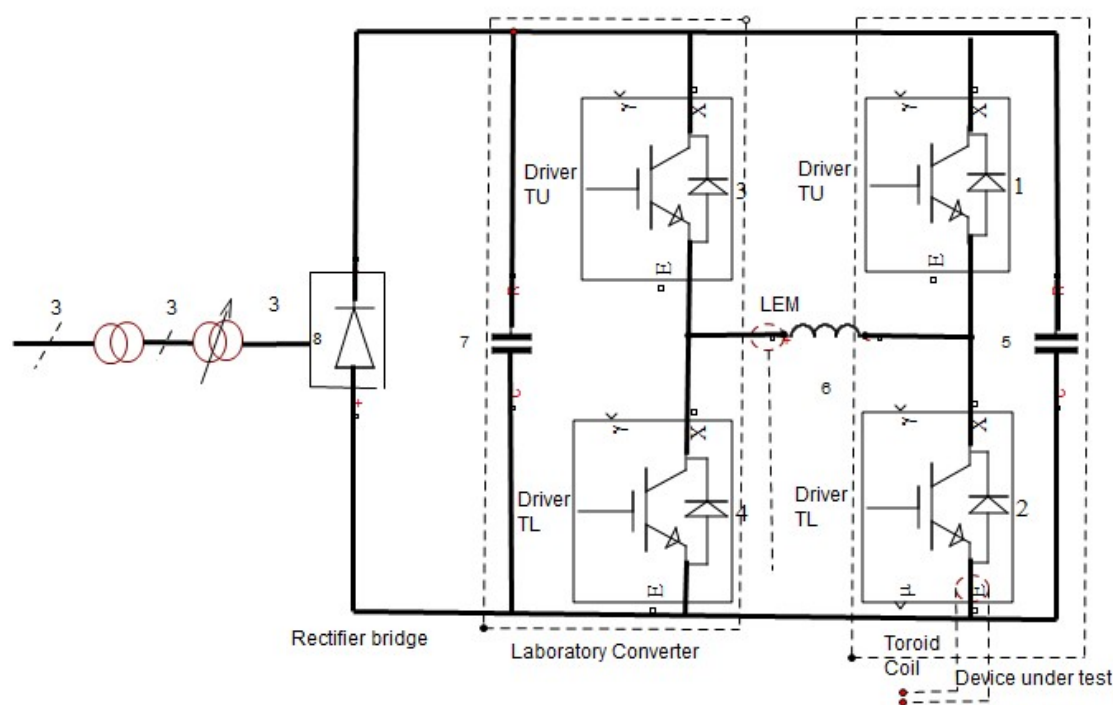


Fig. 27 Principle of measurement setup [66]

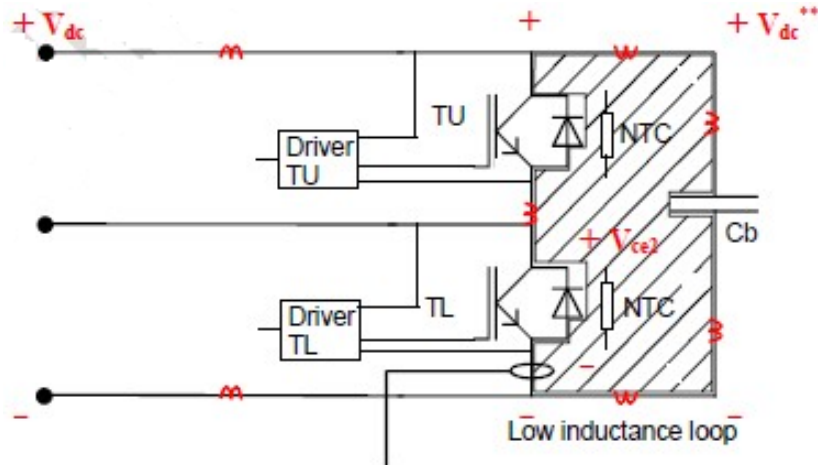


Fig. 28 Area which contributes to stray inductance in the loop between the capacitor and the transistor (From SINTEF Memo) [65]

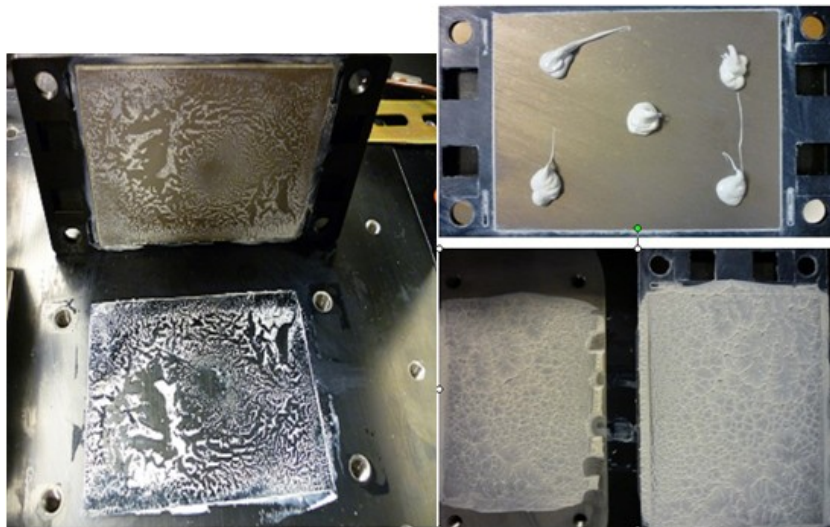


Fig. 29 The break IGBT footprint (a) and the best covering method (b)

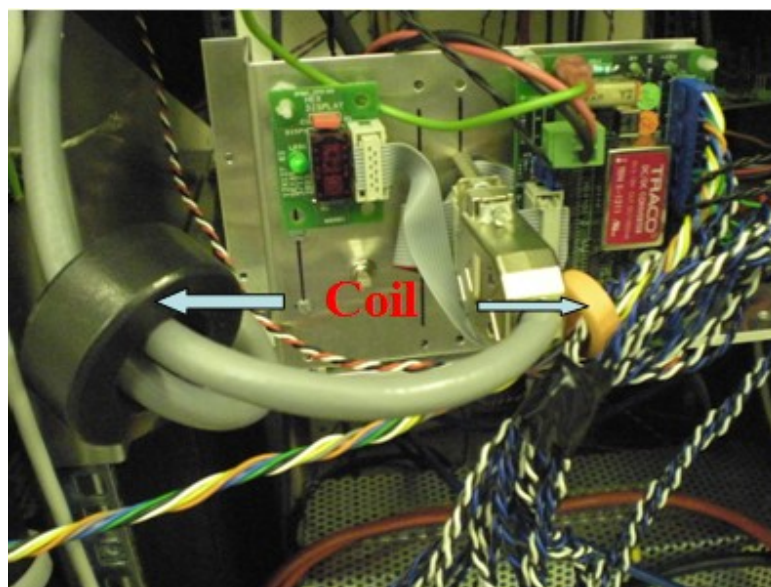


Fig. 30 Coil for filter noise





### 6.3 Double Pulse Switch Testing Setup

Base on the principle of double pulse switch testing (Chapter 5.3), and Fig. 27, two double pulse switch testing were built before and after stressful test conducted (ie. repetitive switch and power cycling test). The first setup as shown in Fig. 32 was used to investigate the dynamic performance of IGBT including the turn-on and turn-off energy losing, turn-on and turn-off time at different temperatures and power levels. The second setup was used to testing the dynamic performance of Tyco IGBT and IXYS IGBT after expose stressful condition for some time. Keeping two setups have the same external condition (ie. inductor, stray inductor, and converter) is very important for testing results comparison. Two new IGBT modules tested at the same voltage, current and juncture temperature on different setups repetitively. The comparison result is shown in Fig. 31 which proves that two setups have exactly the same performance. Both IXYS IGBT modules and Tyco IGBT module tested at different conditions is shown in Table 7. The gate resistance for the IXYS IGBT module test was  $4.125 \Omega$ , and Tyco IGBT module tested at three different gate resistances, that is  $2.2 \Omega$ ,  $3.9 \Omega$ , and  $4.7 \Omega$ . All of the double pulse switch testing, the first turn-off waveforms and second turn-on waveforms were captured and the gate voltage was  $\pm 15V$ .

Table 7 Available switching waveforms of IXYS and Tyco IGBT at 23 °C, 80 °C, 125 °C

| $V_{DC}/I_{CE}$ | 10 A   | 25 A   | 50 A   | 100 A  | 200 A  | 300 A  | 400 A  |
|-----------------|--------|--------|--------|--------|--------|--------|--------|
| 50 V            | ON/OFF |        |        |        |        |        | N/A    |
| 100 V           |        |        |        | ON/OFF | ON/OFF |        | N/A    |
| 200 V           |        |        | ON/OFF |        |        |        | ON/OFF |
| 400 V           |        |        |        | ON/OFF | ON/OFF |        | ON/OFF |
| 600 V           |        | ON/OFF | ON/OFF | ON/OFF | ON/OFF | ON/OFF | ON/OFF |

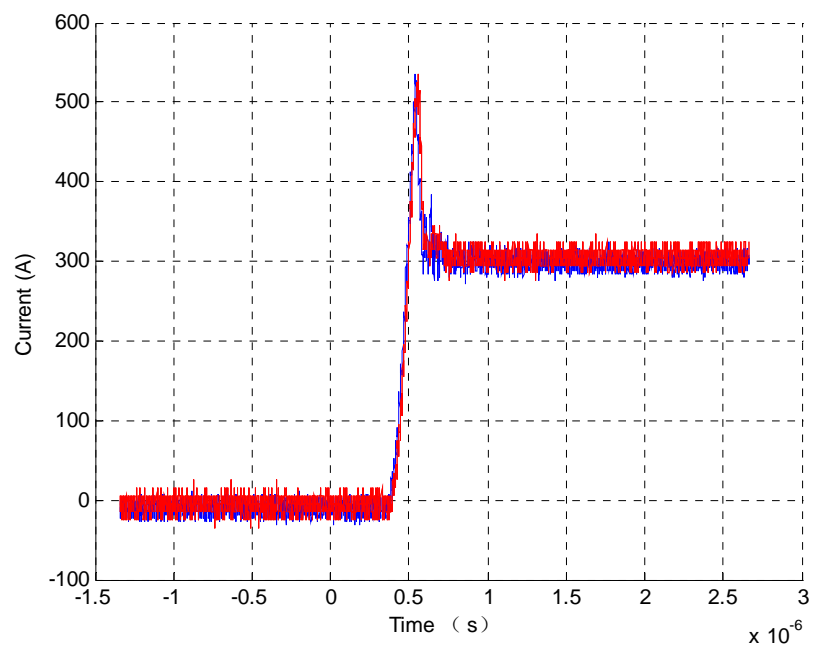


Fig. 31 Compare First setup (red) and Second setup (blue) at 600 V, 300 A, and 25 °C

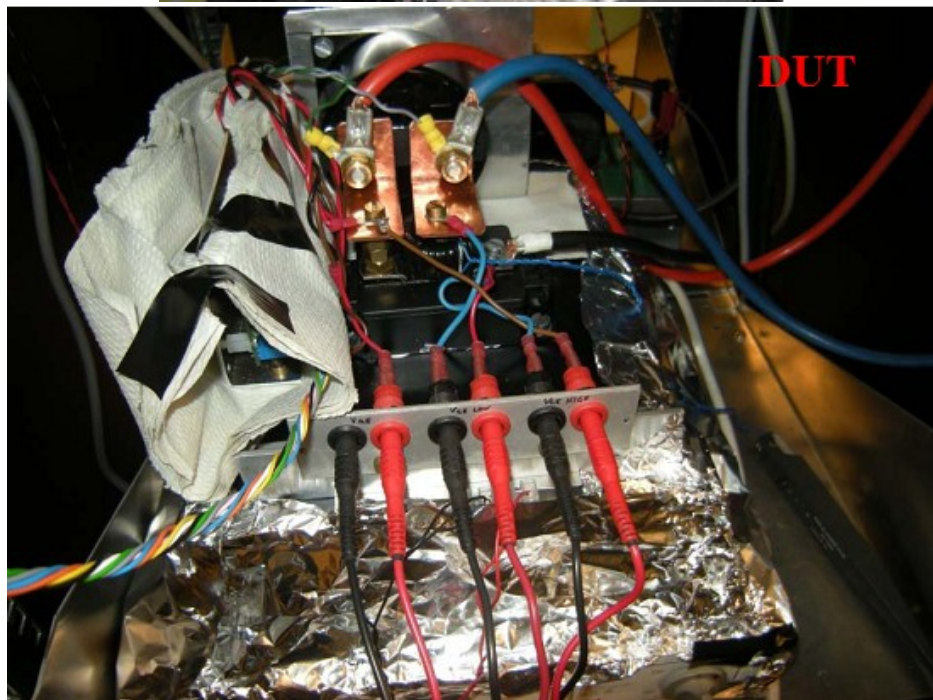
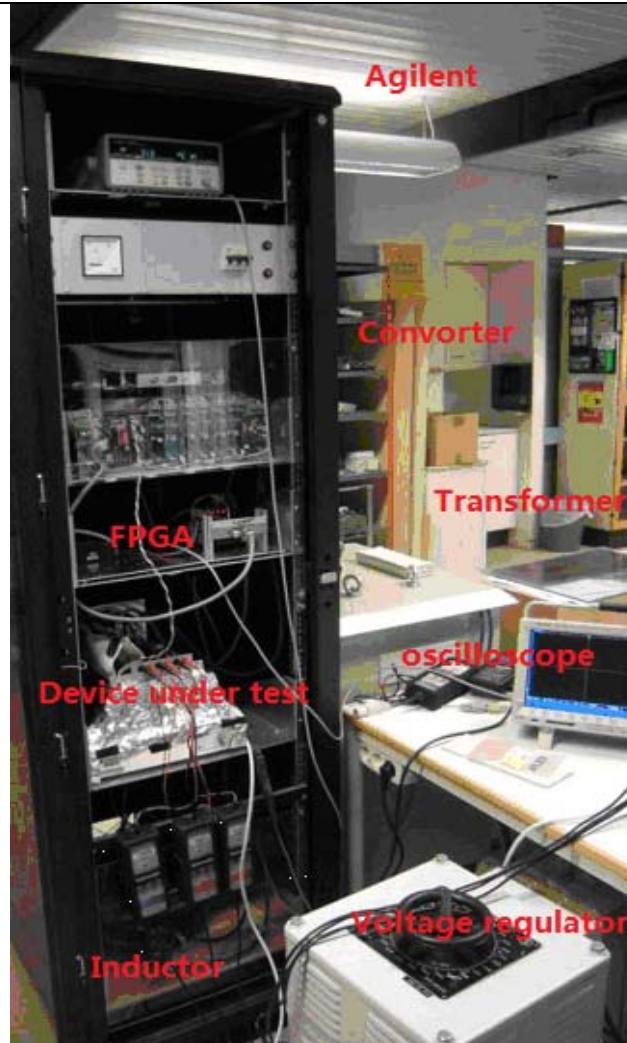


Fig. 32 Double Pulse Switch Testing setup



## 6.4 Repetitive Switch Testing Setup

Repetitive switch test setup was built up base on chapter 5.4 and chapter 6.2, as shown in Fig. 33. The signal generator produced 10 kHz square waveform signal to control the 50 Hz sinuous waveform (PWM control). The air conditioner keeps the ambient temperature at 20 °C. The heat sink can get the thermal balance temperature at 80 °C when set the voltage at 600 V and current at 105 A with fan cools it down constantly. The Agilent recorded different parameters as shown in Table 8, and the sampling frequency is 5 s. After three month repetitive switching, employing the double pulse switch testing again to measure the dynamic characteristics.

Table 8 Agilent channel and parameter

|           |                 |                  |                  |         |                 |                  |
|-----------|-----------------|------------------|------------------|---------|-----------------|------------------|
| Channel   | 101             | 102              | 103              | 104     | 106             | 107              |
| Parameter | IGBT A<br>Temp. | Diode A<br>Temp. | Ambient<br>Temp. | Current | IGBT B<br>Temp. | Diode B<br>Temp. |
| Channel   | 108             | 109              |                  | 105     | 110             | 111              |
| Parameter | 101<br>alarm 2  | 102<br>alarm 2   |                  | Voltage | 106<br>alarm 2  | 107<br>alarm 2   |

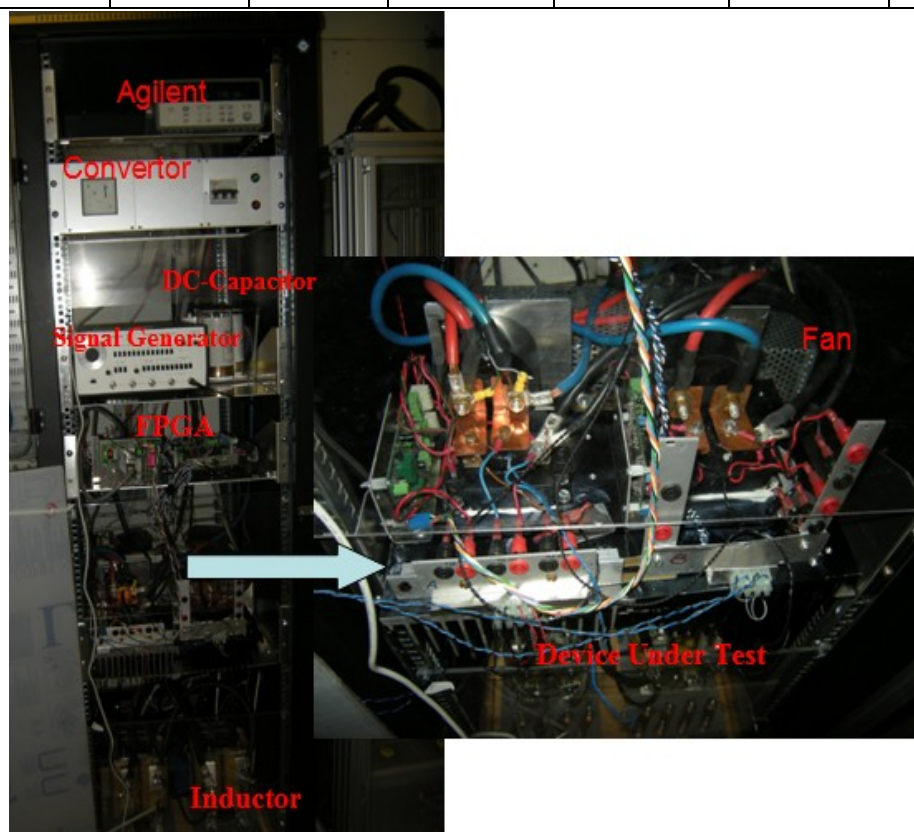


Fig. 33 Repetitive Switch Testing setup



## 6.5 Power Cycling Testing Setup

The power cycling testing setup is shown in Fig. 34. The power supply with 105 A and 20 V heating the IGBT module up to 80 °C, and the fan cools it down to 40 °C, the cycle waveform as shown in Fig. 35, power supply and fan are interlocked. This cycling process controlled by Agilent. The recoded parameters as show in Table 9, and the sampling frequency is 5 s.

Because of some bugs at the Agilent software and computer, made the IGBT module temperature out of control (the fan can not start again) result in the failure of the experiment and one of the IGBT modules broken. The high temperature caused the outside package plastic softy as shown in Fig. 36, some documents has shown that the temperature must higher than 230 °C to melt the plastic. The two tested IGBT module connected in series, and the energy produced by IGBT chips which means IGBT modules work at extremely high temperature (higher than 125 °C) for quite a while (longer than 250 s) based on the temperature increase rate. This ‘happy accident’ proves that measure the dynamic characteristic of IGBT module at higher temperature, ie. 180 °C, is possible.

Table 9 Channel and parameter of power cycling

|           |                    |                   |                        |                   |                  |                  |
|-----------|--------------------|-------------------|------------------------|-------------------|------------------|------------------|
| Channel   | 101                | 102               | 103                    | 104               | 105              | 106              |
| Parameter | Up Diode A Temp.   | Low IGBT A Temp.  | Up IGBT A Temp.        | Low Diode A Temp. | Up Diode B Temp. | Low IGBT B Temp. |
| Channel   | 107                | 108               | 109                    | 110               | 111              | 112              |
| Parameter | Low IGBT B Temp.   | Low Diode B Temp. | Heat sink output Temp. | Ambient Temp.     | 102 alarm 2      | Current          |
| Channel   | 113                | 114               | 115                    | 116               |                  |                  |
| Parameter | Low IGBT A voltage | Up IGBT A voltage | Low IGBT B voltage     | Up IGBT B voltage |                  |                  |



Fig. 34 Power cycling testing setup

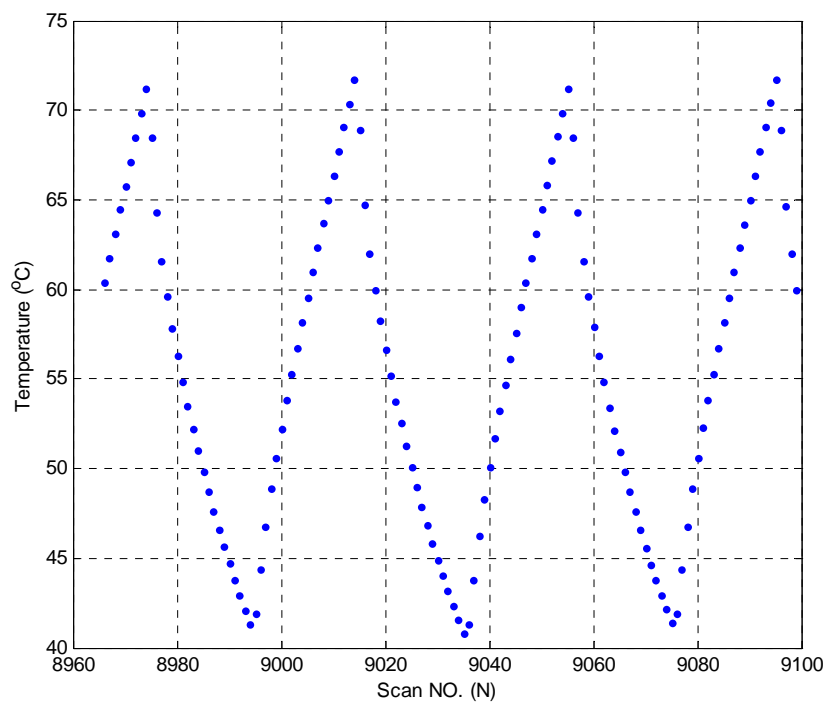


Fig. 35 Power cycles



Fig. 36 melted plastic due to temperature out of control



---

*This page intentionally left blank*





---

## 7. Results and Analysis

The parameters of turn-on and turn-off time, and turn-on and turn-off energies decide the performance of IGBT module, and thus the converter design. Those parameters under different voltage and current levels and different temperatures were investigated in this project by employing the double pulse switch testing. Repetitive switch test and power cycling test as the stress testing investigated the long-term stability of IGBT module which is very important at the industrial application. This chapter analyzed the results of both before and after stressful testing, and explored the influence of gate resistance, temperature, voltage and current level on both IGBT chips and the FWD chips. This chapter also compared the IXYS and Tyco IGBT module performance, verified the credibility of the testing methodology and gained the short-term and long-term stability information. The influence of snubber and stray inductance have been investigated at semester project report [33] thus will not cover at here.

### 7.1 Conduction Voltage

Conduction voltage is an important factor to decide the power loss of IGBT. The relation between conducting voltage of IGBT and temperature is shown in Fig. 37. The conducting voltage increased only 0.15 V when temperature increased from 40 °C to 80 °C, which means that conducting voltage only slightly influenced by temperature for this IXYS IGBT module. Therefore, increase the temperature will not result in lager additional power loss at the IXYS IGBT module. The testing results show that the conducting voltage is about 6 V which match the datasheet data (4.5 V  $\sim$  6.5 V). If IGBT working at rated current, the power losses were 2.4 kW.

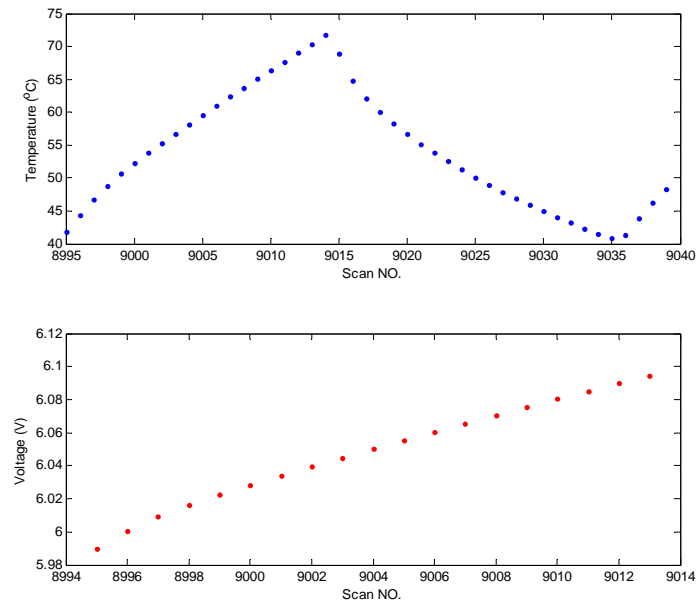


Fig. 37 Conducting Voltage vs. Temperature

## 7.2 Gate Resistance Influence

The Tyco IGBT was tested at two different gate resistances ie.  $2.2 \Omega$  and  $4.7 \Omega$ , and the results is shown in Fig. 38. Decrease the gate resistance can decrease the turn-on delay time, but increased the overshoot and fluctuation of the current waveform, thus a trade-off between them always should be made. In addition, decrease the gate resistance will increase the FWD stress [3, 33], and the influence on turn-off process was less than that of on turn-on process.

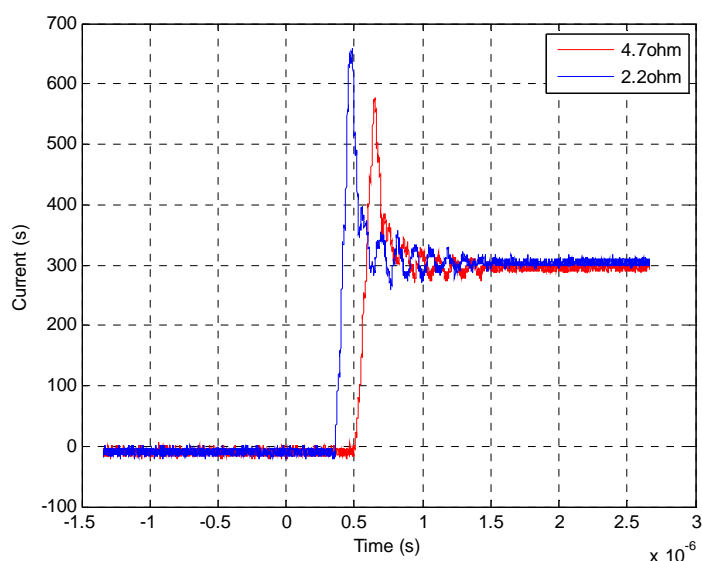


Fig. 38 Influence of gate resistances (Tyco IGBT module at 600 V 300 A and 25 °C )

### 7.3 Influence of Temperature

Based on the double pulse switch testing, the turn-on and turn-off time at 600 V was measured at different temperatures and different current levels. Both of the turn-on and turn-off time definitions are base on the IEC 60747-9 standard [7]. Turn-on time at different collector currents and three different temperatures are shown in Fig. 39. Turn-off time at same current levels and temperatures are shown in Fig. 40 and the 2-D figure of IGBT switching at 600 V and 400 A but different temperatures are shown in Fig. 41, and more figures please refer to Appendix. Setting  $V_{CE}$  and  $I_C$  to 600 V and 300 A, respectively, and junction temperature heated to 125 °C. Measured turn-on and turn-off time were 211.4 nsec and 683.2 nsec respectively. Module datasheet [67] stated 230 nsec and 730 nsec. The gate resistance used during this measurement was 4.125  $\Omega$  compared to 4.7  $\Omega$  in the datasheet, which cause this slight difference.

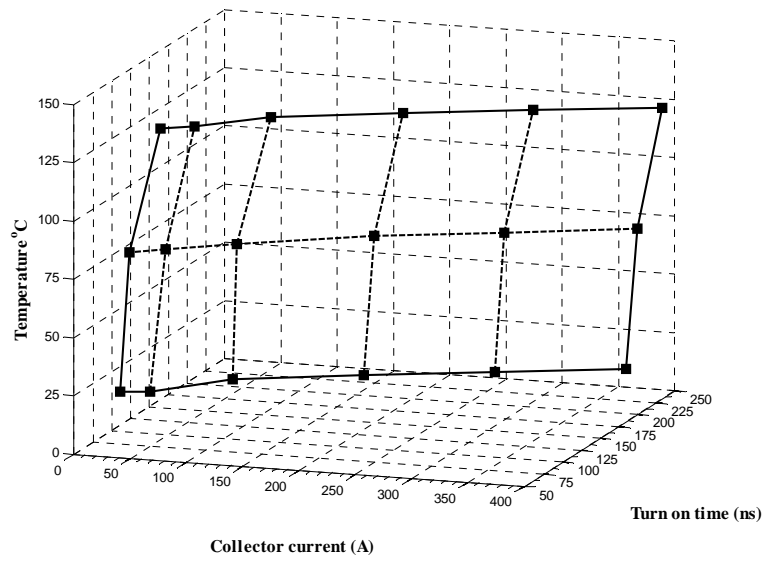


Fig. 39 Turn-on time at different currents and temperatures ( $V_{CE} = 600$  V)

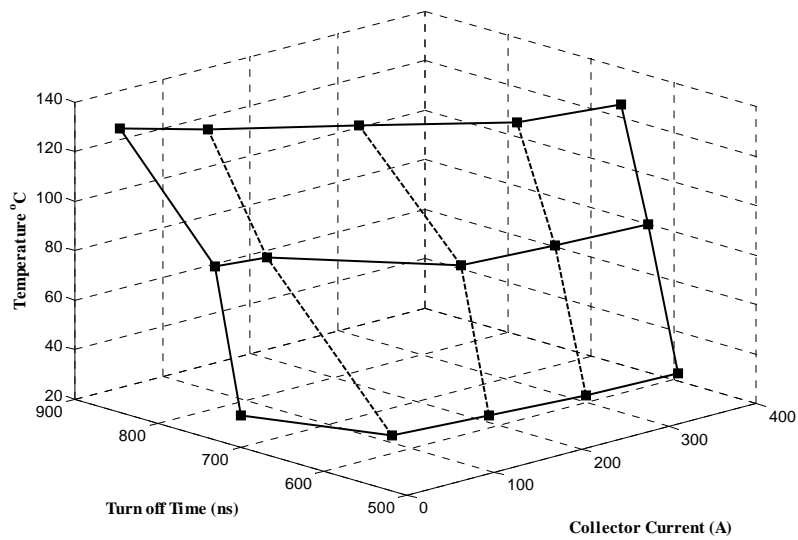


Fig. 40 Turn-off time at different currents and temperatures ( $V_{CE} = 600$  V)

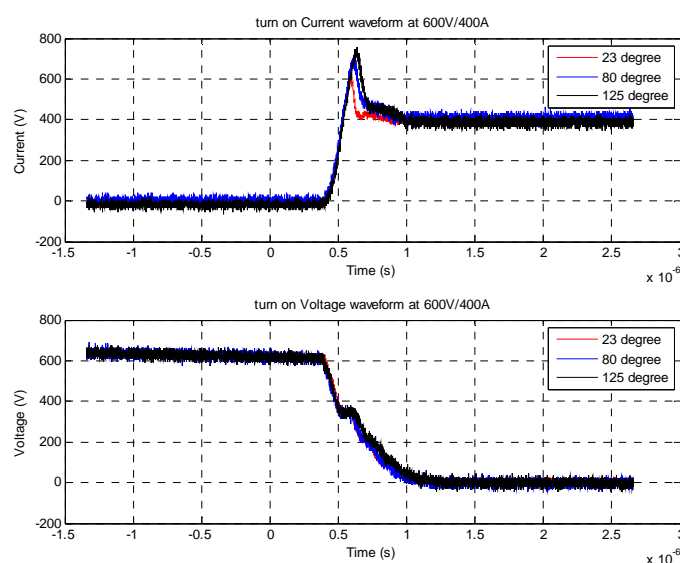


Fig. 41 Turn-on current and voltage waveforms at different temperature (600 V, 400 A)

Turn-on and Turn-off energy losses decided the reliability and lifetime [63, 68-69] of IGBT modules. According the IEC standard, the turn-on (turn-off) energy is the energy dissipated inside the IGBT during the turn-on (turn-off) of a single collector current pulse which can be calculated by formula (2.1) and (2.2). The power dissipations inside the IGBT chip during the turn-on period is shown in Fig. 42 and the turn-off period is shown in Fig. 43. This power pulse commences when the collector current start rising up and continues as far as the device is not fully on i.e.  $V_{CE}$  is higher than  $V_{CE(on)}$ . The turn-on and turn-off energy losses at different current levels and temperatures are displayed in 3-D plot as shown in Fig. 44 and Fig. 45. At the conditions of 600 V, 300 A, and 125 °C ambient temperature, the calculated turn-on and turn-off energy dissipation based on the experimental results and Eq. (2.1) and Eq. (2.2) are 40.0 mJ and 34.3 mJ, respectively. Datasheet given values are 44.0 mJ and 30.0 mJ respectively. The slightly lower gate resistance leads to a faster turn-on and turn-off transients and thus a lower energy loss.

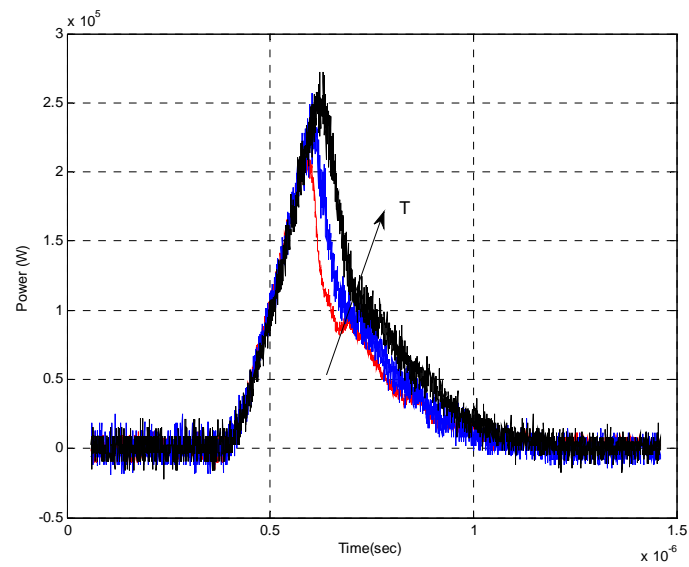


Fig. 42 Turn-on power dissipation at 600 V/400 A/ (23 °C, 80 °C and 125 °C)

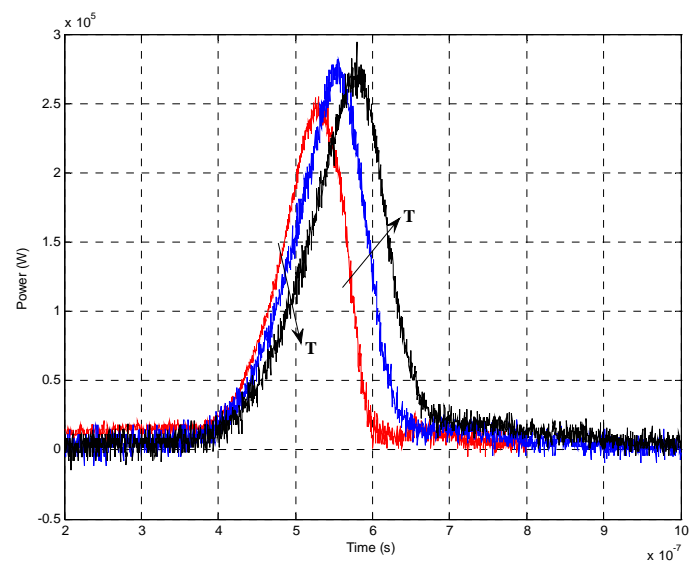


Fig. 43 Turn-off power dissipation at 600 V/400 A/ (23 °C, 80 °C and 125 °C)

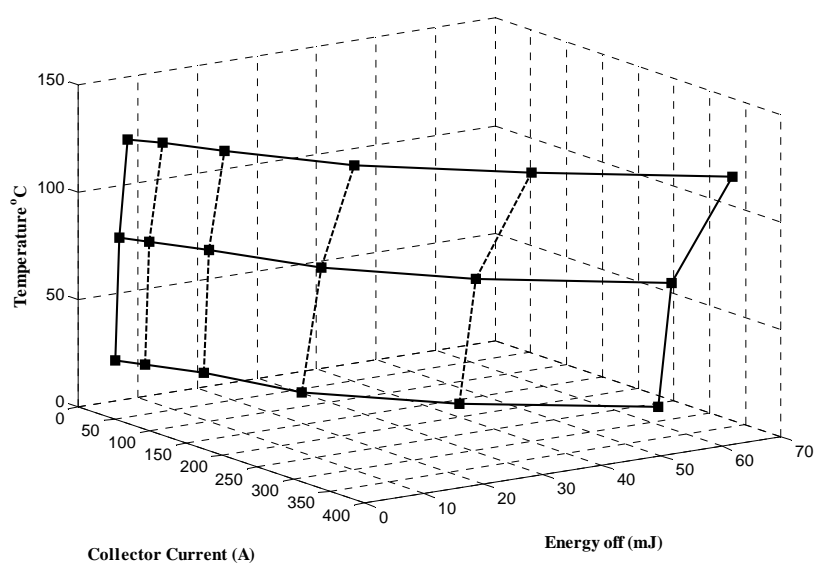


Fig. 44 Turn-on energy loss at different current and temperatures ( $V_{CE} = 600$  V)

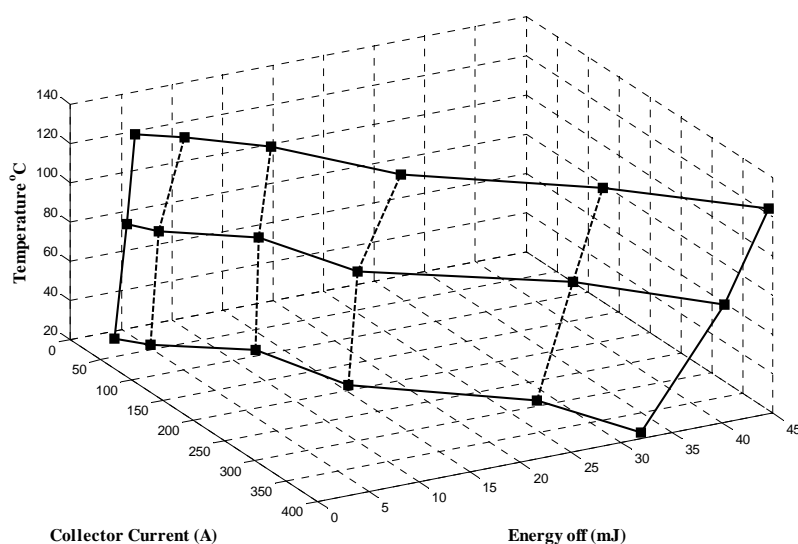


Fig. 45 Turn-off energy loss at different current and temperatures ( $V_{CE} = 600$  V)

## 7.4 Influence of Power

The turn-on time increase with the increasing of voltage and current levels on the IGBT module. Thus the energy dissipation at IGBT module also increases with the temperature. However, the turn-off time decrease with the increasing temperature as shown in Fig. 46 and the turn-off power losses increase with temperature is shown in Fig. 47. Table 10 shows the relation between turn-off time and turn-off energy



dissipation. More waveforms can refer to Appendix. This is because most of the energy loss occurs at the rise time not at the delay time. The delay time is decreasing as current increase.

Table 10 Turn-off time and energy loss at 600 V and 125 °C

| $I_C$          | 400 A | 300 A | 200 A | 100 A | 50 A  |
|----------------|-------|-------|-------|-------|-------|
| $t_{off}$ (ns) | 663.8 | 683.2 | 768.8 | 845.2 | 898.8 |
| $E_{off}$ (mJ) | 44.5  | 34.3  | 20.4  | 13.7  | 8.2   |

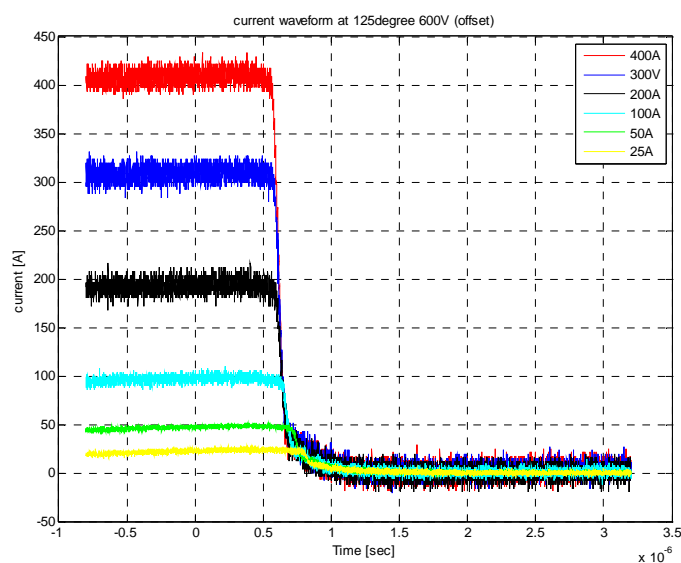


Fig. 46 IGBT turn-off current waveforms at 600 V and 125 °C

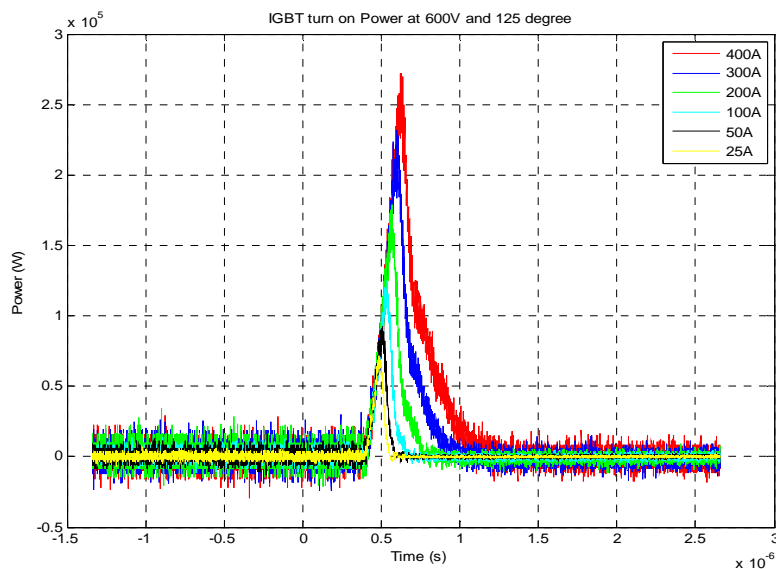


Fig. 47 turn-on power loss at different current





---

## 7.5 FWD Performance

Medium and high voltage level modules employ PiN freewheeling diodes. With necessary high injection level of free carrier to reduce on-state resistance, PiN exhibits a recovery of this storage charge at turn-off. This leads to reduction in switching speed and increase in the turn-on energy losses of the nearby IGBT, thus the performance of FWD impacts IGBT module performance. The reverse recovery charge can be calculated by;

$$Q_{rr} = I_{rr} t_{rr} / 2 \quad (3)$$

With minority carrier lifetime increases with temperature [3], peak reverse recovery current and energy loss during recovery also increase. The waveforms of voltage and current when turn-on the IGBT at different temperatures but the same voltage and current i.e. 600 V and 300 A are shown in Fig. 48 and Fig. 49, the experiment results show that the reverse recovery time  $t_{rr}$  are 0.9 ns at 23 °C and 1.8 ns at 125 °C, where peak reverse recovery current are 225 A and 405 A, respectively. Again power loss can be calculated using Eq. (2.1). The calculated energies dissipation in FWD are 21.6 mJ and 10.2 mJ when the IGBT is turned on at 23 °C and 125 °C, respectively. Calculated energies are 5.1 mJ and 3.8 mJ during IGBT turn off at 23 °C and 125 °C, respectively.

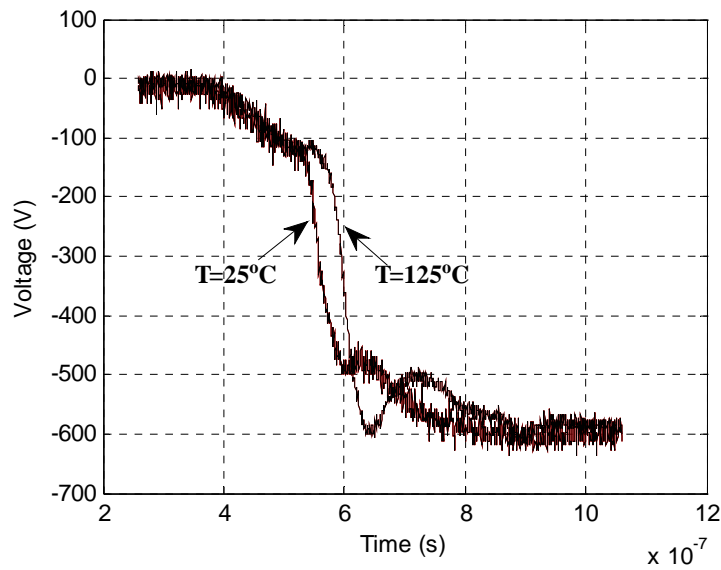


Fig. 48. FWD Voltage waveforms at ( $23^{\circ}\text{C}$  and  $125^{\circ}\text{C}$ )

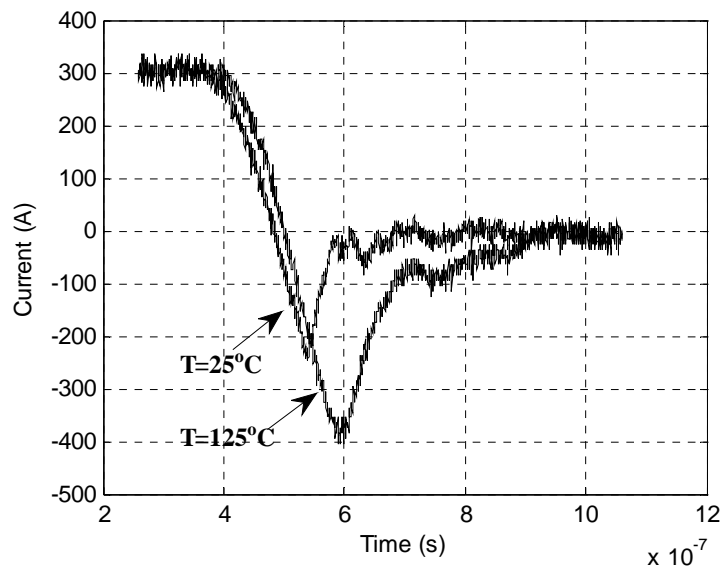


Fig. 49. FWD Current waveforms at ( $23^{\circ}\text{C}$  and  $125^{\circ}\text{C}$ )

## 7.6 Long-term Stability

The double pulse switch testing results of turn-on waveforms before and after the repetitive test is shown in Fig. 50. The results show that after 90 days of stressful switching, the IGBT modules still exactly exhibit the same performance as before. No sign of degradation is noticed. Moreover, the IGBT modules worked under power cycling (refer to chapter 6.5) until one of the IGBT modules were destroyed by



over-temperature. Testing the survived IGBT again after it undergo 21,073 cycles and extremely high temperature for a while. The compared result is shown in Fig. 51. It is very impressive that after undergoing such strong stress the dynamic characterizes and performances not show degradation. Therefore, it is quite safe to conclude that IGBT modules have very good long-term stability.

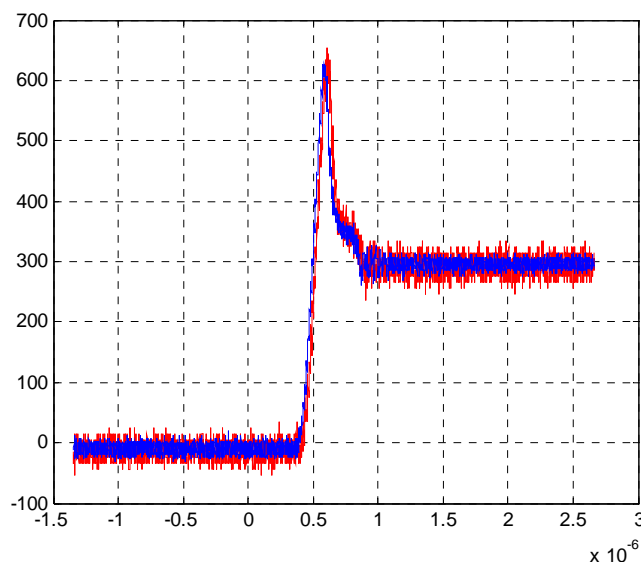


Fig. 50. Turn-on current before and after repetitive switching test

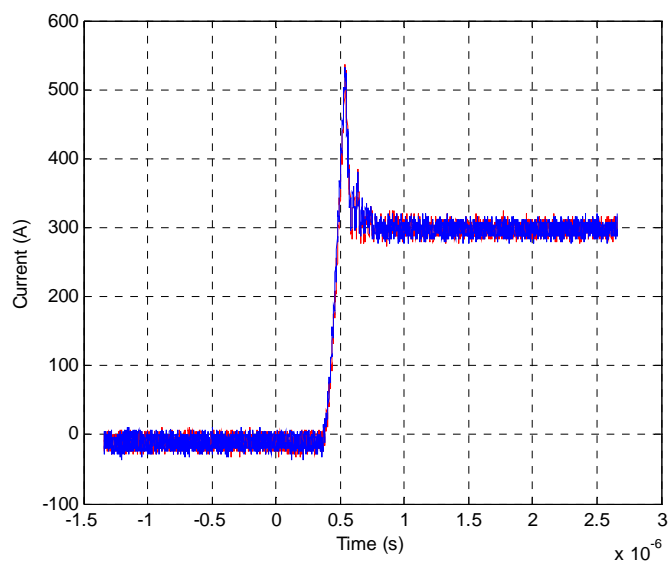


Fig. 51. Turn-on waveforms before and after power cycling test



## 7.7 Tyco-IGBT Performance

The turn-on and turn-off waveforms of Tyco IGBT are shown in Fig. 52, and the turn-off waveform tested by SINTEF [65] as shown in Fig. 53. The rise time are much faster at the new testing than the old one (tested by SINTEF), but due to the two experiments tested at different external conditions, it is hard to judge the accuracy of the Tyco IGBT testing, thus more measurements need to conduct.

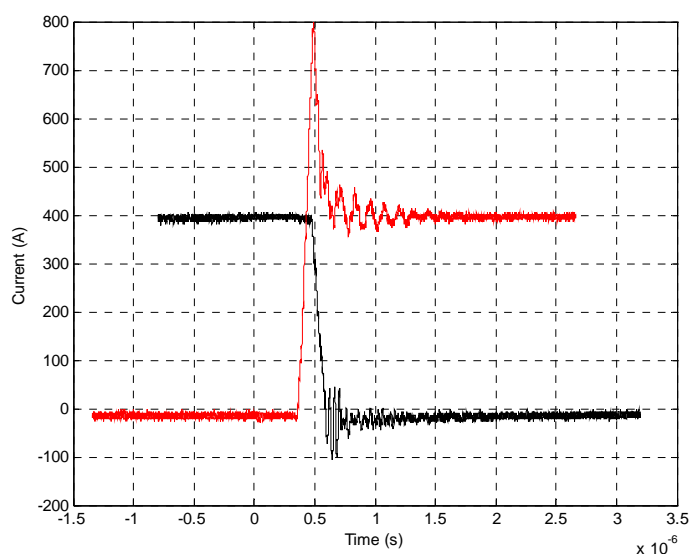


Fig. 52 Tyco IGBT turn-on (red) and turn-off current waveforms

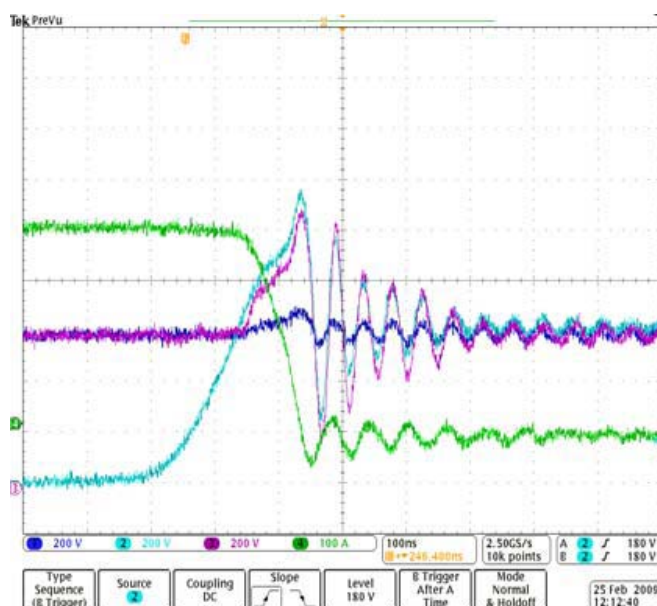


Fig. 53 Tyco turn-off waveform at 600 V and 400 A (from SINTEF memo)



## 7.8 Tyco vs. IXYS IGBT Module

The Tyco IGBT module and IXYS IGBT module were tested at the same conditions, and the results are shown in Fig. 54. The Tyco IGBT has short turn-on time but higher overshoot. The Tyco IGBT should have less energy loss, but the FWD will undergo heavier stress than IXYS IGBT. Observing the faults of IXYS IGBT module repetitive switch test setup due to the bad contact with the heat-sink, the Tyco IGBT module should have better long-term stability because the baseplate has a certain curve which makes the contact much well when screw it up to heatsink.

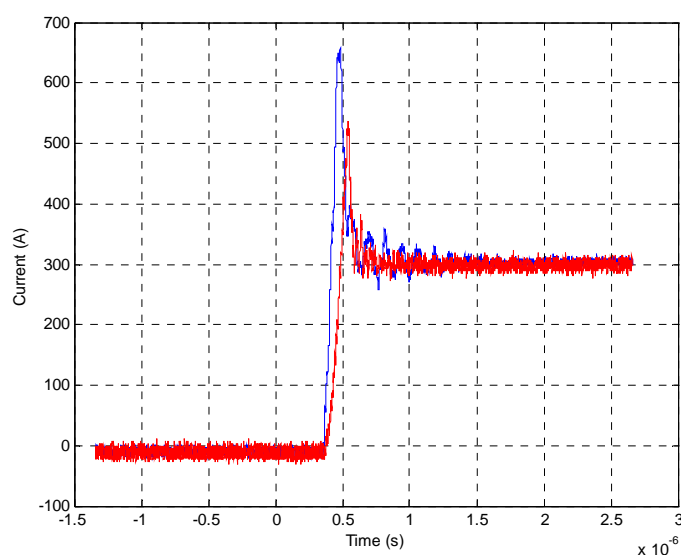


Fig. 54 IXYS (red) vs. Tyco (blue) IGBT at 600 V, 400 A and 25 °C



## 7.9 Verification of Test Results and Error Evaluation

To ensure results soundness and accuracy, four identical IGBT modules in total were measured at the same test conditions and results were compared. Fig. 55 shows the turn-on and turn-off waveforms for the four modules result at  $V_{CE}= 600\text{ V}$ ,  $I_C= 300\text{ A}$ , and  $125\text{ }^\circ\text{C}$ . Turn-on and turn-off time were the same, with same switching power losses. This shows measurements accuracy and credibility of the used methodology. Errors exist in every experiment, but the acceptance of error rang were proved at semester project report [33].

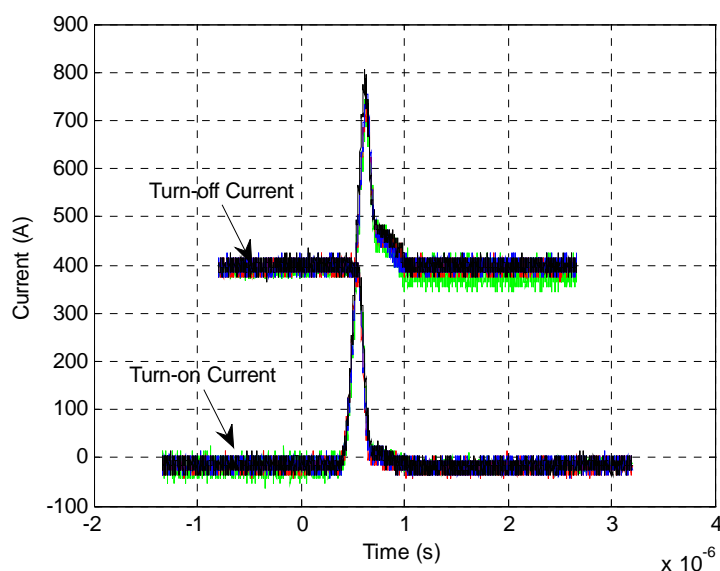


Fig. 55. Four IGBT modules Turn-on and turn-off waveform at 600 V/400 A /125 °C



---

## 8. Conclusion and Outlook

The chip and module technology will be extended to cover higher insulation levels and lower power dissipations. Employing new materials, especially the SiC, is another new development trend for high temperature conditions.

As the traditional wire-bond IGBT module is still the most popular component for industrial applications, three types of experiment setups were designed and build up to explore the dynamic performance and long-term stability of the IXYS<sup>TM</sup> IGBT module. The double pulse switch tests were conducted to investigate the dynamic characteristics. The repetitive switching tests and power cycling tests were conducted to explore the long-term stability by exposing the module to stress over certain period.

The experiments demonstrate that the turn-on and turn-off time and energy losses depend on the IGBT operation conditions including gate resistance, device voltage and current level, and junction temperature. Reducing the gate resistance value would reduce switching time and switching loss but increase the reverse recovery peak current, which would put heavy stresses on the FWD. Therefore, the gate resistance value should be chosen carefully. Under the same  $V_{CE}$  and junction temperature, increasing the collector current increases the turn-on time while the decrease the turn-off time. However, the turn-off energy loss increases. The higher energy losses can be explained by the higher charge recovery of the FWD and the longer tail current. Generally, energy loss increases as the temperature increases. During the turn-on, the delay time is almost constant for different temperatures, while the  $I_C$  rise time increases. This leads to higher loss during the turn-on. For example, turn-on energy was increased by 25.4%, when the temperature rises from 25 °C to 125 °C for same  $V_{CE}$  and  $I_C$ . During the turn-off, energy losses increase with temperature. A 39.5% increase in  $E_{off}$  was recorded when the temperature rises from 25 °C to 125 °C. The reverse recovery loss doubles when temperature increases from 25 °C to 125 °C, while turn-on loss increases by 34.2%. The double pulse switch test conducted after repetitive switching test shows no change in IGBT performance. When the double



---

pulse switch test is repeated after the power cycling test, the dynamic characteristics of survived IGBT shows no degradation even the accidental high temperature broke one of the IGBT modules and melted the package plastic. Therefore, the IXYS<sup>TM</sup> has a much great long-term stability. The Tyco<sup>TM</sup> IGBT module should have a better long-term stability than the IXYS<sup>TM</sup> IGBT because of the better package structure which can effectively conduct the produced energy to heatsink. By repeating the same experiment on different modules, the accuracy and credibility of used methodology were confirmed.

As the testing has shown that the IGBT module can survive at extremely high temperature for a limited time period, measuring the IGBT dynamic characteristics at 180 °C is possible and necessary. The power cycling test employed in this project was much less stressful than the standard testing method. Further tests should follow the mounting tips or use better thermal grease to ensure good contact with the heatsink, and then run it under the standard conditions [61].





## Reference

- [1] V. K. Khanna, *Insulated Gate Bipolar Transistor IGBT Theory and Design*, 1 ed.: Willey-IEEE Press, 2003.
- [2] S. Linder, *Power Semiconductors*, 1st ed.: EPFL Press, 2006.
- [3] Ned Mohan, *et al.*, *Power Electronics: Converters, Applications, and Design*: Wiley, 2002.
- [4] K.J.Um, "IGBT Basic II," *Fairchild Semiconductor, Application Note 9020*, 2001.
- [5] SIEMENS, "Insulated Gate Bipolar Transistor(IGBT)," *Semiconductor Group*, 2003.
- [6] R. P. C. William W. Sheng, *Power Electronic Modules: Design and Manufacture* CRC Press, 2004.
- [7] IEC, "IEC 60747-9 International Standard, Part 9: Insulated-gate bipolar transistors (IGBTs)," ed. Switzerland, 2003.
- [8] K.S.Oh, "IGBT Basic 1," *Fairchild Semiconductor, Application Note 9016*, 2001.
- [9] A. Sattar, "Insulated Gate Bipolar Transistor (IGBT) Basics," *IXYS Corporation*, vol. IXAN0063, 1999.
- [10] A. Kopta, *et al.*, "New plasma shaping technology for optimal high voltage diode performance," in *Power Electronics and Applications, 2007 European Conference on*, 2007, pp. 1-10.
- [11] R. S. a. J. Lutz, "Axial Lifetime Control by Radiation Induced Centers in Fast Recovery Diodes."
- [12] P. Hazdra, *et al.*, "Axial lifetime control in silicon power diodes by irradiation with protons, alphas, low- and high-energy electrons," *Microelectronics Journal*, vol. 35, pp. 249-257, 2004.
- [13] J. Vobecký, *et al.*, "Helium irradiated high-power P-i-N diode with low ON-state voltage drop," *Solid-State Electronics*, vol. 47, pp. 45-50, 2003.
- [14] J. Vobecky and P. Hazdra, "High-power P-i-N diode with the local lifetime control based on the proximity gettering of platinum," *Electron Device Letters, IEEE*, vol. 23, pp. 392-394, 2002.
- [15] D. Xiao, "Reliablity of Power Electronics (IGBT) -- summer job report," 2009.
- [16] A. K. M. Rahimo, S. Eicher, ABB Switzerland Ltd, Semiconductors, Switzerland, "Next Generation Planar IGBTs with SPT+ Technology," *Power Electronics Europe Magazine*, 2005.
- [17] U. S. M. Rahimo, A. Kopta, R. Schnell, S. Linder, "SPT+, the Next Generation of Low-Loss HV-IGBTs," *PCIM PCIM Power Electronics Conference*, p. 6, 2005.
- [18] M. M. Bakran, *et al.*, "Next generation of IGBT-modules applied to high power traction," in *Power Electronics and Applications, 2007 European Conference on*, 2007, pp. 1-9.
- [19] S. Eicher, *et al.*, "4.5kV press pack IGBT designed for ruggedness and reliability," in *Industry Applications Conference, 2004. 39th IAS Annual Meeting. Conference Record of the 2004 IEEE*, 2004, pp. 1534-1539 vol.3.
- [20] S. Kaufmann, *et al.*, "Innovative press pack modules for high power IGBTs," in *Power Semiconductor Devices and ICs, 2001. ISPSD '01. Proceedings of the 13th International Symposium on*, 2001, pp. 59-62.
- [21] S. Kaufmann and F. Zwick, "10 kV IGBT press pack modules with series connected chips," in



- Power Semiconductor Devices and ICs, 2002. Proceedings of the 14th International Symposium on, 2002, pp. 89-92.*
- [22] S. Gunturi and D. Schneider, "On the operation of a press pack IGBT module under short circuit conditions," *Advanced Packaging, IEEE Transactions on*, vol. 29, pp. 433-440, 2006.
- [23] N. K. HIDEO MATSUDA, MICHIAKI HIYOSHI, SATOSHI TERAMAE, and KAZUNOBU NISHITANI, "A Highly Reliable Press Packed IGBT," *Electrical Engineering in Japan*, vol. Vol. 131, 2000.
- [24] R. Kolessar and H. P. Nee, "A new physics-based circuit model for 4H-SiC power diodes implemented in SABER," in *Applied Power Electronics Conference and Exposition, 2001. APEC 2001. Sixteenth Annual IEEE, 2001*, pp. 989-994 vol.2.
- [25] P. W. Dominique Tournier, Phillippe Godignon, L. Coulbeck, José Millán, Roger Bassett, "4.5 kV-8 A SiC-Schottky Diodes / Si-IGBT Modules," in *Materials Science Forum (Volumes 527 - 529)* vol. Silicon Carbide and Related Materials 2005, ed, October, 2006, pp. 1163-1166.
- [26] B. S. a. A. Benfdila, "Recent Trends in IGBT Technology," *African Physical Review*, 2008.
- [27] R. Singh, *et al.*, "SiC power Schottky and PiN diodes," *Electron Devices, IEEE Transactions on*, vol. 49, pp. 665-672, 2002.
- [28] Y. Sui, *et al.*, "High-Voltage Self-Aligned p-Channel DMOS-IGBTs in 4H-SiC," *Electron Device Letters, IEEE*, vol. 28, pp. 728-730, 2007.
- [29] J. W. B. W. Williams, "A simulation study of high voltage 4H-SiC IGBTs," *Semicond. Sci. Technol.*, vol. 13, pp. 806-815, 1998.
- [30] H. Iwamoto, *et al.*, "Turn-off behaviour of epitaxial planar and trench gate IGBTs and nonepitaxial planar gate IGBT under hard and soft switchings," *IEE Proceedings - Electric Power Applications*, vol. 148, pp. 443-448, 2001.
- [31] F. W. F. a. M. M. M. Helsper, "Comparison of Planar- and Trench-IGBT-Modules for resonant applications."
- [32] M. Rahimo, *et al.*, "Novel Enhanced-Planar IGBT Technology Rated up to 6.5kV for Lower Losses and Higher SOA Capability," in *Power Semiconductor Devices and IC's, 2006. ISPSD 2006. IEEE International Symposium on, 2006*, pp. 1-4.
- [33] D. Xiao, "Investigate the reliability of IGBT module (2009 semest project)," p. 70, 2009.
- [34] E. H. a. S. Dewar, "Reliability of LoPak with SPT-Narrow time-to-failure distributions indicate mature product," *PCIM Europe Magazine*, 2001.
- [35] W. L. M. Rahimo, C. von Arx, A. Kopta, R. Schnell, S. Dewar, S. Linder, "Novel Soft-Punch-Through (SPT) 1700V IGBT Sets Benchmark on Technology Curve," *Proc. PCIM'01*, 2001.
- [36] S. L. S. Dewar, C. von Arx, A. Mukhitinov, G. Debled, "Soft Punch Through (SPT) – Setting new Standards in 1200V IGBT," *PCIM*, p. 7, 2000.
- [37] U. Florin, "IGBTs:concept, state-of-the-art technologies, and derivatives," *Cambridge University, short-course at ISPSD 2009*, 2009.
- [38] T. Uesugi, "Power Devices for Automotive Applications- Reviews of Technologies for Low Power Dissipation and High Ruggedness," *T&D Review of Toyota CRDL*, vol. 35, 2000.
- [39] M. Avram, *et al.*, "Contributions to development of high power SiC-IGBT," in *Semiconductor Conference, 2005. CAS 2005 Proceedings. 2005 International, 2005*, pp. 365-368 vol. 2.
- [40] M. Avram, *et al.*, "Contributions to development of power SiC devices," in *Semiconductor Conference, 2004. CAS 2004 Proceedings. 2004 International, 2004*, pp. 303-306 vol.2.



- 
- [41] M. R. C. M. Johnson, N. G. Wright, D. A. Hinchley, A. B. Horsfall, D. J. Morrison, "Characterisation of 4H-SiC Schottky Diodes for IGBT Applications," 2000.
- [42] D. M. Brown, *et al.*, "Silicon carbide MOSFET technology," *Solid-State Electronics*, vol. 39, pp. 1531-1542, 1996.
- [43] A. Elasser, *et al.*, "Switching characteristics of silicon carbide power PiN diodes," *Solid-State Electronics*, vol. 44, pp. 317-323, 2000.
- [44] F. Schafmeister, *et al.*, "Evaluation of 1200 V-Si-IGBTs and 1300 V-SiC-JFETs for application in three-phase very sparse matrix AC-AC converter systems," in *Applied Power Electronics Conference and Exposition, 2003. APEC '03. Eighteenth Annual IEEE*, 2003, pp. 241-255 vol.1.
- [45] Z. Hui and L. M. Tolbert, "Efficiency of SiC JFET-Based Inverters," in *Industrial Electronics and Applications, 2009. ICIEA 2009. 4th IEEE Conference on*, 2009, pp. 2056-2059.
- [46] B. Ozpineci, *et al.*, "A 55 kW three-phase inverter with Si IGBTs and SiC Schottky diodes," in *Applied Power Electronics Conference and Exposition, 2006. APEC '06. Twenty-First Annual IEEE*, 2006, p. 7 pp.
- [47] X. Perpiñà, *et al.*, "Failure-relevant abnormal events in power inverters considering measured IGBT module temperature inhomogeneities," *Microelectronics Reliability*, vol. 47, pp. 1784-1789.
- [48] M. Ciappa, "Selected failure mechanisms of modern power modules," *Microelectronics Reliability*, vol. 42, pp. 653-667.
- [49] X. Perpiñà, *et al.*, "Self-heating experimental study of 600 V PT-IGBTs under low dissipation energies," *Microelectronics Journal*, vol. 35, pp. 841-847, 2004.
- [50] C. Gillot, *et al.*, "Double-sided cooling for high power IGBT modules using flip chip technology," *Components and Packaging Technologies, IEEE Transactions on*, vol. 24, pp. 698-704, 2001.
- [51] G. Mitic, *et al.*, "Reliability of AlN substrates and their solder joints in IGBT power modules," *Microelectronics Reliability*, vol. 39, pp. 1159-1164.
- [52] J.-H. F. a. S. G. Amina Hamidi, "Packaging-related failure mechanisms of high power IGBT modules," *The 2005 International Power Electronics Conference*, 2005.
- [53] H. Ye, *et al.*, "Failure modes and FEM analysis of power electronic packaging," *Finite Elements in Analysis and Design*, vol. 38, pp. 601-612, 2002.
- [54] P. Rose, *et al.*, "Investigations on the stability of dynamic avalanche in IGBTs," in *Power Semiconductor Devices and ICs, 2002. Proceedings of the 14th International Symposium on*, 2002, pp. 165-168.
- [55] M. Rahimo, *et al.*, "A study of switching-self-clamping-mode "SSCM" as an over-voltage protection feature in high voltage IGBTs," in *Power Semiconductor Devices and ICs, 2005. Proceedings. ISPSD '05. The 17th International Symposium on*, 2005, pp. 67-70.
- [56] A. K. M. Rahimo, S. Eicher, U. Schlapbach, S. Linder, "Switching-Self-Clamping-Mode "SSCM", a breakthrough in SOA performance for high voltage IGBTs and Diodes," *Proceedings of 2004 International Symposium on Power Semiconductor Devices & ICs, Kitakyushu*, 2004.
- [57] C. t. m. amor, "Characterization of 3.3kv IGCTs for Medium power application," PHD PHD, Génie Electrique, DOCTEUR DE L'INSTITUT NATIONAL POLYTECHNIQUE DE TOULOUSE, 2005.



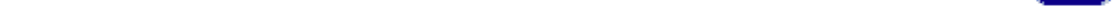
- 
- [58] V. A. Sankaran, *et al.*, "Power cycling reliability of IGBT power modules," in *Industry Applications Conference, 1997. Thirty-Second IAS Annual Meeting, IAS '97., Conference Record of the 1997 IEEE*, 1997, pp. 1222-1227 vol.2.
- [59] G. Coquery and R. Lallemand, "Failure criteria for long term Accelerated Power Cycling Test linked to electrical turn off SOA on IGBT module. A 4000 hours test on 1200A-3300V module with AlSiC base plate," *Microelectronics Reliability*, vol. 40, pp. 1665-1670.
- [60] P. Cova and F. Fantini, "On the effect of power cycling stress on IGBT modules," *Microelectronics Reliability*, vol. 38, pp. 1347-1352.
- [61] J. Lutz, "Power device packaging and reliability," *Stockholm Mach 31,2009*, 2009.
- [62] T. L. Skvarenina, Ed., *The Power Electronics Handbook (Industrial Electronics)*. CRC, 2002, p.^pp. Pages.
- [63] W. Wuchen, *et al.*, "Investigation on the long term reliability of power IGBT modules," in *Power Semiconductor Devices and ICs, 1995. ISPSD '95. Proceedings of the 7th International Symposium on*, 1995, pp. 443-448.
- [64] A. Morozumi, *et al.*, "Reliability of power cycling for IGBT power semiconductor modules," *Industry Applications, IEEE Transactions on*, vol. 39, pp. 665-671, 2003.
- [65] A. Petterteig, "Preparing and testing pressure tolerant phase-leg IGBT module V23990-P669-F02 from Tyco," SINTEF Energy Research, Trondheim2008.
- [66] L. R. Ljøkelsøy K., "AN 00.12.49 Driver interface board, v 4.0 – Documentation 2. edition," *Open Worknote SINTEF*, 2007.
- [67] IYYS, "IGBT module datasheet MII400-12E4," *IXYS*, 2007.
- [68] L. Feller, *et al.*, "Lifetime analysis of solder joints in high power IGBT modules for increasing the reliability for operation at 150 °C," *Microelectronics Reliability*, vol. 48, pp. 1161-1166.
- [69] A. Hamidi, *et al.*, "Reliability and lifetime evaluation of different wire bonding technologies for high power IGBT modules," *Microelectronics Reliability*, vol. 39, pp. 1153-1158.



---

## Appendix

As there is too much data to cover all of them at here, just parts of the results and pictures will present at here. For the full double pulse switch testing results of IXYS NO.1 can refer to “Original Data for IXYS”, and all of the data has recorded with Excel File. The data of power cycling test and repetitive switching test also recorded in Excel Files. All of the data can get by send e-mail to [dix@stud.ntnu.no](mailto:dix@stud.ntnu.no). The IGBT datasheets download from IXYS<sup>TM</sup> and Tyco<sup>TM</sup> official documents. The gate driver and the inverter circuit abstract form SINTEF Memo.



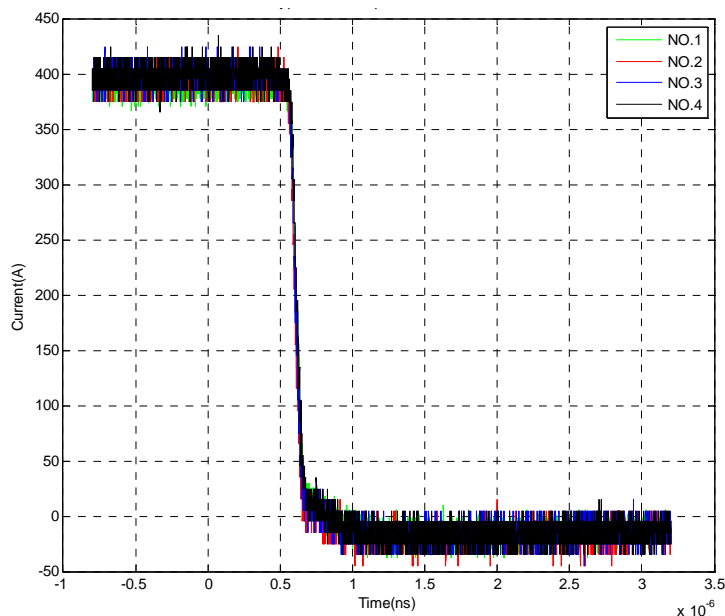


**Fig A1. Four IXYS IGBT module turn off at same conditions**

Table A. Switching time and energy losses at different current and temperature levels

| 600V | 23°C switching time (ns) and energy (mJ) |                  |                 |                  | 80°C switching time (ns) and energy (mJ) |                  |                 |                  | 125°C switching time (ns) and energy (mJ) |                  |                 |                  |
|------|--|------------------|-----------------|------------------|--|------------------|-----------------|------------------|---|------------------|-----------------|------------------|
|      | t <sub>on</sub>                          | t <sub>off</sub> | E <sub>on</sub> | E <sub>off</sub> | t <sub>on</sub>                          | t <sub>off</sub> | E <sub>on</sub> | E <sub>off</sub> | t <sub>on</sub>                           | t <sub>off</sub> | E <sub>on</sub> | E <sub>off</sub> |
| 400A | 184.4                                    | 594.2            | 49.3            | 31.9             | 200                                      | 630.8            | 51.5            | 40.2             | 232.8                                     | 663.8            | 61.8            | 44.5             |
| 300A | 160                                      | 600              | 27.9            | 27.7             | 173.2                                    | 636              | 30.6            | 31.3             | 211.4                                     | 683.2            | 40.0            | 34.3             |
| 200A | 136                                      | 612.5            | 13.5            | 15.2             | 149.6                                    | 645.8            | 16.8            | 16.1             | 188                                       | 768.8            | 22.3            | 20.4             |
| 100A | 111.2                                    | 624              | 9.1             | 12.2             | 116.2                                    | 774.8            | 9.8             | 12.5             | 161.6                                     | 845.2            | 12.4            | 13.7             |
| 50A  | 76.6                                     | 753.2            | 5.2             | 4.8              | 97.2                                     | 784              | 5.8             | 5.6              | 134.8                                     | 898.8            | 8.1             | 8.2              |
| 25A  | 73.6                                     | 594.2            | 3.1             | N/A              | 85.6                                     | 630.8            | 3.8             | 4.0              | 127.2                                     | 663.8            | 5.2             | 4.8              |

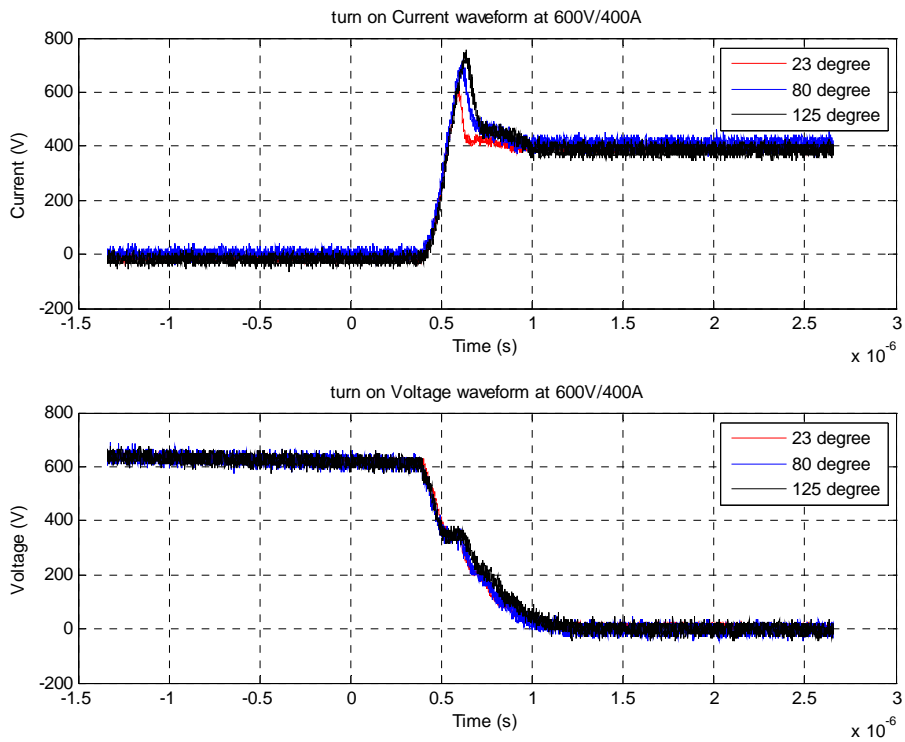


Fig A2. Turn on time comparison at different temperatures

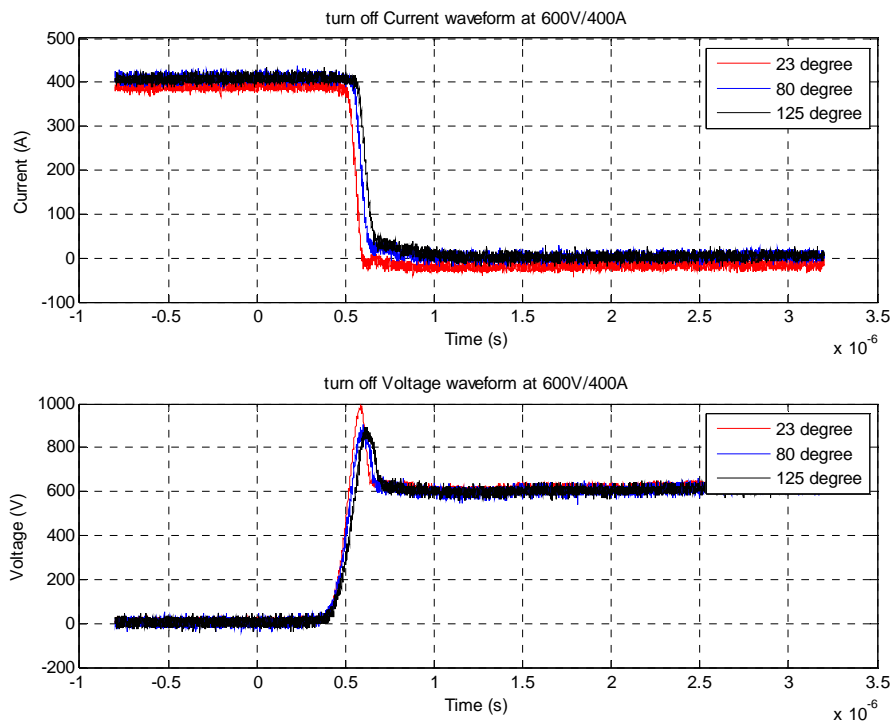


Fig A3. Turn off current waveform at different temperatures



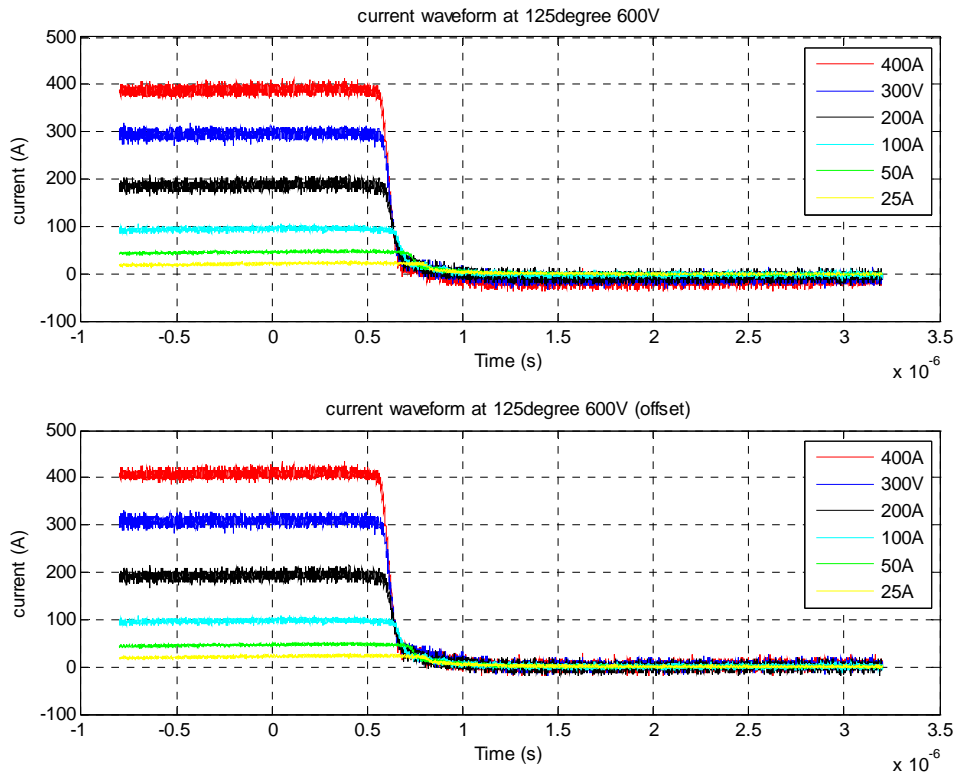


Fig A4. Current waveform before and after offset

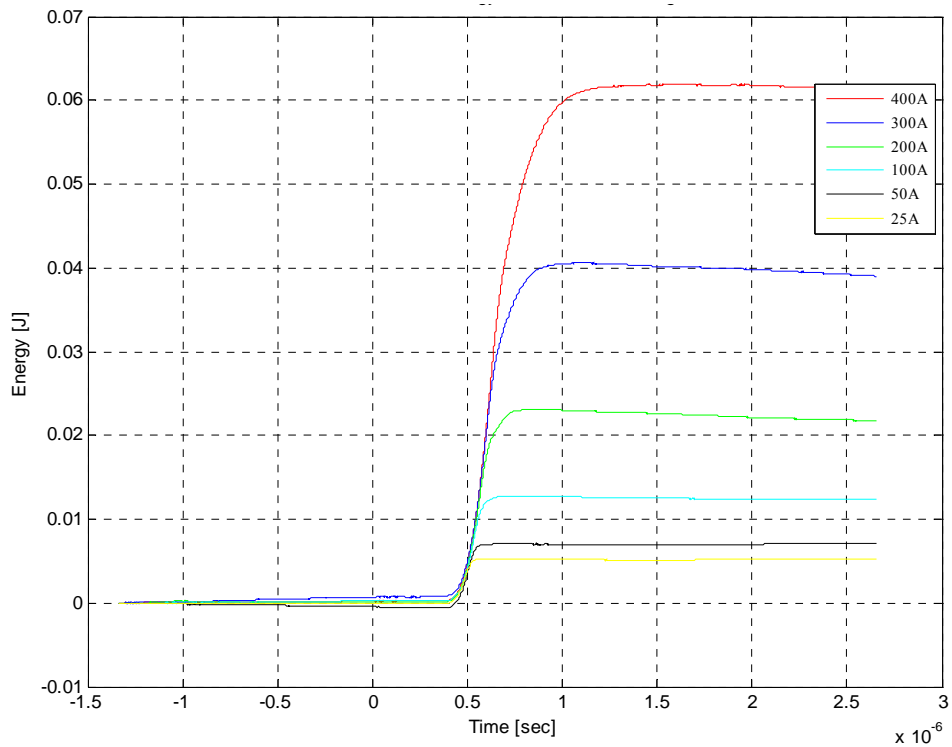


Fig A5. Turn-on Energy loss at different current levels

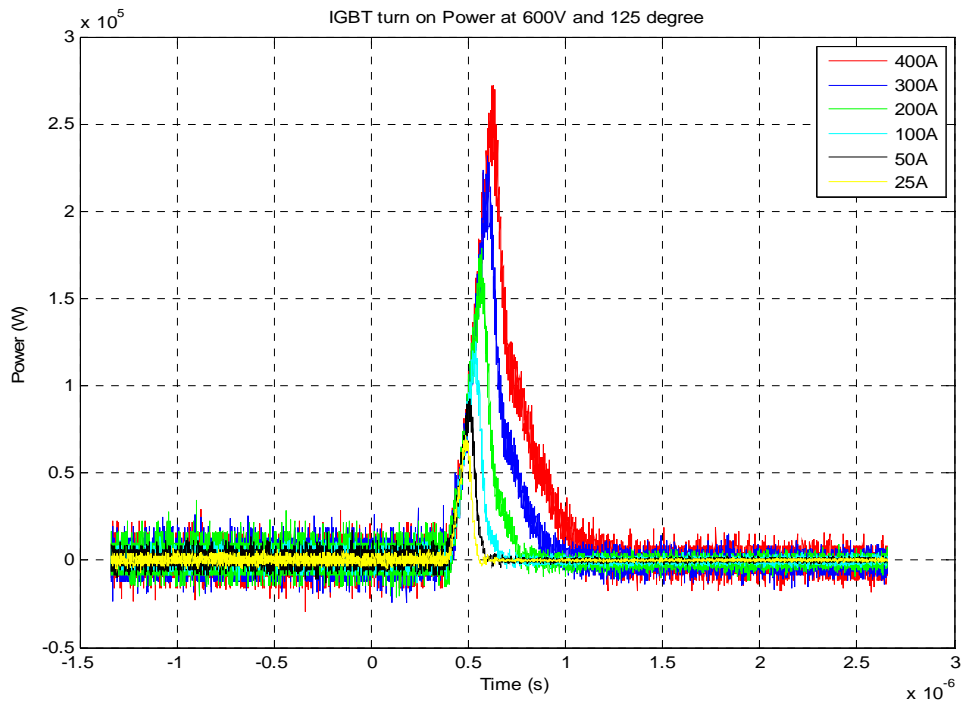


Fig A6. turn-on power loss at different current

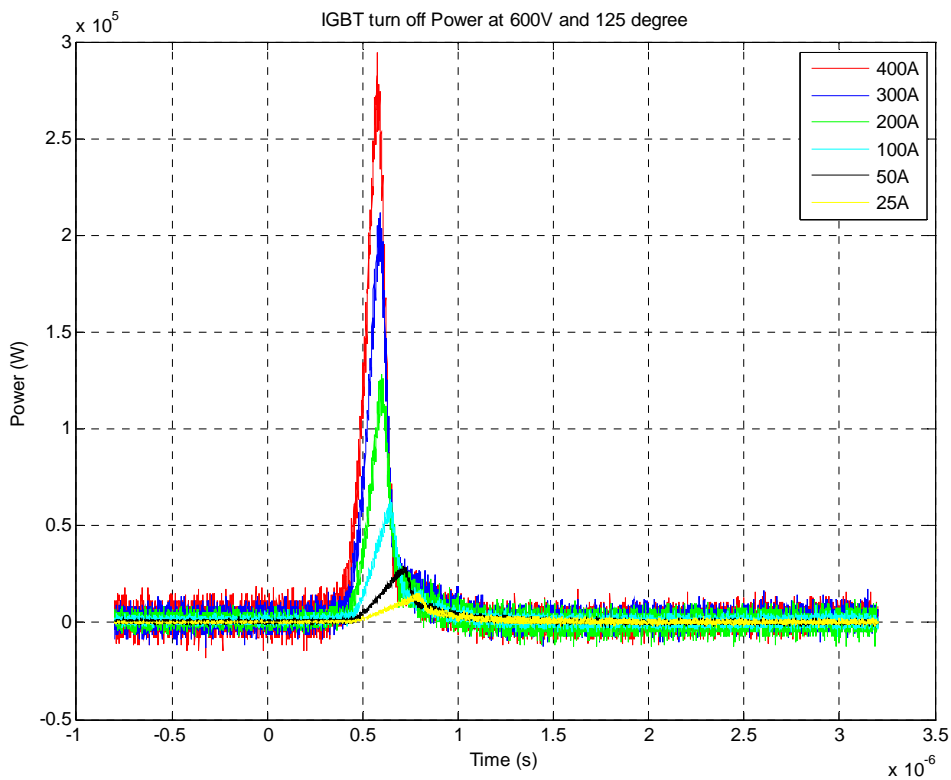


Fig A7. turn-on power loss at different current

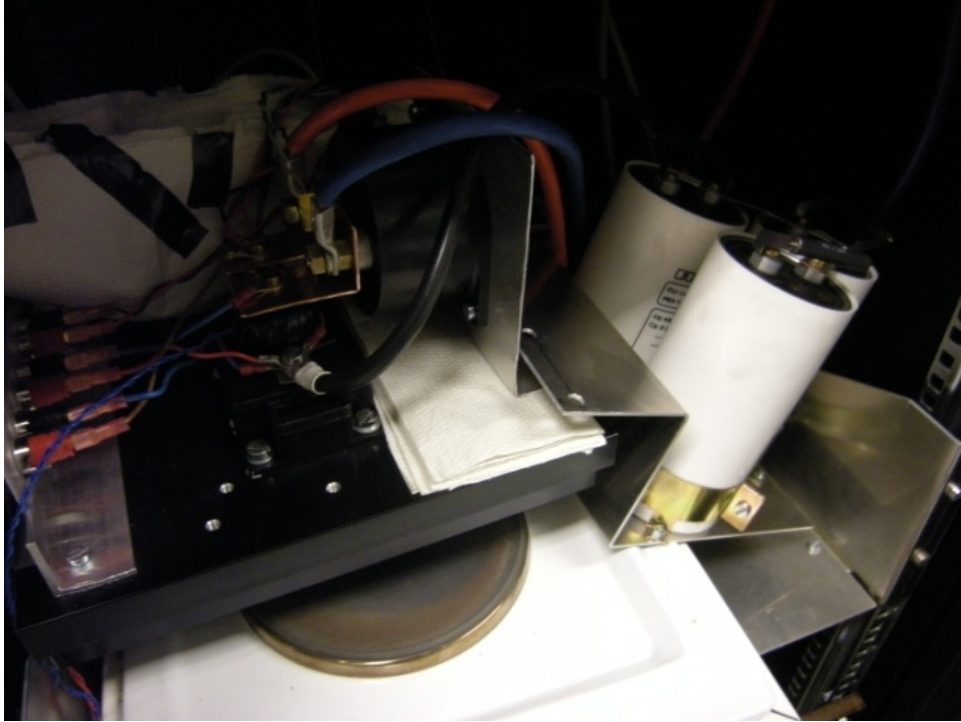


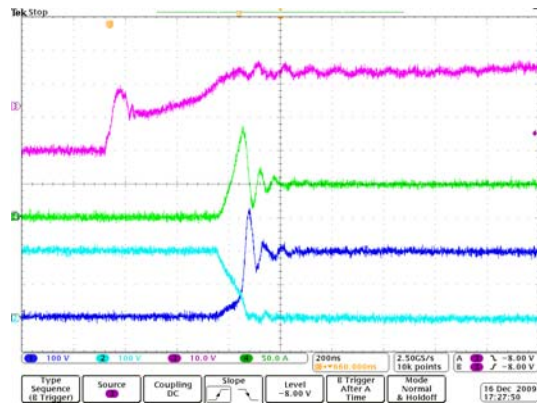
Fig A8. Capacitor location whiter (first time) and black (Later) to reduce the stray inductance



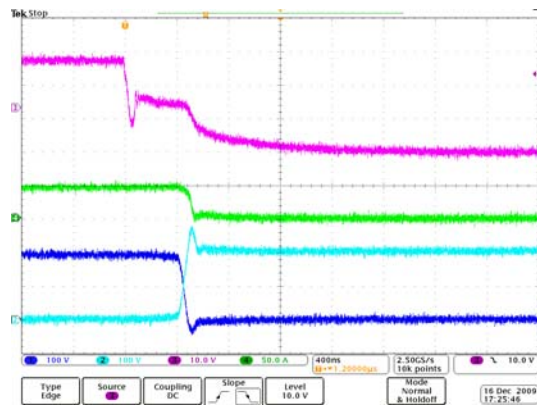
# IXYS IGBT module NO.2 at 23 °C

200V 50A 23 °C

Turn on

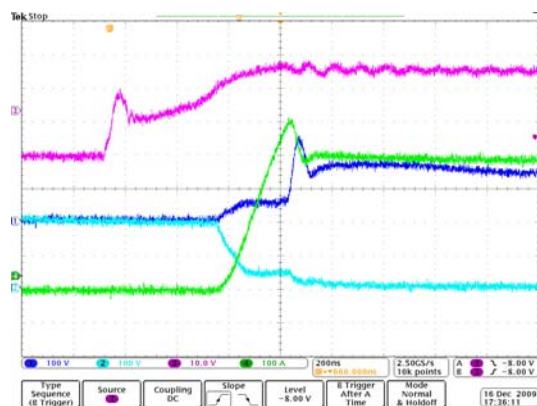


Turn off

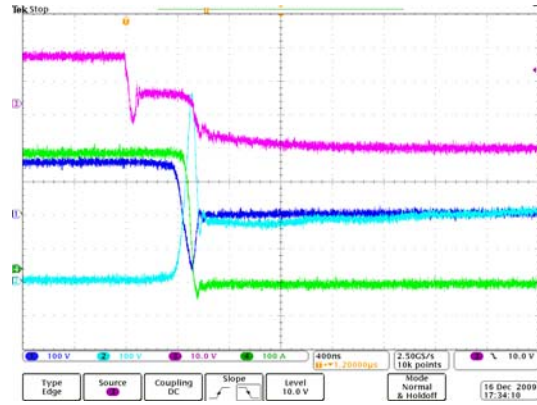


200 V 400 A 23 °C

Turn on

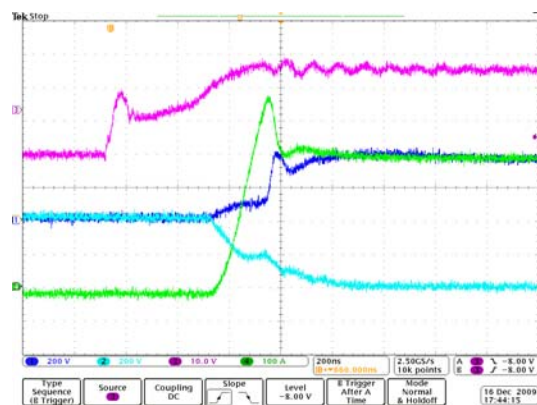


Turn off

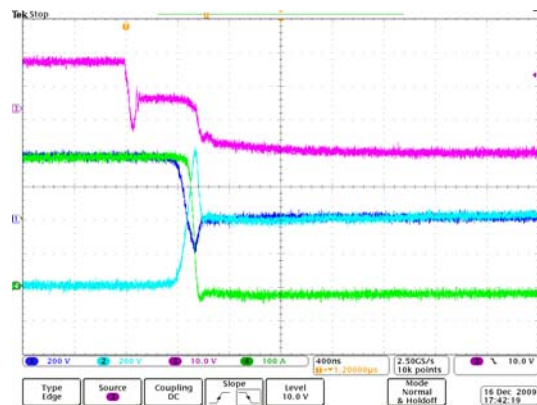


400 V 400 A 23 °C

Turn on



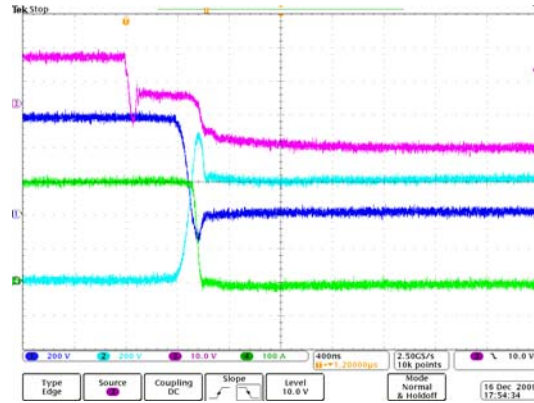
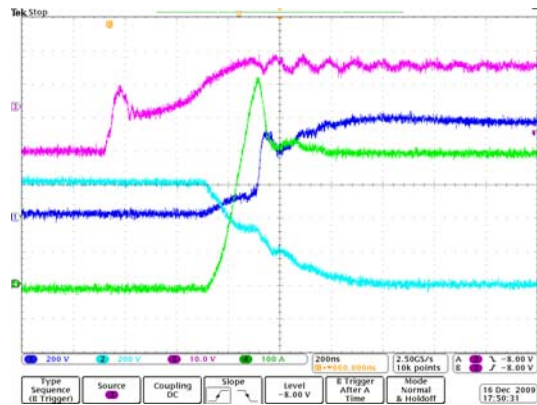
Turn off





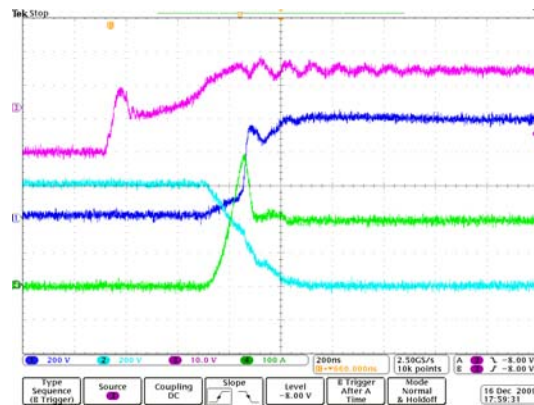
600 V 400 A 23 °C

Turn on

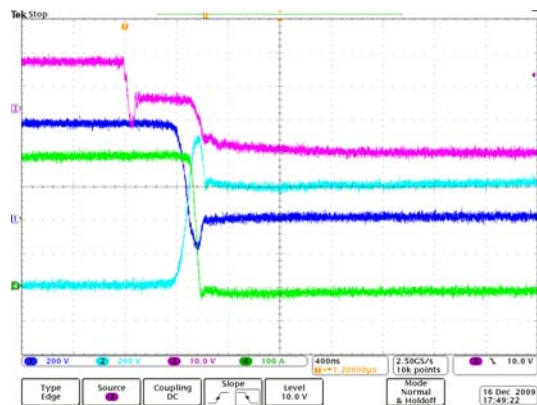


600 V 200 A 23 °C

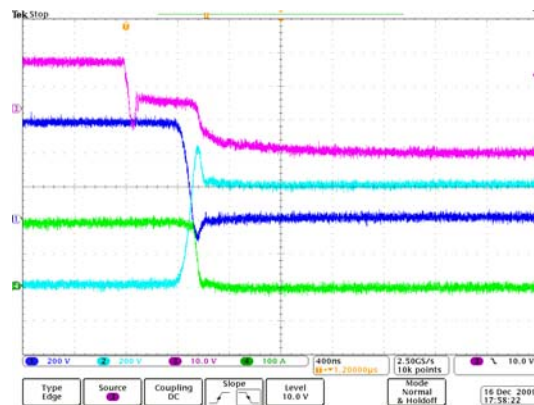
Turn on



Turn off

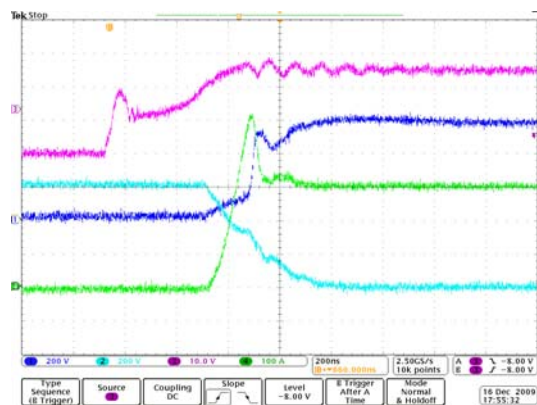


Turn off



600V 300A 23 °C

Turn on

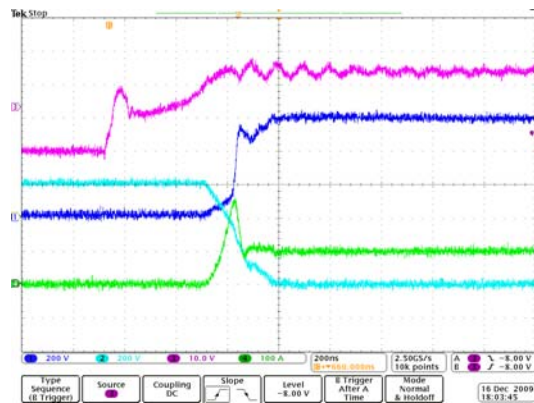


Turn off

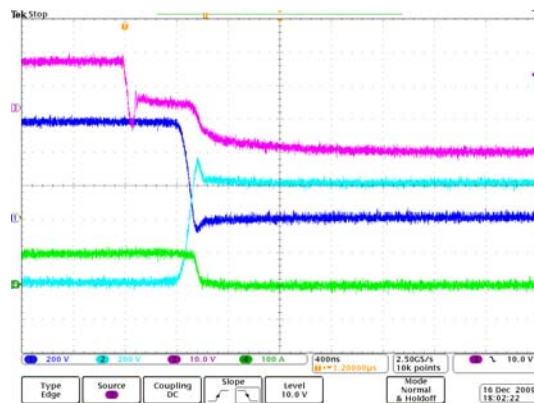


600V 100A 23 °C

Turn on

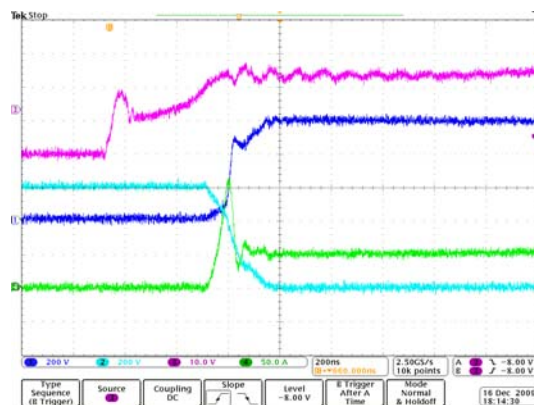


Turn off

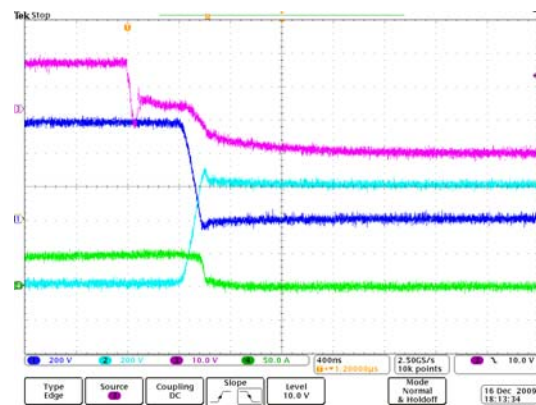


600V 50A 23 °C

Turn on



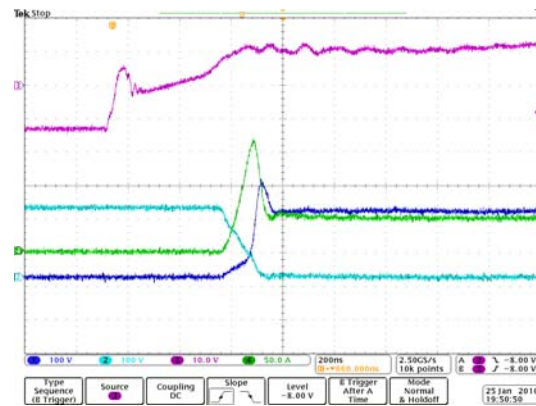
Turn off



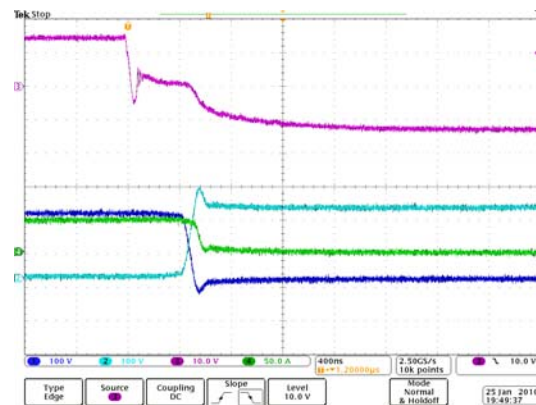
IXYS IGBT NO.2 at 80 °C

200 V 50 A 80 °C

Turn on

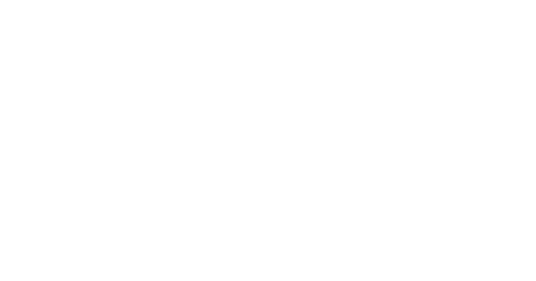


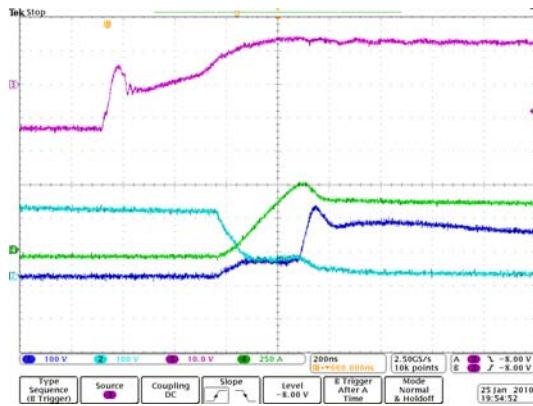
Turn off



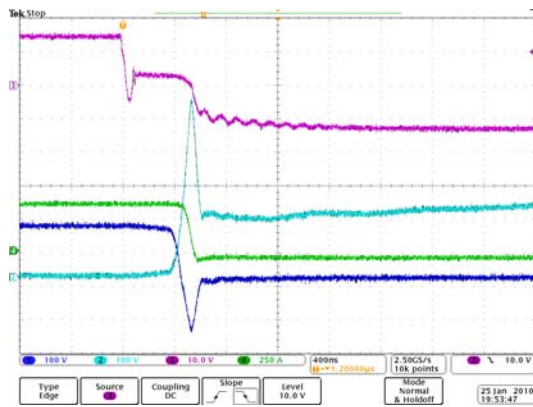
200 V 400 A 80 °C

Turn on



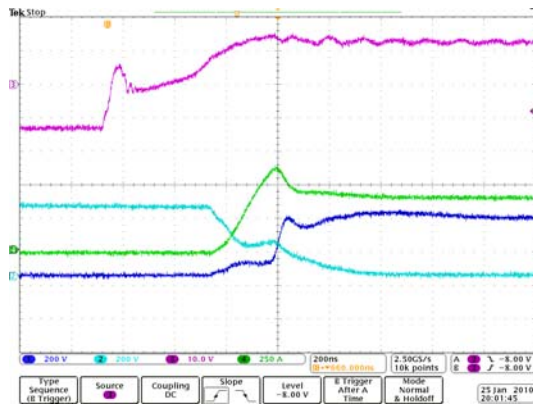


Turn off

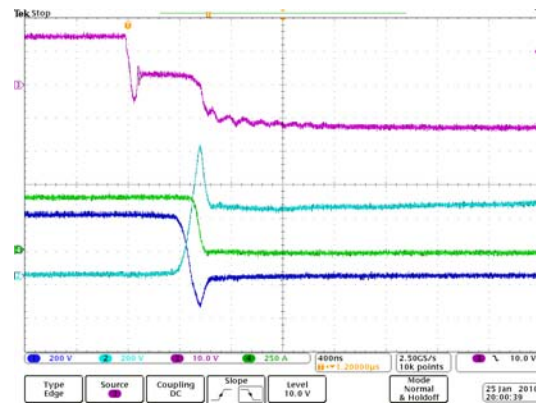


400V 400A 80 °C

Turn on

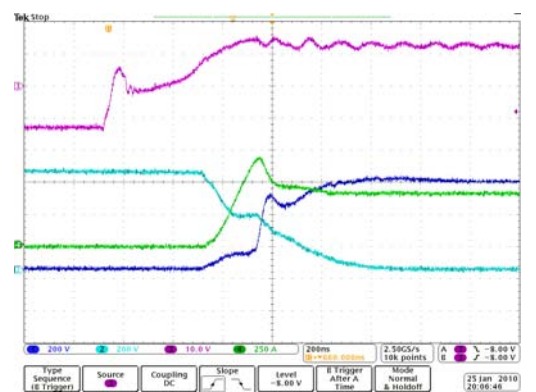


Turn off

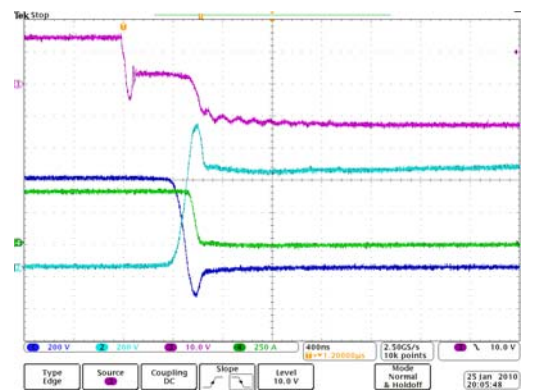


600V 400A 80 °C

Turn on

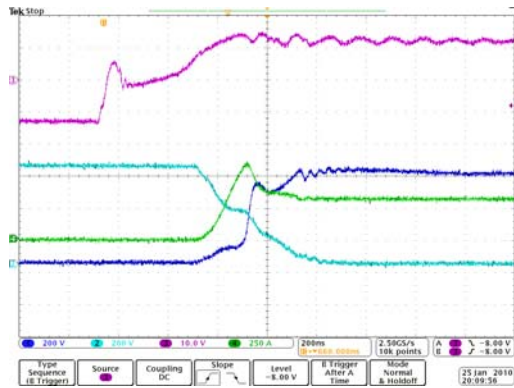


Turn off

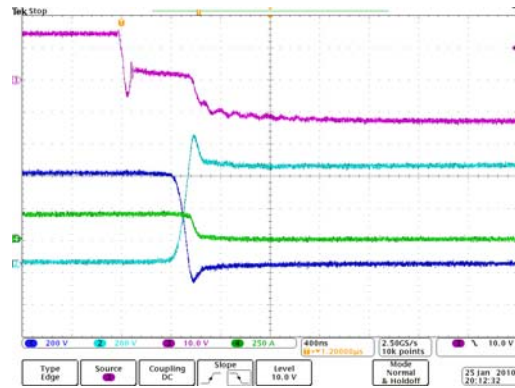


600V 300A 80 °C

Turn on

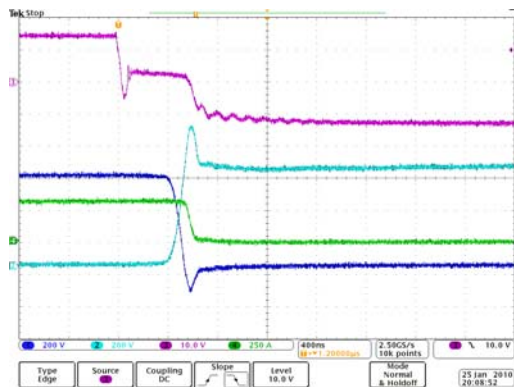


Turn off



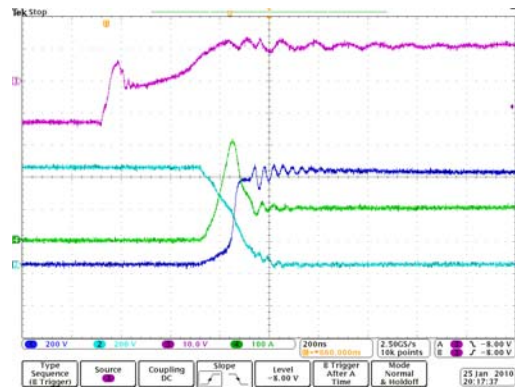
600 V 100 A 80 °C

Turn on

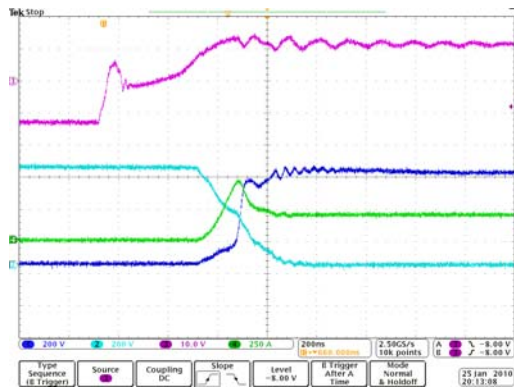


600V 200A 80 °C

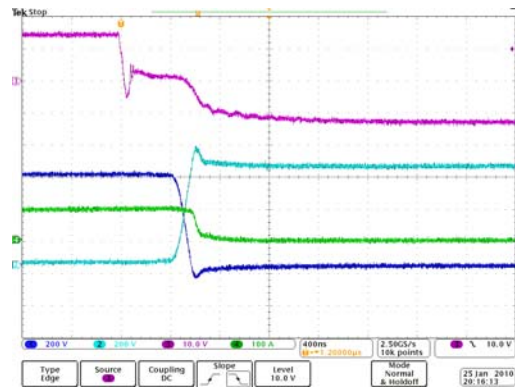
Turn on



Turn off



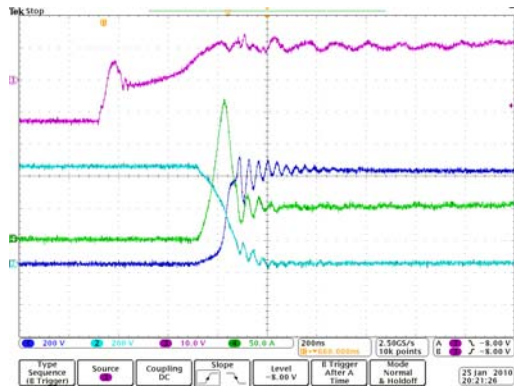
Turn off



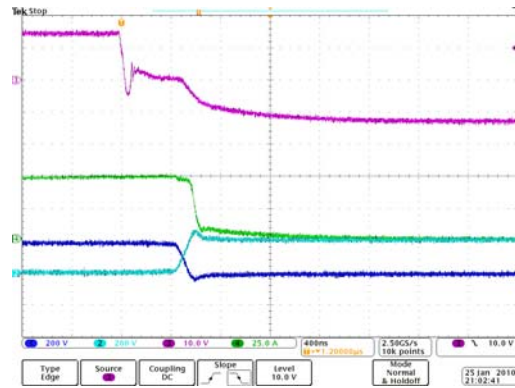
600 V 50 A 80 °C

Turn on



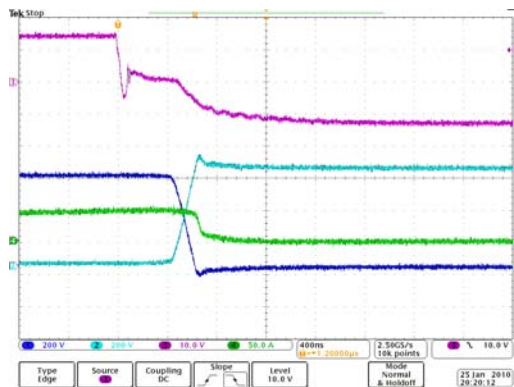


Turn off



200 V 400 A 125 °C

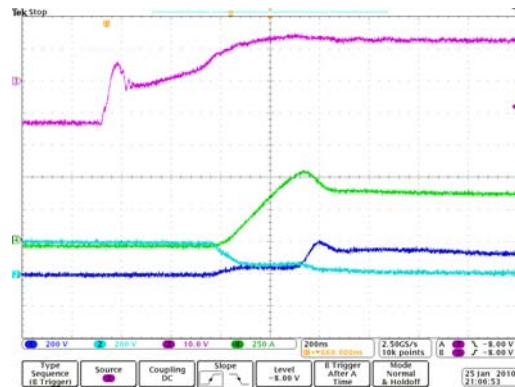
Turn on



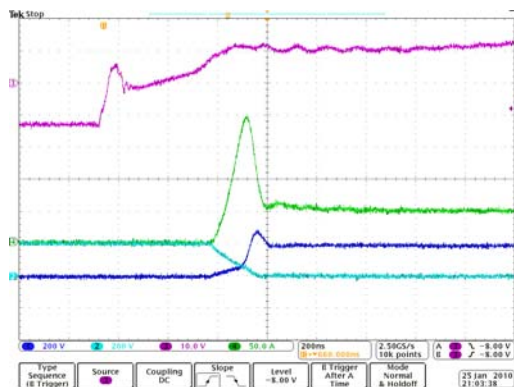
IXYS IGBT NO.2 at 125 °C

200 V 50 A 125 °C

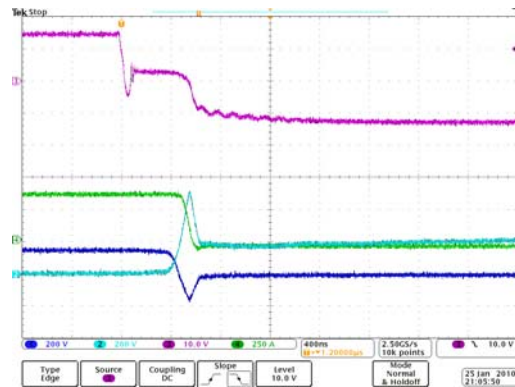
Turn on



Turn off



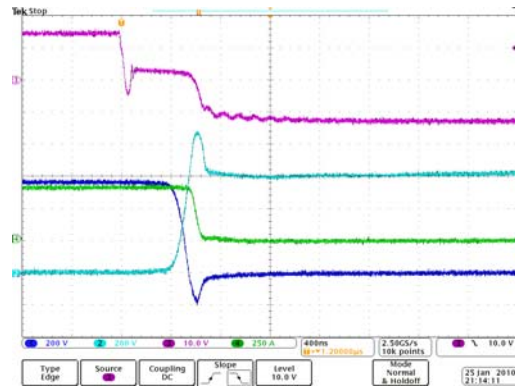
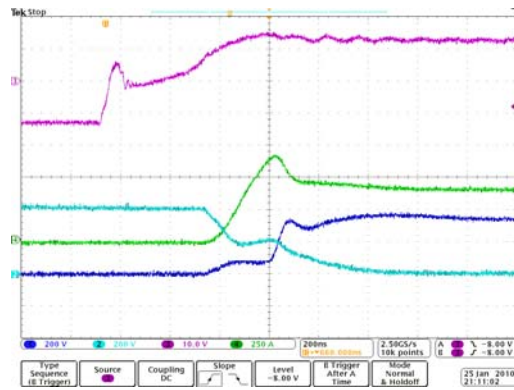
Turn off





400 V 400 A 125 °C

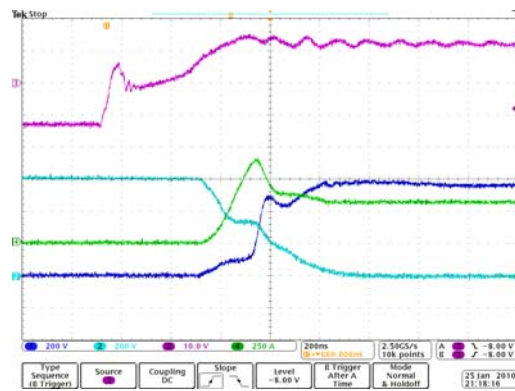
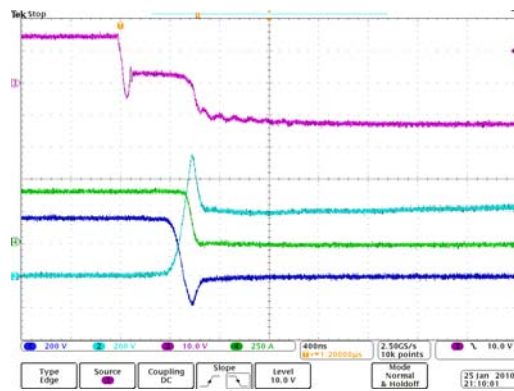
Turn on



600 V 300 A 125 °C

Turn on

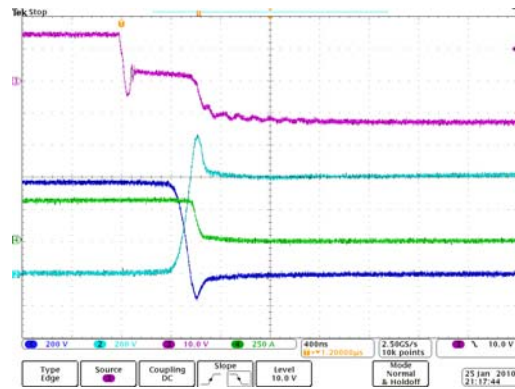
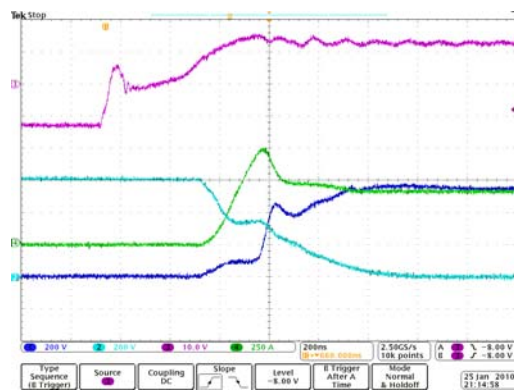
Turn off



600 V 400 A 125 °C

Turn on

Turn off

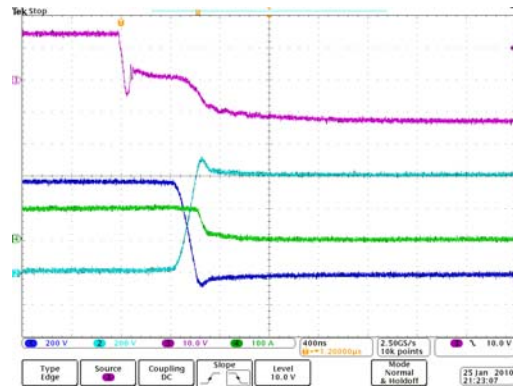
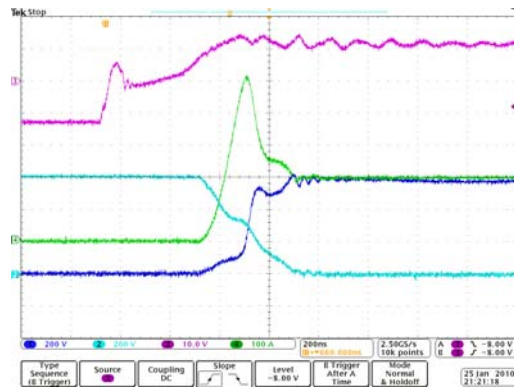


Turn off

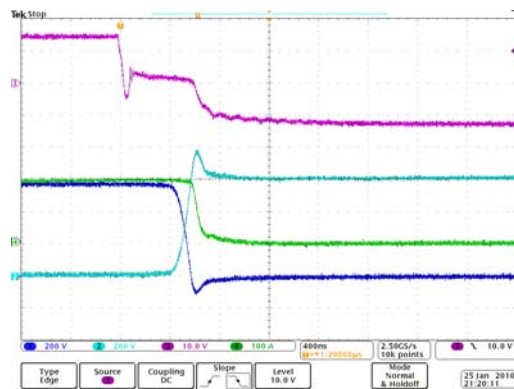


600V 200A 125 °C

Turn on

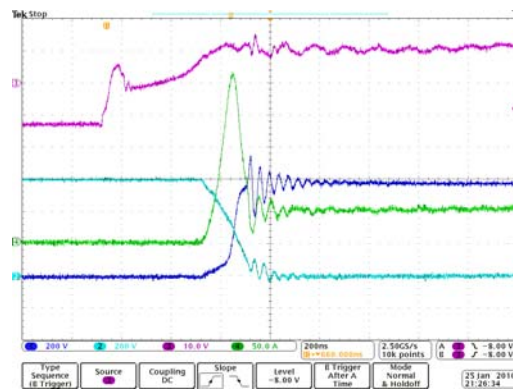


Turn off



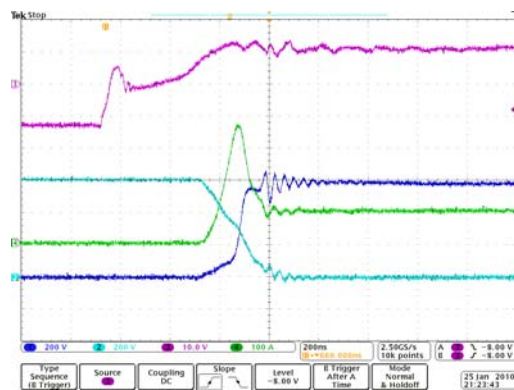
600V 200A 125 °C

Turn on

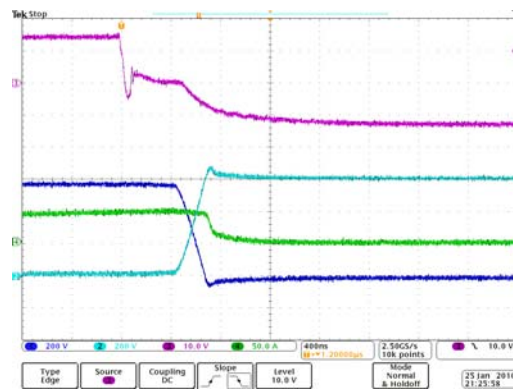


600 V 100 A 125 °C

Turn on



Turn off



Turn off



## Some Useful MATLAB Command

```
Info_loading = xlsread('filename', 1); %loading excel file sheet 1.
Time=Info_loading(2:end, 1); %Time is the matrix of column 1 in sheet 1.
CH1=Info_loading(2:end,2); %CH1 is the matrix of column 2 in sheet 1.
CH2=Info_loading(2:end, 3);
CH3=Info_loading(2:end, 4);
CH4=Info_loading(2:end, 5);
plot(Time, CH1, 'k'); % plot the figure of Time-CH1, and curve is black.
Energy loss calculator:
clear P98
RCH298=CH298; %IGBT Voltage, Off set voltage
RCH498=CH498+15; %IGBT Current, Off set current
P98=RCH298.*RCH498; % Power Calculator
clear E
detaT= Time98(6)-Time98(5)
E(1)=P98(1)*detaT
for i=2:10000; %Energy loss calculator
    E(i)=E(i-1)+P98(i)*detaT;
end
plot(Time98,E)
grid on
hold off
```

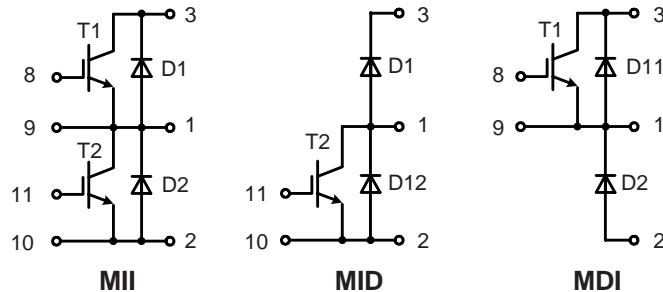
# IGBT Module

phaseleg and chopper topologies

**MII 400-12E4**  
**MID 400-12E4**  
**MDI 400-12E4**

**$I_{C25} = 420 \text{ A}$**   
 **$V_{CES} = 1200 \text{ V}$**   
 **$V_{CE(sat) \text{ typ.}} = 2.2 \text{ V}$**

Preliminary



### IGBTs T1-T2

| Symbol              | Conditions  | Maximum Ratings |               |
|---------------------|---|-----------------|---------------|
| $V_{CES}$           | $T_{VJ} = 25^\circ\text{C to } 150^\circ\text{C}$   | 1200            | V             |
| $V_{GES}$           |   | $\pm 20$        | V             |
| $I_{C25}$           | $T_C = 25^\circ\text{C}$  | 420             | A             |
| $I_{C80}$           | $T_C = 80^\circ\text{C}$  | 300             | A             |
| $I_{CM}$            | $V_{GE} = \pm 15 \text{ V}; R_G = 4.7 \ \Omega; T_{VJ} = 125^\circ\text{C}$   | 450             | A             |
| $V_{CEK}$           | <b>RBSOA</b> , Clamped inductive load; $L = 100 \ \mu\text{H}$  | $V_{CES}$       |               |
| $t_{SC}$<br>(SCSOA) | $V_{CE} = 900 \text{ V}; V_{GE} = \pm 15 \text{ V}; R_G = 4.7 \ \Omega; T_{VJ} = 125^\circ\text{C}$<br>non repetitive | 10              | $\mu\text{s}$ |
| $P_{tot}$           | $T_C = 25^\circ\text{C}$  | 1700            | W             |

### Features

- IGBT
  - low saturation voltage
  - positive temperature coefficient
  - fast switching
  - short tail current for optimized performance in resonant circuits
- HiPerFRED™ diodes
  - fast and soft reverse recovery
  - low operating forward voltage
  - low leakage current
- Package
  - low inductive current path
  - screw connection to high current main terminals
  - use of non interchangeable connectors for auxiliary terminals possible
  - kelvin emitter terminal for easy drive
  - isolated ceramic base plate

| Symbol  | Conditions   | Characteristic Values<br>( $T_{VJ} = 25^\circ\text{C}$ , unless otherwise specified) |                        |                      |               |
|---|--|--|------------------------|----------------------|---------------|
|   |  | min.   | typ.                   | max.                 |               |
| $V_{CE(sat)}$                                 | $I_C = 300 \text{ A}; V_{GE} = 15 \text{ V}; T_{VJ} = 25^\circ\text{C}$<br>$T_{VJ} = 125^\circ\text{C}$  |  | 2.2<br>2.6             | V<br>V               |               |
| $V_{GE(th)}$                                  | $I_C = 10 \text{ mA}; V_{GE} = V_{CE}$   | 4.5  |                        | 6.5 V                |               |
| $I_{CES}$                                     | $V_{CE} = V_{CES}; V_{GE} = 0 \text{ V}; T_{VJ} = 25^\circ\text{C}$<br>$T_{VJ} = 125^\circ\text{C}$  |  | 0.8<br>3.5             | mA<br>mA             |               |
| $I_{GES}$                                     | $V_{CE} = 0 \text{ V}; V_{GE} = \pm 20 \text{ V}$  |  |                        | 600 nA               |               |
| $t_{d(on)}$<br>$t_r$<br>$t_{d(off)}$<br>$t_f$ | Inductive load, $T_{VJ} = 125^\circ\text{C}$<br>$V_{CE} = 600 \text{ V}; I_C = 300 \text{ A}$<br>$V_{GE} = \pm 15 \text{ V}; R_G = 4.7 \ \Omega$ |  | 150<br>60<br>680<br>50 | ns<br>ns<br>ns<br>ns |               |
| $E_{on}$                                      |  |  | 36                     | mJ                   |               |
| $E_{off}$                                     |  |  | 30                     | mJ                   |               |
| $C_{ies}$                                     |  | $V_{CE} = 25 \text{ V}; V_{GE} = 0 \text{ V}; f = 1 \text{ MHz}$                     |                        | 17                   | nF            |
| $Q_{Gon}$                                     |  | $V_{CE} = 600 \text{ V}; V_{GE} = 15 \text{ V}; I_C = 300 \text{ A}$                 |                        | 2.25                 | $\mu\text{C}$ |
| $R_{thJC}$<br>$R_{thJH}$                      | (per IGBT)<br>with heatsink compound   |  | 0.15                   | 0.08 K/W<br>K/W      |               |

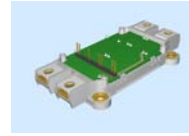
### Applications

- drives
  - AC
  - DC
- power supplies
  - rectifiers with power factor correction and recuperation capability
  - UPS

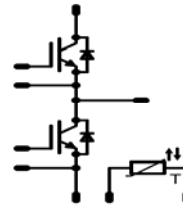


**flowPHASE 2**
**1200V / 300A**
**Features**

- Reliable solder and screw contacts
- Compact and low inductive design

**flowSCREW 2 housing**

**Target Applications**

- Motor Drive
- Uninterruptable Power Supply (UPS)
- Welding

**Schematics**

**Types**

- V23990-P610-F02-PM with connector PCB

## Maximum Ratings

| Parameter                            | Symbol      | Condition   | Value          | Unit       |
|--------------------------------------|-------------|---|----------------|------------|
| <b>Transistor Inverter</b>           |             |   |                |            |
| Collector-emitter break down voltage | $V_{CE}$    |   | 1200           | V          |
| DC collector current                 | $I_C$       | $T_j = T_{j,max}$<br>$T_h = 80^\circ C$<br>$T_c = 80^\circ C$ | 278<br>tbd     | A          |
| Repetitive peak collector current    | $I_{cpuls}$ | tp limited by $T_{j,max}$                                     | 900            | A          |
| Power dissipation per IGBT           | $P_{tot}$   | $T_j = T_{j,max}$<br>$T_h = 80^\circ C$<br>$T_c = 80^\circ C$ | 560<br>tbd     | W          |
| Gate-emitter peak voltage            | $V_{GE}$    |   | $\pm 20$       | V          |
| SC withstand time*                   | $t_{SC}$    | $T_j \leq 125^\circ C$<br>$V_{GE} = 15V$<br>$V_{CC} = 900V$   | 10             | $\mu s$    |
| Maximum junction temperature         | $T_{j,max}$ |   | 150 $^\circ C$ | $^\circ C$ |

\* It is recommended to not exceed 1000 short circuit situations in the lifetime of the module and to allow at least 1s between short circuits

**Diode Inverter**

|                                 |             |   |                |            |
|---------------------------------|-------------|---|----------------|------------|
| DC forward current              | $I_F$       | $T_j = T_{j,max}$<br>$T_h = 80^\circ C$                       | 130            | A          |
| Repetitive peak forward current | $I_{FRM}$   | tp limited by $T_{j,max}$                                     | 2000           | A          |
| Power dissipation per Diode     | $P_{tot}$   | $T_j = T_{j,max}$<br>$T_h = 80^\circ C$<br>$T_c = 80^\circ C$ | 280<br>tbd     | W          |
| Maximum junction temperature    | $T_{j,max}$ |   | 150 $^\circ C$ | $^\circ C$ |

## Maximum Ratings

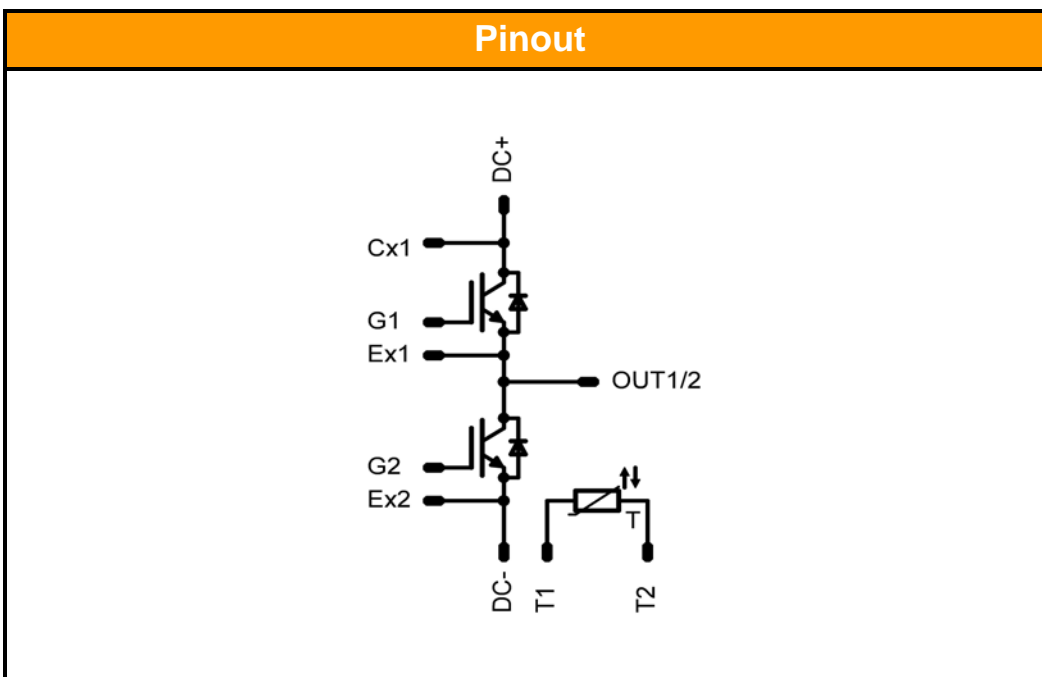
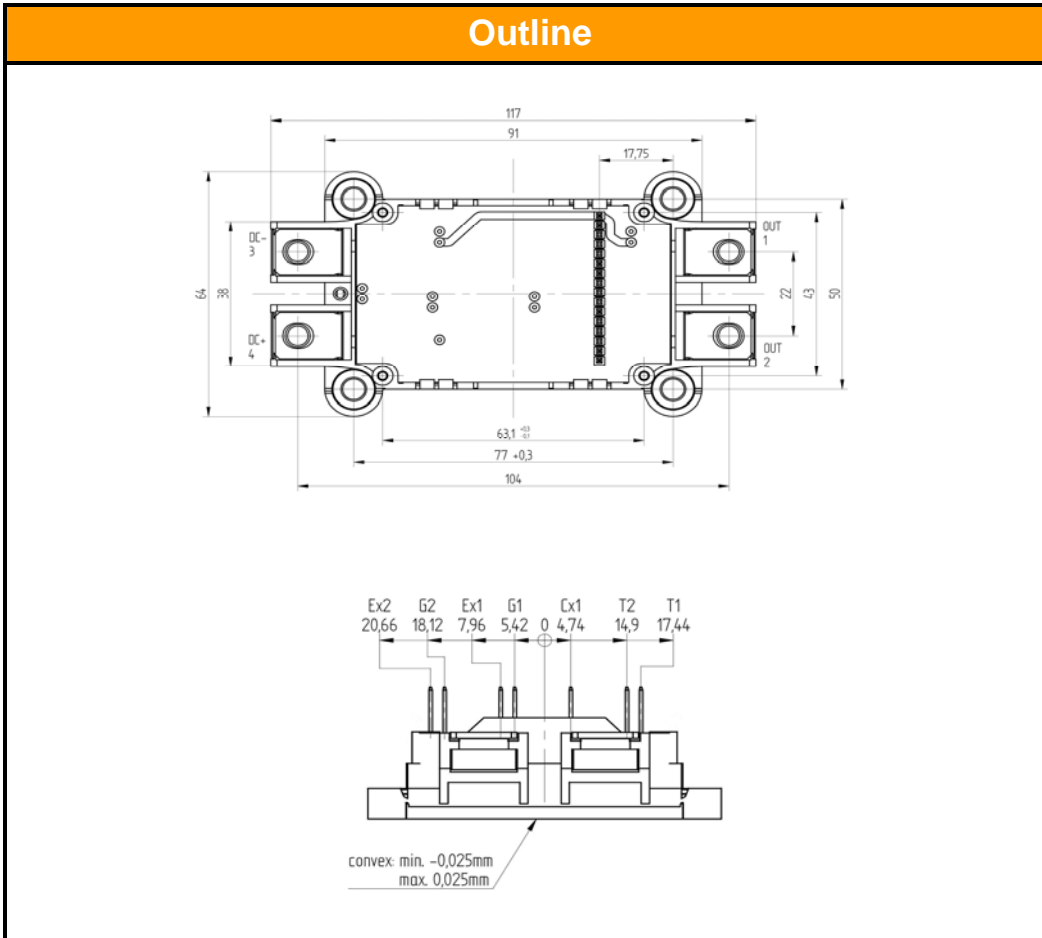
| Parameter                    | Symbol    | Condition | Value      | Unit |
|------------------------------|-----------|-----------|------------|------|
| <b>Thermal properties</b>    |           |           |            |      |
| Storage temperature          | $T_{stg}$ |           | -40...+125 | °C   |
| Operation temperature        | $T_{op}$  |           | -40...+125 | °C   |
| <b>Insulation properties</b> |           |           |            |      |
| Insulation voltage           | $V_{is}$  | t=1min    | 4000       | Vdc  |
| Creepage distance            |           |           | min 12,7   | mm   |
| Clearance                    |           |           | min 12,7   | mm   |



**Characteristic Values**

| Parameter  | Symbol         | Conditions   |  |                                  |              |                     | Value |          |      | Unit |     |
|--|----------------|--|--|----------------------------------|--------------|---------------------|-------|----------|------|------|-----|
|  |                | $V_{GE}(V)$ or $V_{GS}(V)$                           | $V_r(V)$ or $V_{CE}(V)$ or $V_{DS}(V)$ | $I_c(A)$ or $I_f(A)$ or $I_D(A)$ | $T(C^\circ)$ | Min                 | Typ   | Max      |      |      |     |
| <b>Transistor Inverter</b>                       |                |  |  |                                  |              |                     |       |          |      |      |     |
| Gate emitter threshold voltage                   | $V_{GE(th)}$   | VCE=VGE  |  |                                  | 0,012        | Tj=25°C<br>Tj=125°C | 5     | 5,8      | 6,5  | V    |     |
| Collector-emitter saturation voltage             | $V_{CE(sat)}$  |  | 15                                     |                                  | 300          | Tj=25°C<br>Tj=125°C | 1,3   | 1,8<br>2 | 2,2  | V    |     |
| Collector-emitter cut-off                        | $I_{CES}$      |  | 0                                      | 1200                             |              | Tj=25°C<br>Tj=125°C |       |          | 2    | mA   |     |
| Gate-emitter leakage current                     | $I_{GES}$      |  | 30                                     | 0                                |              | Tj=25°C<br>Tj=125°C |       |          | 1400 | nA   |     |
| Integrated Gate resistor                         | $R_{gint}$     |  |  |                                  |              |                     |       | 2,5      |      | Ohm  |     |
| Turn-on delay time                               | $t_{d(on)}$    | Rgoff=2Ω<br>Rgon=2Ω                                  | ±15                                    | 600                              | 300          | Tj=25°C<br>Tj=125°C |       | 310      |      | ns   |     |
| Rise time  | $t_r$          |  |  |                                  |              | Tj=25°C<br>Tj=125°C |       | 40       |      | ns   |     |
| Turn-off delay time                              | $t_{d(off)}$   |  |  |                                  |              | Tj=25°C<br>Tj=125°C |       | 540      |      | ns   |     |
| Fall time  | $t_f$          |  |  |                                  |              | Tj=25°C<br>Tj=125°C |       | 170      |      | ns   |     |
| Turn-on energy loss per pulse                    | $E_{on}$       |  |  |                                  |              | Tj=25°C<br>Tj=125°C |       | 52       |      | mWs  |     |
| Turn-off energy loss per pulse                   | $E_{off}$      |  |  |                                  |              | Tj=25°C<br>Tj=125°C |       | 32       |      | mWs  |     |
| SC withstand time                                | $t_{SC}$       |  |  |                                  |              |                     |       |          |      | μs   |     |
| Input capacitance                                | $C_{ies}$      | f=1MHz   | 0                                      | 25                               |              | Tj=25°C<br>Tj=125°C |       | 22       |      | nF   |     |
| Output capacitance                               | $C_{oss}$      |  | 0                                      | 25                               |              | Tj=25°C<br>Tj=125°C |       | 4,2      |      | nF   |     |
| Reverse transfer capacitance                     | $C_{rss}$      |  | 0                                      | 25                               |              | Tj=25°C<br>Tj=125°C |       | 3,6      |      | nF   |     |
| Gate charge                                      | $Q_{gate}$     |  | ±15                                    |                                  |              | Tj=25°C<br>Tj=125°C |       | 2800     |      | nC   |     |
| Thermal resistance chip to heatsink per chip     | $R_{thJH}$     | Thermal grease<br>thickness ≤ 50 μm<br>λ = 0,61 W/mK |  |                                  |              |                     |       | 0,125    |      | K/W  |     |
| Coupled thermal resistance diode-transistor      | $R_{thJH}$     |  |  |                                  |              |                     |       |          | tbd  |      | K/W |
| Coupled thermal resistance transistor-transistor | $R_{thJH}$     |  |  |                                  |              |                     |       |          | tbd  |      | K/W |
| <b>Diode Inverter</b>                            |                |  |  |                                  |              |                     |       |          |      |      |     |
| Diode forward voltage                            | $V_F$          |  |  |                                  | 300          | Tj=25°C             | 1     | 1,85     | 2,4  | V    |     |
| Peak reverse recovery current                    | $I_{RM}$       | Rgon=2Ω<br>diF/dt=6000 A/us                          | 0                                      | 600                              | 300          | Tj=25°C<br>Tj=125°C |       | 300      |      | A    |     |
| Reverse recovery time                            | $t_{rr}$       | Rgon=2Ω<br>diF/dt=6000 A/us                          | 0                                      | 600                              | 300          | Tj=25°C<br>Tj=125°C |       | 800      |      | ns   |     |
| Reverse recovery charge                          | $Q_{rr}$       | Rgon=2Ω<br>diF/dt=6000 A/us                          | 0                                      | 600                              | 300          | Tj=125°C            |       | 77       |      | μC   |     |
| Reverse recovery energy                          | $E_{rec}$      | Rgon=2Ω<br>diF/dt=6000 A/us                          | 0                                      | 600                              | 300          | Tj=25°C<br>Tj=125°C |       | 30       |      | mWs  |     |
| Thermal resistance chip to heatsink per chip     | $R_{thJH}$     | Thermal grease<br>thickness ≤ 50 μm<br>λ = 0,61 W/mK |  |                                  |              |                     |       | 0,25     |      | K/W  |     |
| Thermal resistance chip to case per chip         | $R_{thJC}$     |  |  |                                  |              |                     |       |          | tbd  |      | K/W |
| Coupled thermal resistance transistor-diode      | $R_{thJH}$     |  |  |                                  |              |                     |       |          | tbd  |      | K/W |
| Coupled thermal resistance diode-diode           | $R_{thJH}$     |  |  |                                  |              |                     |       |          | tbd  |      | K/W |
| <b>NTC Thermistor</b>                            |                |  |  |                                  |              |                     |       |          |      |      |     |
| Rated resistance                                 | $R_{25}$       |  |  |                                  |              | Tj=25°C             | 4,46  | 4,7      | 4,94 | kOhm |     |
| Deviation of R100                                | $D_{R/R}$      | R100=226Ω  |  |                                  |              | Tc=100°C            |       | 3        |      | %/K  |     |
| Power dissipation given Epcos-Type               | $P$            |  |  |                                  |              | Tj=25°C             |       | 210      |      | mW   |     |
| B-value  | $B_{(25/100)}$ | Tol. ±3%   |  |                                  |              | Tj=25°C             |       | 4500     |      | K    |     |

### Package Outline and Pinout



**PRODUCT STATUS DEFINITIONS**

| <b>Datasheet Status</b> | <b>Product Status</b>  | <b>Definition</b>   |
|-------------------------|------------------------|---|
| Target                  | Formative or In Design | This datasheet contains the design specifications for product development. Specifications may change in any manner without notice. The data contained is exclusively intended for technically trained staff.  |
| Preliminary             | First Production       | This datasheet contains preliminary data, and supplementary data may be published at a later date. Tyco Electronics reserves the right to make changes at any time without notice in order to improve design. The data contained is exclusively intended for technically trained staff. |
| Final                   | Full Production        | This datasheet contains final specifications. Tyco Electronics reserves the right to make changes at any time without notice in order to improve design. The data contained is exclusively intended for technically trained staff.  |

**DISCLAIMER**

Tyco Electronics reserves the right to make changes without further notice to any products herein to improve reliability, function or design. Tyco Electronics does not assume any liability arising out of the application or use of any product or circuit described herein; neither does it convey any license under its patent rights, nor the rights of others.

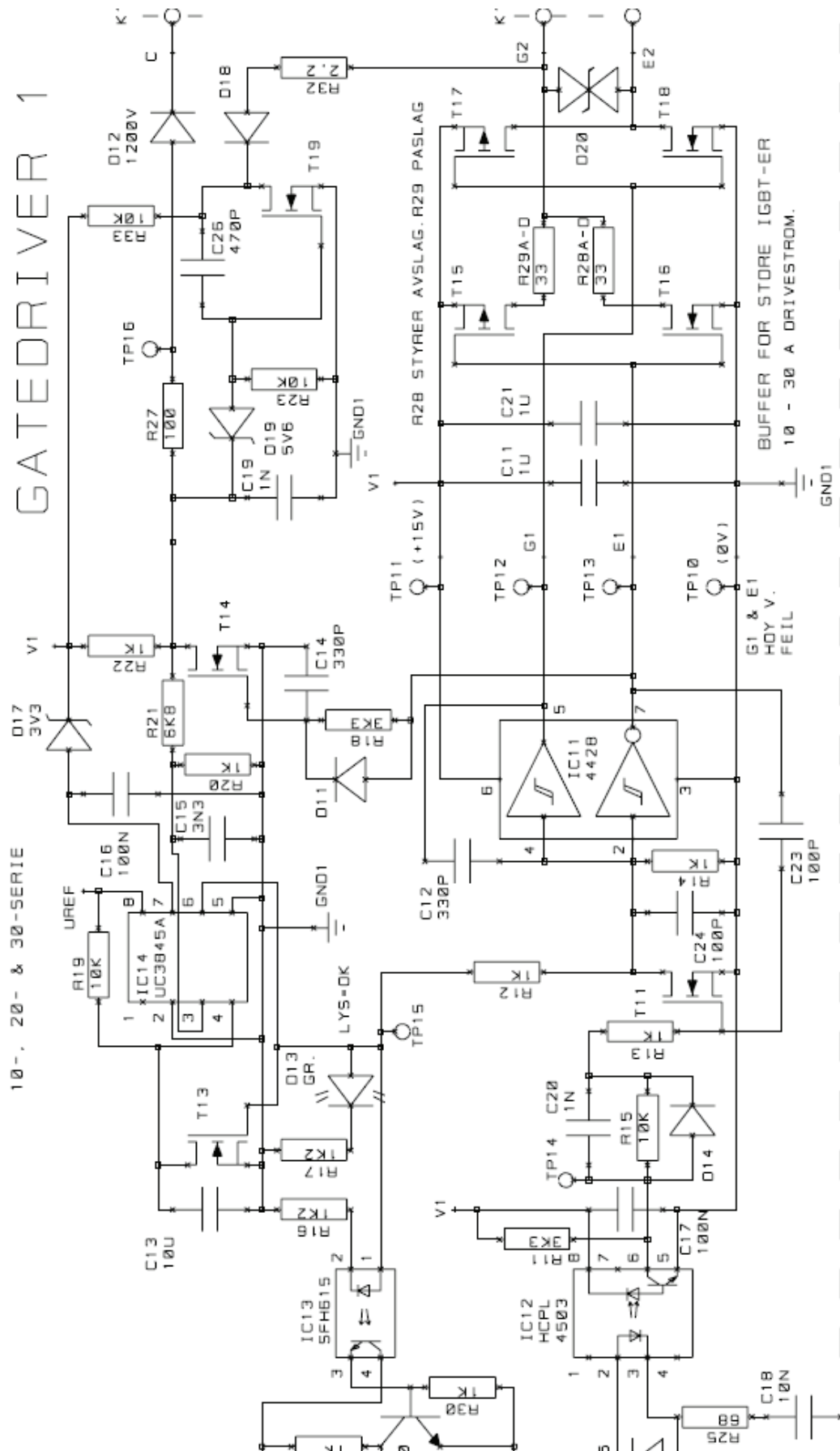
**LIFE SUPPORT POLICY**

Tyco Electronics products are not authorised for use as critical components in life support devices or systems without the express written approval of Tyco Electronics.

As used herein:

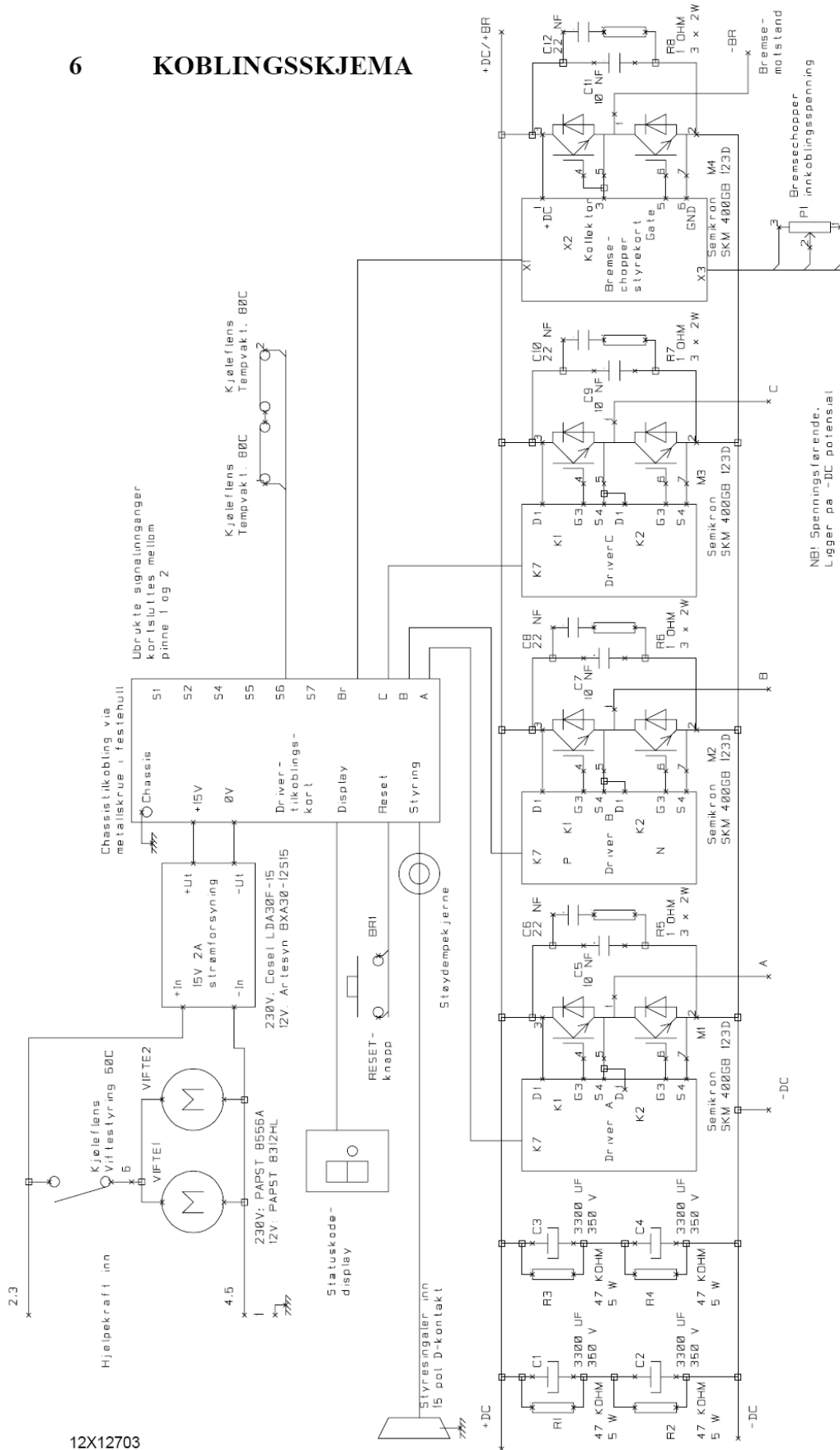
1. Life support devices or systems are devices or systems which, (a) are intended for surgical implant into the body, or (b) support or sustain life, or (c) whose failure to perform when properly used in accordance with instructions for use provided in labelling can be reasonably expected to result in significant injury to the user.
2. A critical component is any component of a life support device or system whose failure to perform can be reasonably expected to cause the failure of the life support device or system, or to affect its safety or effectiveness.

# APPENDIX B: EFI Gate Driver [4]



# APPENDIX C: 20kW Laboratory Inverter [3]


## 6 KOBLINGSSKJEMA



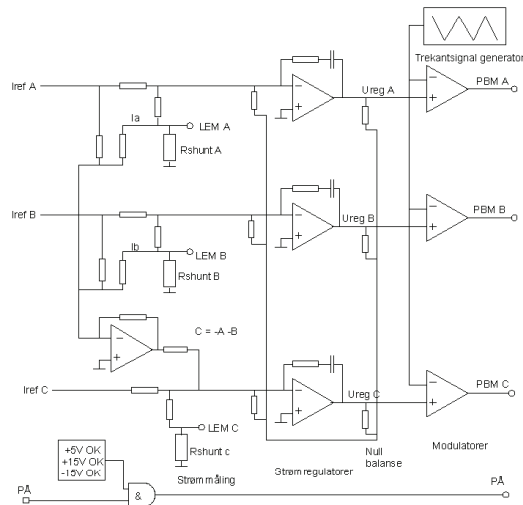
|   |
|---|
| FILE: Lab vekselretter skjema.scm                               |
| UTLEGG REF. PROSJ. 12x134.03                                    |
| KONSTRUERT K.Ljøkelsøy DATO: 17/4-2002                          |
| 20 kW lab-<br>veksleretterenhet.<br>Variant 1                   |
| <b>SINTEF</b><br>Energiforskning AS Per Ekoblet kondensatorbank |

12X12703

## APPENDIX D: Analog Current Control Board [13]

|  |           |  |                |
|--|-----------|--|----------------|
|  <p><b>SINTEF Energiforskning AS</b></p> <p>Postadresse: 7034 Trondheim<br/>Resepsjon: Sem Sælands vei 11<br/>Telefon: 73 59 72 00<br/>Telefaks: 73 59 72 50</p> <p>http://www.energy.sintef.no</p> <p>F. nr.: NO 939 350 675</p> |           | <b>ARBEIDSNOTAT</b>  |                |
|  |           | <p>GJELDER</p> <p><b>Analog strømregulatorkort. v1.0</b></p> |                |
|  |           | GÅR TIL  |                |
| AN NR.   | GRADERING | GJENOMGÅTT AV  |                |
| <b>AN98.13.44</b>  | Åpen      | Terje Rogne  |                |
| ELEKTRONISK ARKIVKODE  |           | FORFATTER(E)   | DATO           |
| J:\DOK\13\kj\98004216.DOC  |           | Kjell Ljøkelsoy  | 1998-11-17     |
| PROSJEKTNR.  |           |  | ANTALL SIDER   |
| 13X081.01  |           | Kjell.Ljokelsoy@energy.sintef.no                             | 14             |
| AVDELING   |           | BESØKSADRESSE  | LOKAL TELEFAKS |
| Elektriske anlegg  |           | Sem Sælandsvei 11  | 73 59 72 50    |

*Dokumentet inneholder: Skjema, komponentplassering, delaliste, tilkoblingsliste, kommentarer.*



Kortet inneholder tre analoge strømregulatorer med tilhørende pulsbreddemodulatorer, samt shuntmotstander for strømmåling med LEM transfoshunter.

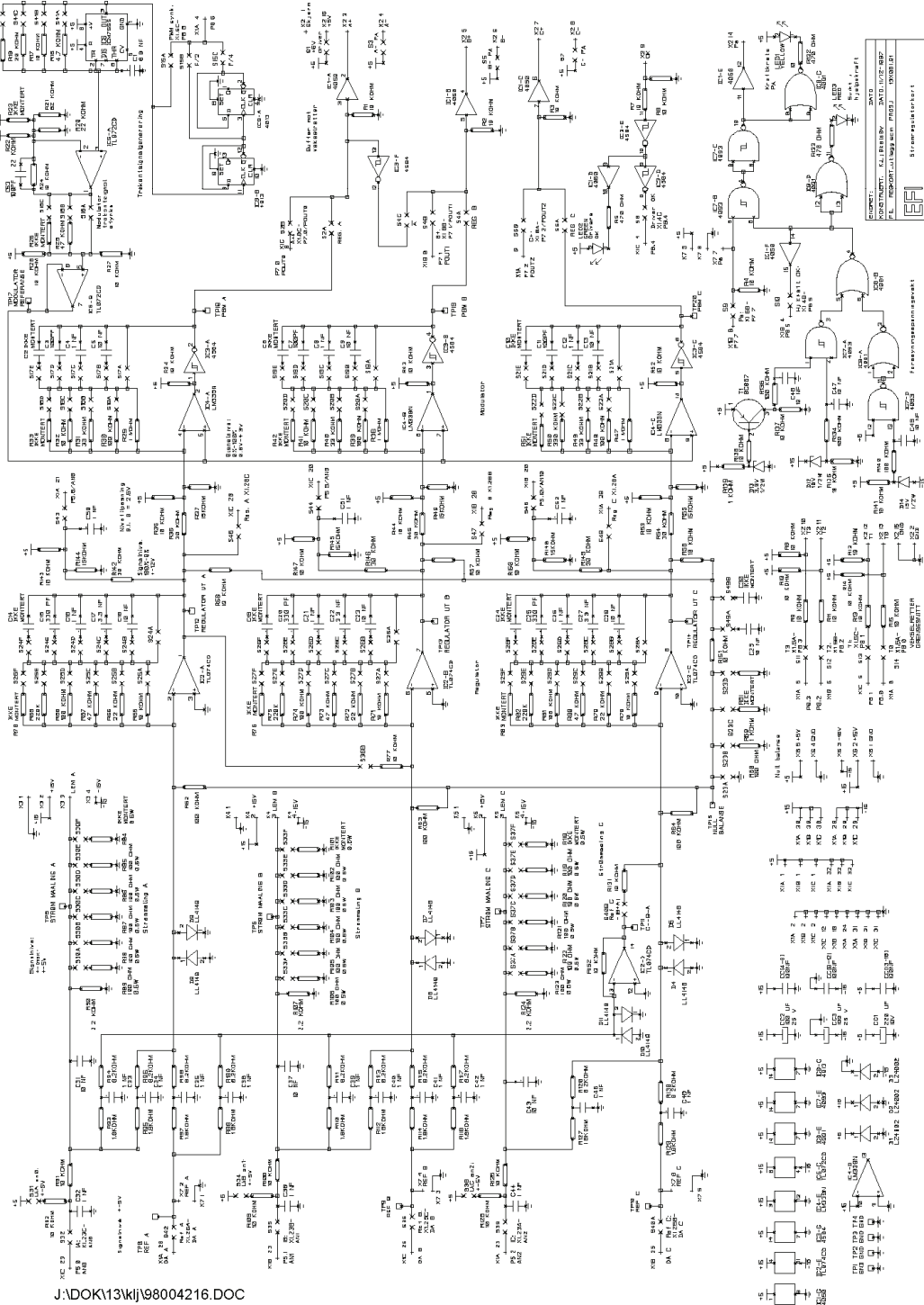
Regulatorinnstillinger og konfigurering bestemmes av et sett med strappinger.

Ved bruk i motorstyringer kan kortet konfigureres slik at kun to strømmålinger og referansesignaler benyttes. En nullpunktsbalanseringskrets sikrer da en midlere utstyring på 50%

Dette notat inneholder prosjektinformasjon og foreløpige resultater, som internt og uformelt underlag for endelig prosjektrapport fra SINTEF Energiforskning AS. SINTEF Energiforskning AS hefter ikke for notatets innhold, og resultatene/ data vil i den godkjente prosjektrapport kunne avvike fra notatets opplysninger uten spesielt varsel eller henvisning til dette. Innholdet får ikke gjengis uten skriftlig tillatelse fra SINTEF Energiforskning AS.



2 SKJEMA



J:\DOK113\kij\98004216.DOC

|       | Name   | Conditions  | Standards  |
|-------|--|---|--|
| HTRB  | Hot reverse test                                 | MOS/IGBT: 1000h, $T_{vjmax}$ ,<br>$V_{CEmax} (\leq 2.0 \text{ kV}), 0.8 * V_{CEmax} (>2.0 \text{ kV})$<br>Conv.: 1000h, $T_j = 125^\circ\text{C}$ ,<br>$V_{RM} = 0.9 * V_{RRM}$ ,<br>$V_{RM}/V_{DM} = 0.8 * V_{RRM}/V_{DRM}$ <sup>a</sup>   | IEC 60747-2/6<br>Kap. V<br>IEC 60747-9:<br>1998  |
| HTGS  | High temperature gate stress test                | 1000h, $\pm V_{GEmax}$ , $T_j = 125^\circ\text{C}$  | IEC 60747-9:<br>1998                             |
| H3TRB | High humidity high temperature reverse bias test | 1000h, $85^\circ\text{C}$ , 85%RH,<br>$V_{CE} = 0.8 * V_{CEmax}$ , however max. 80 V,<br>$V_{GE} = 0\text{V}$   | IEC 60749:<br>1996                               |
| TST   | Thermal shock <sup>1</sup>                       | $T_{stgmin} - T_{stgmax}$ , typ. $-40^\circ\text{C}$ to $+125^\circ\text{C}$ ,<br>but $\Delta T_{max} \leq 165\text{K}$ , $t_{storage} \geq 1\text{h}$ ,<br>$t_{change} \leq 30 \text{ s}$<br>High power, standard: 20 cycles<br>High power, traction: 100 cycles<br>Medium power: 50 cycles<br>Conv.: 25 cycles <sup>a</sup> | IEC 60749:<br>1996                               |
| TC    | Temperature cycling <sup>1</sup>                 | External heating and cooling<br>2 min. $< t_{cycl} < 6 \text{ min}$ ; $\Delta T_c = 80\text{K}$ ,<br>$T_{cmin} = 25^\circ\text{C}$<br>High power, standard: 2 000 cycles<br>Medium power: 5 000 cycles<br>Conv.: 5000 cycles <sup>a</sup>   | IEC 60747-2/6<br>Kap. IV<br>IEC 60747-9:<br>1998 |
| TC    | Temperature cycling <sup>2</sup>                 | External heating and cooling<br>$T_{stgmin} - T_{stgmax}$ 100 cycles<br>Conv. modules: 25 cycles <sup>a</sup>   | IEC 60068-2-<br>14 test Na                       |
| PC    | Power cycling <sup>1</sup>                       | Internal heating and external cooling<br>$0.5 < t_{cycl} < 10 \text{ sec}$ ; $\Delta T_j = 60\text{K}$ ,<br>$T_{jmax} = 125^\circ\text{C}$ , 130 000 cycles   | IEC 60747-9:<br>1998                             |
| PC    | Power cycling <sup>2</sup>                       | Internal heating and external cooling<br>$\Delta T_j = 100\text{K}$ , 20 000 cycles<br>Conv. modules: 10 000 cycles <sup>a</sup>  | IEC 60747-9:<br>1998                             |
| V     | Vibration  | Sinusoidal sweep, 5g, 2 h per axis<br>(x, y, z)   | IEC 60068-2-6<br>Test Fc                         |
| MS    | Mechanical shock                                 | Half sine puls, 30g, 3 times<br>each direction ( $\pm x, \pm y, \pm z$ )  | IEC 60068-2-<br>27 Test Ea                       |
| PC    | Power cycling <sup>1</sup>                       | Internal heating and external cooling<br>$0.5 < t_{cycl} < 10 \text{ sec}$ ; $\Delta T_j = 60\text{K}$ ,<br>$T_{jmax} = 125^\circ\text{C}$ , 130 000 cycles   | IEC 60747-9:<br>1998                             |
| PC    | Power cycling <sup>2</sup>                       | Internal heating and external cooling<br>$\Delta T_j = 100\text{K}$ , 20 000 cycles<br>Conv. modules: 10 000 cycles <sup>a</sup>  | IEC 60747-9:<br>1998                             |